Tampere University

Heidi Peussa

CHARACTERIZATION OF A STRETCHING AND COMPRESSION DEVICE AND ITS APPLICATION ON EPITHELIAL CELLS

Faculty of Medicine and Health Technology
Master of Science Thesis
April 2020

ABSTRACT

Heidi Peussa : Characterization of a Stretching and Compression Device and its Application on Epithelial Cells
Master of Science Thesis
Tampere University
Master's Degree Programme in Bioengineering
April 2020

Whether originated from the environment, surrounding cells or from the cell itself, all cells in a human being are subjected to mechanical signals. These signals, along with biochemical and electrical signals, control all cellular functions. Cells sense mechanical signals through a process called mechanotransduction. This allows cells to detect mechanical forces such as compression, stretching and shear stress, as well as the topography and toughness of the substrate. Mechanotransduction can affect cells directly at the protein level or through gene expression, and it affects, for example, differentiation, proliferation, viability and migration of cells.

This Master of Science thesis focuses on a silicone based device designed to apply static or cyclic compression or stretching on cells. The development of this device has been ongoing for years, and as the latest advance a new version was designed. The new version is a step toward productization as it streamlines the manufacture of the device. The aim of this thesis was to characterize this new version of the device.

The work can be divided into three parts. First, several commercial polydimethylsiloxane (PDMS) films were compared in order to choose the one that best suits the requirements of the device. This aimed to improve the efficiency of manufacture as well. Then, the stretching performance and repeatability of the device were characterized. Finally, the device was used in cell culture to apply compression to epithelial cells.

Three commercial PDMS films in two thicknesses were compared for their autofluorescence, optical resolution, biocompatibility and performance in the device. Differences between samples were small, but SILPURAN® (Wacker Chemie AG) in the thickness of 200 µm was chosen. In addition to showing good results in the tested parameters, the film is packed in a user-friendly way and showed no problems in adsorbing surface molecules.

Also several modifications to the current device were tested. The actual characterization was carried out with a device with a slightly expanded vacuum chamber and a stabilator ring that decreased z-displacement. The maximum stretching was 8.6 ± 0.6 % and the undesired z-displacement less than 100 µm. Variation from device to device was 0.6 %-units and repeatability within a single device 0.2 %-units. Therefore, the variation originates from manufacture flaws, not the performance of the device itself

Cell experiments were done with Madin-Darby Canine Kidney (MDCK) epithelial cells. One cell line expressed a genetically labeled occludin protein, and thus allowed the inspection of cell boarders in live cells. The other MDCK cell line expressed jRGECO1a, a live calcium indicator, and was used to study calcium signaling. After a six day culture period on a statically stretched device, strain was released thus creating a 15 % decrease in cell culture area. Cells were imaged before and after compression. The results show that epithelial cells became tightly packed due to compression. Average cross-sectional area of cells decreased 40 %, thus indicating active rearrangement of the cytoskeleton. Interestingly, calcium signaling decreased after compression. This was probably a consequence of the tight packing. When cells had smaller space, they had less possibilities to change shape and migrate, which was seen as a decrease in calcium activity.

All in all, the device was reliable and usable in cell culture conditions. However, further development is required to improve maximum stretching and linearity of stretching, and to make the setup more compact. Additionally, despite the advances in the manufacture of the device, production remains inefficient and calls for improvements.

Keywords: Mechanotransduction, mechanobiology, PDMS, stretching, compression, cell culture, MDCK epithelial cells

TIIVISTELMÄ

Heidi Peussa : Venytys- ja kompressiolaitteen karakterisointi ja sen soveltaminen epiteelisoluille
Diplomityö
Tampereen yliopisto
Biotekniikan diplomi-insinöörin tutkinto-ohjelma
Huhtikuu 2020

Kaikki ihmisen solut altistuvat mekaanisille voimille. Näitä voimia voivat tuottaa solut itse, naapurisolut tai ne voivat olla peräisin ympäristöstä. Yhdessä biokemiallisten ja sähköisten signaalien kanssa nämä signaalit säätelevät solujen kaikkea toimintaa. Solut tulkitsevat mekaanisia voimia, kuten venytystä, kompressiota, leikkausvoimia sekä pinnanmuotoja, muuntamalla ne biokemiallisiksi signaaleiksi. Tätä kustutaan mekanotransduktioksi. Se vaikuttaa soluihin proteiinitasolla sekä geenien ekspression kauttta, ja säätelee esimerkiksi solujen erilaistumista, jakautumista, elossa pysymistä ja liikkumista.

Tämä diplomityö keskittyy silikonipohjaiseen mekanobiologiseen soluviljelyalustaan, jolla voidaan tuottaa soluille joko syklistä tai staattista venytystä tai kompressiota. Laitetta on kehitetty jo pitkään, ja diplomityön aihe oli karaktersoida laitteen uusin versio. Uuden version valmistaminen on tehokkaampaa, mikä on täten askel kohti laitteen tuotteistamista.

Työ jakautuu kolmeen osaan. Valmistuksen tehokkuuden edistämiseksi itsetehty silikonikalvo haluttiin korvata kaupallisella. Tätä varten määritettiin vertailtavien kaupallisten kalvoehdokkaiden ominaisuuksia, jotta voitiin valita laitteen toimintaan parhaiten soveltuva kalvo. Kalvon valinnan jälkeen laitteen venymisen toiminta ja toistettavuus karakterisoitiin, ja lopulta laitetta testattiin soluviljelyssä.

Kalvojen autofluoresenssi, optinen resoluutio, bioyhteensopivuus sekä toiminta venytyslaitteessa määritettiin. Näytteiden väliset erot olivat pieniä, mutta 200 µm paksuinen SILPURAN® (Wacker Chemie AG) valittiin kalvoksi. Hyvien mittaustulosten lisäksi kalvon pakkaus oli käyttäjäystävällinen, ja se adsorboi pintamolekyylejä ongelmitta.

Ennen karakterisointia laitetta muokattiin vielä hieman. Vakuumikammiota korotettiin 4 mm:iin ja ulkoreunaa vasten lisättiin stabilointirengas vähentämään kalvon z-suuntaista liikettä. Maksimivenymäksi saatiin 8.6 ± 0,6 % ja z-suunnan ei-toivottu liike oli alle 100 µm. Eri laitteiden välillä havaittiin 0,6 %-yksikköä variaatiota venymässä, ja yhden laitteen venymän variaatio oli 0,2 %-yksikköä eri mittauskertojen välillä. Toimintaerot johtuvat pienistä valmistusvirheistä, eivät laitteen perimmäisestä toiminnasta.

Solutestit tehtiin Madin-Darby Canine Kidney (MDCK) -epiteelisoluilla. Toisen solulinjan okludiini oli geneettisesti leimattu emerald-fluoresenssileimalla. Okludiini on solu-soluliitosproteiini, joten solulinja mahdollisti solun reunojen kuvantamisen elävistä soluista. Toinen solulinja puolestaa ekspressoi jRGECO1a-kalsiumindikaattoria, jolloin solujen kalsiumaktiivisuutta voitiin seurata. Soluja kasvatettiin kuusi päivää venytetyllä laitteella. Tämän jälkeen venytys vapautettiin, mikä aikaansai kasvatuspinta-alan 15 % kutistumisen. Solut kuvattiin ennen ja jälkeen kompression, jolloin havaittiin että solujen keskimääräinen poikkipinta-ala pieneni 40 %. Tämä on enemmän kuin kasvatuspinta-alan pieneneminen, mikä viittaa siihen, että solut muuttivat muotoaan aktiivisesti. Kalsiumaktiivisuus puolestaan heikkeni kompression myötä, mikä todennäköisesti johtui pakkautumisesta. Kun tilaa on vähemmän, solujen mahdollisuudet liikkua ja muuttaa muotoaan pienenevät, mikä näkyy kalsiumsignaloinnin vähenemisenä.

Voidaan siis todeta, että laite on luotettava ja sitä voidaan käyttää soluviljelyssä solujen mekaaniseen stimulointiin. Laite kuitenkin vaatii lisäkehitystä, jotta venymä saadaan suuremmaksi ja lineaarisemmaksi, ja jotta laitteisto kokonaisuudessaan olisi käyttäjäystävällisempi. Lisäksi, vaikka karakterisoitu versio on edellistä tehokkaampi valmistaa, suurien erien valmistus on edelleen hidasta.

Avainsanat: Mekanotransduktio, mekanobiologia, PDMS, venytys, kompressio, soluviljely, MDCK-epiteelisolut

PREFACE

The thesis was done in co-operation between the Micro and Nanosystems research group and the Cellular Biophysics research group from the faculty of Medicine and Health Technology in Tampere University. I want to thank my instructors Joose Kreutzer, who focused on the technical side, and Teemu Ihalainen, who's expertise is in mechanobiology and microscopy. I am grateful for the interesting topic, and for all the help and support during my thesis work. I also want to thank my examiners Soile Nymark and Pasi Kallio. An additional thanks goes to Pasi, PI of Micro and Nanosystems research group, for giving me the opportunity to do my thesis work in his group.

Most importantly, I am grateful to the whole work community that I got to be a part of. Thanks for all the help, the useful tips, the peer support, the occasionally overtime luch breaks and the good laughs. Without you this project would not have been as fun as it was.

In Tampere, Finland, on 14 April 2020

Heidi Peussa

CONTENTS

LIST OF FIGURES

LIST OF TABLES

LIST OF SYMBOLS AND ABBREVIATIONS

CAD	Computer-aided design
ECM	Extra cellular matrix
FAK	Focal adhesion kinase
FBS	Fetal bovine serum
FOV	Field of view
FWHM	Full width at half maximum
Hz	Hertz
jRGECO1a	Modified red intensiometric genetically encoded Ca2+-indicators for optical imaging 1a
kPa	Kilopascal
LINC	Linker of nucleoskeleton and cytoskeleton
LMW	Low molecular weight
Mbar	Millibar
MDCK	Madin-Darby canine kidney cell line
MEM	Minimum essential medium
PA	Phosphatidic acid
PBS	Phosphate-buffered saline
PDMS	Polydimethylsiloxane
PEG	poly (ethylene glycol)
Psi	pounds per square inch
RT	Room temperature
SDS	Sodium dodecyl sulfate
SUN	Sad1p and UNC-84 domain containing protein
UV	Ultra violet
$X_{comp,i}$	X-coordinate of the comparison particle at measurement point i
$X_{comp,-4\ mbar}$	X-coordinate of the comparison particle at the initial measurement point (-4 mbar)
$X_{ref,i}$	X-coordinate of the reference particle at measurement point i
$X_{ref,-4\ mbar}$	X-coordinate of the reference particle at the initial measurement point (-4 mbar)
$Y_{comp,i}$	Y-coordinate of the comparison particle at measurement point i
$Y_{comp,-4\ mbar}$	Y-coordinate of the comparison particle at the initial measurement point (-4 mbar)
$Y_{ref,i}$	Y-coordinate of the reference particle at measurement point i
$Y_{ref,-4\ mbar}$	Y-coordinate of the reference particle at the initial measurement point (-4 mbar)

1. INTRODUCTION

All cellular functions are controlled by signals which rise from the extracellular environment, other cells and from the cells their selves. These signals can be biochemical, electrical or, as this thesis concentrates on, mechanical. By supplying cells with signals that mimic their physiological environment, cell behavior can be controlled. Mechanical stimulation can be used, for example, to improve differentiation of cells in order to develop specific tissues, it can be used to simulate disease conditions, or to study mechanobiological pathways. (Birla, 2014)

This is why a vast amount of mechanobiological platforms exist, designed to stimulate cells with different kinds of mechanical forces such as shear stress, osmotic pressure, hydrostatic pressure, interstitial flow, compression and stretch. The actuation type of these mechanobiological platforms varies from device to device, including piezoelectric, electromagnetic, optical, electrothermal and pneumatic actuation. Likewise, the size of the devices ranges from single cell manipulation to the stimulation of large cell populations or arrays. Many of the devices are custom made by academic research groups, but also some commercial products exist (STREX Cell, CellScale and FlexCell®). Despite the vastness of the field, only a fraction of these devices enable similar stimulation as the device studied in this thesis (Huh *et al.*, 2010; Tse *et al.*, 2012; Huang and Nguyen, 2013; Pavesi *et al.*, 2015).

The device studied in this thesis was developed in the Micro and Nanosystems Research Group in Tampere University. It is actuated by negative pressure and made of polydimethylsiloxane (PDMS), a transparent and bioinert material. The device can be used to create horizontal static compression, static stretching or cyclic stretching on cells. Thanks to the transparency of PDMS, cells can be imaged directly on the device with an inverted microscope.

The development and further improvement of this pneumatic stretching and compression device has been ongoing for many years. Several versions of the device exist, and they have been used to study cardiomyocyte differentiation equiaxially (Kreutzer *et al.*, 2014) and uniaxially (Kreutzer *et al.*, 2019).

As a step towards productization, a new version of this device was developed. This new version is cast from a single mold, whereas the old version was compiled of multiple

parts. The aim of this thesis was to characterize the performance of this new version. Characterization was done by measuring the stretch reached by the device. Several devices were measured so that the similarity of different devices could be determined. Also, the actuation repeatability of a single device was determined.

Additionally, a commercial PDMS film was chosen to replace the previously used lab-made PDMS film. This further supports the potential productization of the device. The best performing commercial film was chosen by comparing the autofluorescence, optical resolution, biocompatibility and stretching of the candidates.

Finally, the device was tested in cell culture to verify its usability and to gain user experience. Two epithelial cell lines were used. One expresses occludin-emerald, a cell-cell junction protein fused to emerald fluorescent protein. This allows the imaging of epithelial cell boarders. The other cell line expresses genetic calcium indicator jRGECO1a, which enables the detection of calcium levels in living cells. Cells were grown on stretched devices, thus allowing the effect of compression to be studied once the strain was released.

The thesis consists of a theory part and an experimental part. The theory in Chapter 2 gives an introduction to the biology of mechanotransduction, followed by a literature review on similar stretching and compression devices, a description of the device studied in this thesis and an overview on PDMS. The materials and methods are described in Chapter 3, which is divided in five sections: manufacture of the device, choosing the best performing commercial PDMS film, optimizing the device, characterizing the performance of the optimized device and finally performing cell experiments on epithelial cells. Results are presented in Chapter 4, followed by discussion and the conclusions.

2. THEORY

The aim of the thesis was to characterize the new version of a cell stretching device developed in the Micro- and Nanosystems research group (faculty of Medicine and Health Technology in Tampere University), and to test it in cell culture. Although the device is originally intended for stretching, in this thesis a method was developed where the same device can be used to apply compression on cells. The characterization data and user experience can be used to further develop the device in the future.

This chapter first discusses the biology of mechanotransduction and the need for mechanical stimulation devices in cell culture. A short review of existing stretching and compression devices is given, followed by a description of the device studied in this thesis. As the device in entirely made of PDMS, the charasteristics of this material are also covered.

2.1 Mechanotransduction

Cells are in constant interaction with their environment, which is constituted of the extracellular matrix (ECM) and of adjacent cells. These interactions are crucial for differentiation, proliferation, cell viability, migration and other cell functions. A significant part of this interaction occurs through mechanical signaling that can be created by neighboring cells, external forces or the cell itself. In order for the mechanical stimulus to produce a response, cells convert it into biochemical activity. This phenomenon is called mechanotransduction. (Sun, Costell and Fässler, 2019)

Mechanotransduction allows cells to sense, for example, the stiffness and topography of their surroundings, and different mechanical forces. These forces include, among others, shear stress, hydrostatic and osmotic pressure, compression and stretching (Figure 1). Mechanical stimulation is especially evident in cells that sense touch and hearing, and in tissues such as muscle, cartilage and bone that are subjected strong mechanical forces, but it is present in all cell types. (Lim, Jang and Kim, 2018)

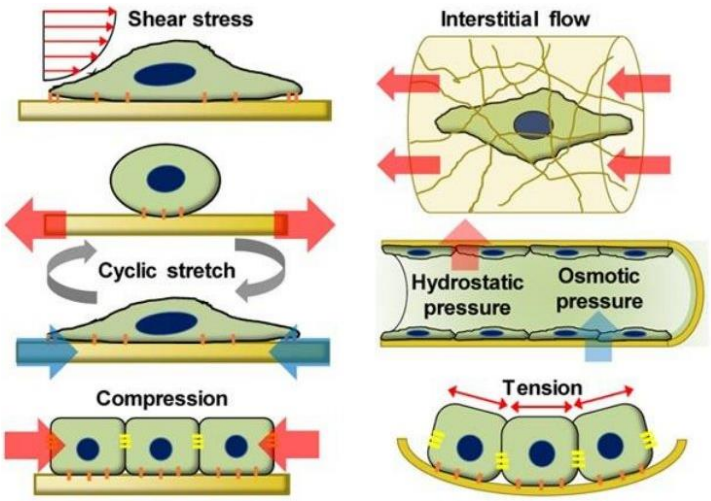

Figure 1. *Types of mechanical forces cells experience* (Uto *et al.*, 2017).

Cells sense mechanical stimulation at their cell membrane with cell-cell and cell-ECM junctions, mechanosensitive ion-channels and possibly with other membrane proteins. Cells then react to these signals both by directly modifying the cytoskeleton and cell junctions, and ultimately altering their gene expression. (Anishkin *et al.*, 2014; Lim, Jang and Kim, 2018; Martino *et al.*, 2018)

Focal adhesions are one of the main mechanosensing elements of cells, and definitely the most studied ones. Focal adhesions can be described as multiprotein bridges between the actin cytoskeleton and the ECM. They are dynamic multiprotein structures located on the cell membrane that undergo constant formation and disassembly according to stimulation. (Martino *et al.*, 2018)

A mature focal adhesion consists of the membrane spanning integrin dimer and a multimolecular plaque that connects the integrin to actin filaments. The main components are depicted in Figure 2. Integrin is linked to actin filaments through talin, which binds to the β-subunit of integrin. Force loading on talin leads to a stepwise revealing of cryptic binding sites for vinculin, another actin binding protein. Therefore, mechanical stimulation leads to recruitment of more actin fibers, and enforcement of the focal adhesion. This is referred to as talin-vinculin mechanosensitivity. (Martino *et al.*, 2018)

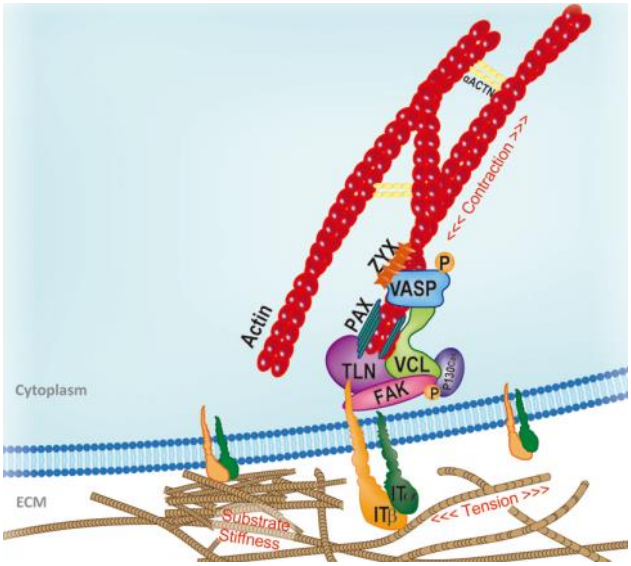

Figure 2. *The structure of a focal adhesion. αACTN = α actinin, FAK = focal adhesion kinase, IT = integrin, PAX = paxillin, TLN = talin, VASP = vasodilator-stimulated phosphoprotein, VCL = vinculin and ZYX = zyxin (Martino et al., 2018).*

In addition to regulating the actin cytoskeleton, mechanical stimulation also activates biochemical pathways. One key player in this activation is focal adhesion kinase (FAK). Depending on the mechanical cues FAK receives, different phosphorylation sites can be activated, which in turn activate numerous signaling pathways. These pathways control for example cell migration by decreasing or increasing actin polymerization, tension created by the cytoskeleton, as well as the assembly or disassembly of entire focal adhesions. Additionally, FAK induced signaling travels to the nucleus, where it affects protein expression, apoptosis, proliferation and differentiation. (Tomakidi *et al.*, 2014)

As calcium is a multipurpose signaling molecule, it plays an important role also in mechanotransduction. Mechanosensitive ion-channels and the primary cilia respond to mechanical stimuli and trigger the release of calcium to the cytosol. There, calcium regulates numerous pathways and receptors in a spatiotemporal way and has therefore an effect on for example gene expression, neurotransmitter release, muscle contraction, metabolism, proliferation, fertility and migration. Calcium also affects the players of mechanotransduction directly. It regulates α-actin structure and dynamics, and actomyosin contraction in both muscle- and non-muscle cells. It also interacts with focal adhesions through a transmembrane protein called polycystin-1. (Jones and Nauli, 2012; Benavides Damm and Egli, 2014)

Finally, the nucleus has its own mechanosensitive system that reacts to mechanical forces in the cytoskeleton. Actin fibers, intermediate filaments and microtubules are connected to the nucleus via the linker of nucleoskeleton and cytoskeleton (LINC) complexes. The main components of LINCs are SUN (Sad1p and UNC-84 domain containing

protein) and nesprin proteins. They form a junction that passes the inner and outer nuclear membranes and connect the cytoskeleton to the nuclear lamina and chromatin. (Martino *et al.*, 2018)

As LINCs are connected to the nuclear lamina, it is hypothesized that they have a role in regulating how tightly DNA is packed. Euchromatin is a lightly packed form of DNA where genes are active, whereas heterochromatin is more dense and therefore less accessible. According to this theory, mechanical signals from the cytoskeleton would have a role in regulating this chromatin packing, and therefore gene expression. (Alam et al., 2016; Martino et al., 2018)

Mechanical signals clearly have a vast impact on the behavior of cells and tissues. Compression has a key role in many developmental and tissue morphogenesis processes, for example in the formation of the optic cup in the eye (Sidhaye and Norden, 2017) and the gut villi (Shyer *et al.*, 2013) during embryonic development. Compression also controls many functions of adult tissues, such as epithelial movements (Marinari *et al.*, 2012; Wyatt *et al.*, 2020) and cartilage development (Sophia Fox, Bedi and Rodeo, 2009; Anderson and Johnstone, 2017; Chen, Kuo and Chen, 2018; Lee *et al.*, 2018; Occhetta *et al.*, 2019). Finally, compression can be a cause or effect of many diseases such as cancer (Tse *et al.*, 2012; Boyle *et al.*, 2018) and asthma (Tschumperlin *et al.*, 2002; Li *et al.*, 2012; Lan *et al.*, 2018). Therefore, compression has significant roles in normal development and function, but also in disease. It can be utilized in *in vitro* models of diseases, and to improve the differentiation and development of tissues.

2.2 Mechanical stimulation platforms

In vitro models are a powerful tool for studying diseases, testing medicines and researching basic cellular functions such as mechanotransduction. *In vitro* culture can also be used to produce tissue and possibly organs for transplantation into patients. (Birla, 2014)

In order to culture cells and to mature them into tissues or organs *in vitro,* cells require an environment that mimics their physiological conditions. These conditions consist of the biochemical and electrical signals, as well as the mechanical stimulation described in Section 2.1. Substrate toughness and topography can be adjusted by choosing correct materials and by manipulating the surface of the substrate, but in order to stimulate cells with mechanical forces, special dynamic platforms are required. (Birla, 2014) As different cell and tissue types require different stimuli, numerous mechanical stimulation platforms have been developed. The following section will concentrate on devices enabling both stretching and compression.

2.2.1 Devices for compressing and stretching cell cultures

As compression and stretching are opposing forces, many devices are applicable for both. However, a majority of devices are designed with the focus on stretching, and are therefore referred to as stretching devices. Nevertheless, similarly as the device used in this thesis, the function of the device is determined only by the status of the stretching device on the moment of cell seeding. If cells are seeded on a relaxed matrix, the device will induce stretching, whereas if cells are seeded on a stretched matrix, relaxation will produce compression. In this section, the focus will be on pneumatic devices usable for stretching and compression. For comparison, some devices designed solely for compression will first be presented.

Lee *et al.* (2018) developed a pneumatic compression device for 3D culture. Positive pressure acts as a piston that compresses the alginate gel where cells are growing (Figure 3). This can be used to apply 14 kPa 1 Hz cyclic compression to chondrocytes. (Lee *et al.*, 2018) The same idea is utilized in a commercial compression device called BioPress™ by FlexCell® (Flexcell® International Corporation, 2020). A similar setup, but much simplified, was used by Tschumperlin *et al.*, but pressurized air was applied from above and cells were grown in 2D (Tschumperlin *et al.*, 2002). Also other publications utilized pistons to create compression, but the piston is often actuated with weights thus allowing only static compression (Tse *et al.*, 2012).

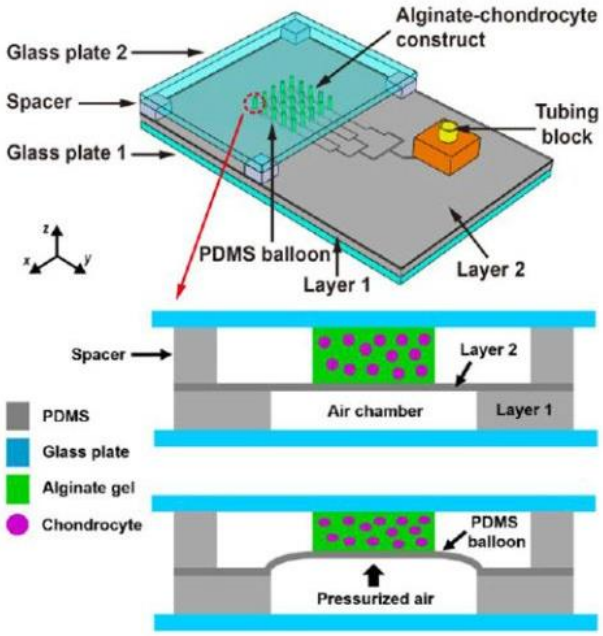

Figure 3. *Pneumatic compression device for 3D cell culture. Positive pressure expands the air chamber and compresses the hydrogel in which cells are cultured.* (Lee *et al.*, 2018)

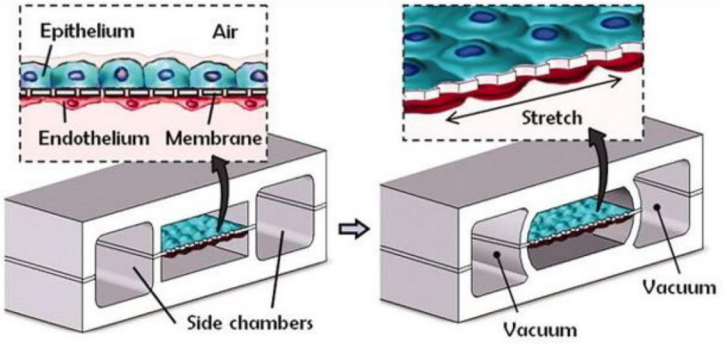

Figure 4. *Pneumatic uniaxial stretching/compression device that allows co-culture of two different cells on opposing sides of a semipermeable PDMS film* (Huh *et al.*, 2010).

Huh *et al*. (2010) developed a lung-on-a-chip that utilizes cyclic negative pressure to simulate the stretching caused by breathing (Figure 4). The device consists of two vacuum chambers on both sides of a cell culture chamber. Negative pressure applied to the side chambers expands the cell culture chamber uniaxially perpendicular to the direction of media flow. Cells are grown on a thin film that is set in the middle of the cell culture chamber to achieve optimal geometry for stretching. The film is semipermeable which allows the co-culture of epithelium and endothelium. (Huh *et al.*, 2010)

Pavesi *et al*. (2015) used a similar approach as Huh *et al.*, but without the co-culture possibility (Figure 5). Instead, they doped the bulk PDMS with carbon nanotubes to make it conductive. This allowed cells to be electrically stimulated in addition to the stretching and media flow.

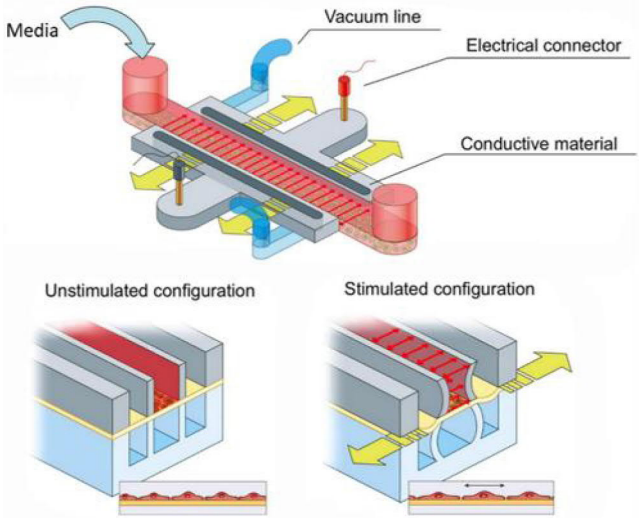

Figure 5. *Pneumatic stretching/compression device that allows uniaxial deformation. The bulk of the device is doped with carbon nanotubes for conductivity. The red chamber contains the cells and the ones marked with blue are the pneumatic chambers. Negative pressure applied to the lateral pneumatic chambers causes the central chamber to stretch. This stretches also the the film on which cells grow.* (Pavesi *et al.*, 2015)

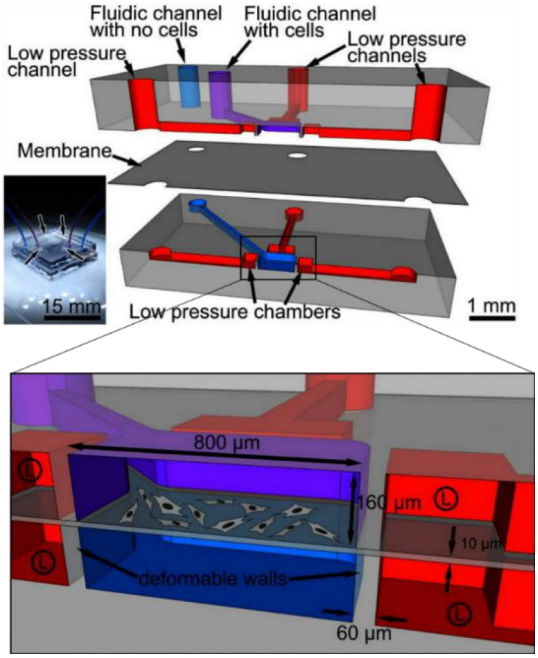

Figure 6. *Stretching/compression device that allows biaxial stretching (Tremblay et al., 2014).*

The same principle was used also by Huang and Nguyen (2013) and Tremblay et *al.* (2014) Tremblay's team added vacuum chambers on the perpendicular side. This allows the possibility of stretching cells in both x- and y-directions in 2D (Figure 6).

Also a commercial pneumatic cell stretching system exists. Flexcell®'s FX-6000™ Tension System comes in a 6 well plate format and has its own pressure controller system and software (Figure 7a). The stretching is based on negative pressure that pulls down and stretches the membrane on which cells are cultured (Figure 7b). Depending on the culture plate type, uniaxial or equiaxial stretch can be applied. The maximum strain varies from 8 % to 33 % depending on the culture plate type. (Flexcell® International Corporation, 2018)

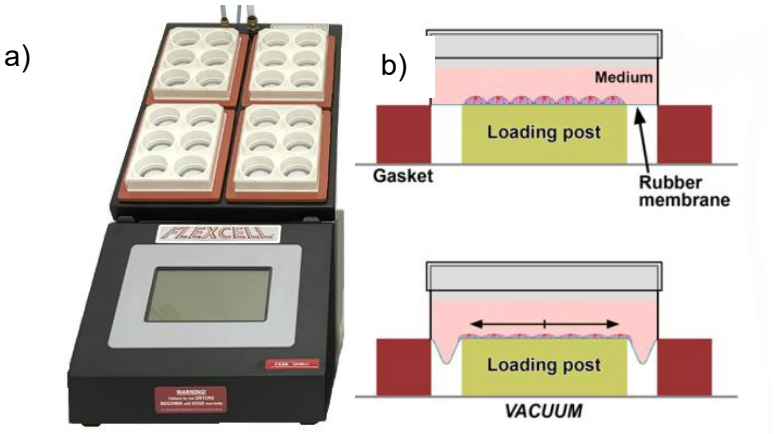

Figure 7. *A) Flexcell® FX-6000 Tension System device and b) the principle of funciton* (Flexcell® International Corporation, 2018).

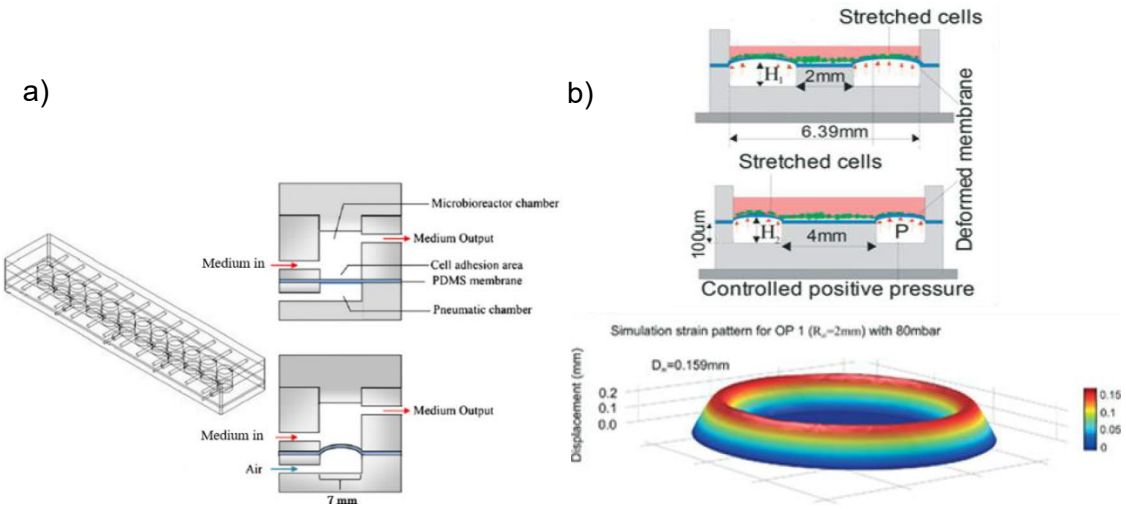

Figure 8. *A) Array-type pneumatic stretching device actuated by positive pressure. The PDMS film expands and becomes convex.* (Wu *et al.*, 2011) *B) Stretching device where stretching occurs as a ring for study of circumferencial alignment. The center remains unstimulated*(Kamble *et al.*, 2018)

In addition to the presented pneumatic devices, numerous others exist. However, in many of them the film on which cells are grown is expanded in a convex manner as shown in Figure 8 (Wu *et al.*, 2011; Heo *et al.*, 2013; Kamble *et al.*, 2018). These systems are usable only for stretching because cells have difficulty in attaching evenly on a substrate that is not flat. Furthermore, also multiple other actuation types can be utilized for stretching or compression devices. These include shape memory alloys, piezoelectric systems, electric motors or manual micromanipulated systems (Iwadate and Yumura, 2009; Deguchi *et al.*, 2015; Schürmann *et al.*, 2016; *STREX Cell Strain Instrument User Manual*, 2020; Wyatt *et al.*, 2020). Likewise as in pneumatic systems, these systems usually rely on an elastic film, often made of PDMS.

Pneumatic actuation systems have several advantages over the other mentioned actuation types. They are not susceptible to erosion like electromagnetic motors, they do not require lubrication that increases the risk of contamination, they do not create heat, and the electric components do not need to be in close proximity to cell culture media. (Kamble *et al.*, 2016) This makes them safer and more long lasting in use.

2.2.2 The pneumatic stretching/compression device used in this study

The stretching device used in this study was developed in the Micro and Nanosystems Research group in Tampere University. The device consists of a cell culture chamber in the center and of a vacuum chamber surrounding it (Figure 9). The bottom of the device is covered with PDMS film. This PDMS film forms the bottom of the cell culture chamber on which cells are cultured, and seals the vacuum chamber.

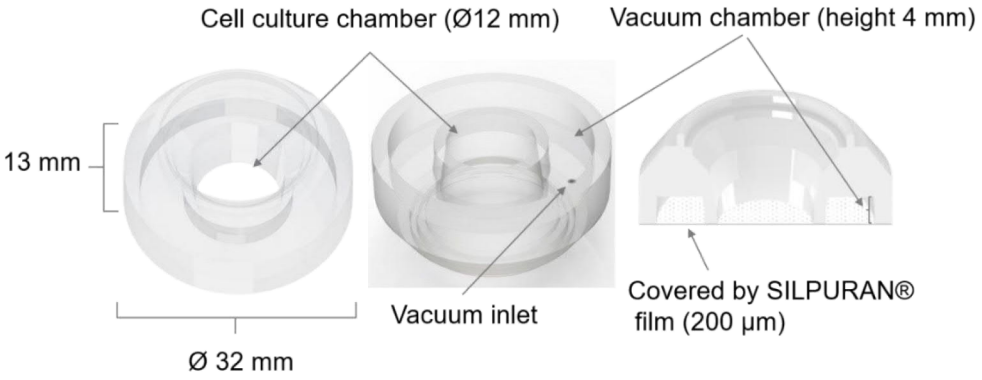

Figure 9. *The current version of the stretching device from above, below and a cross-section.*

The stretching is achieved by applying different amounts of negative pressure (up to -400 mbar) to the vacuum chamber via a small inlet in the roof of the vacuum chamber. Negative pressure in this chamber deforms the PDMS film and the wall of the cell culture chamber symmetrically (Figure 10). This creates an equiaxial stretch to the film in the cell culture chamber. The structure was designed so that minimal fluid shear stress would be created. This is achieved by limiting the vertical movement of the film. (Kreutzer *et al.*, 2014, 2019)

As the actuator is not in direct interaction with the cell culture chamber, the risk of contamination is decreased. The device is controlled with an adjustable pressure device. By changing the waveform, amplitude and frequency of pressure, the device can be used in a cyclic or static stretching mode. (Kreutzer *et al.*, 2014). Additionally, the cells can easily be imaged with an inverted microscope through the PDMS film directly in the device. This is a significant advantage to devices described in Section 2.2.1., where the structure of the device often forms an obstacle between the microscope objective and cells. Also, when imaging from below, the objective does not create a contamination risk to the imaged cells, as it does not have to be in contact with the culture medium.

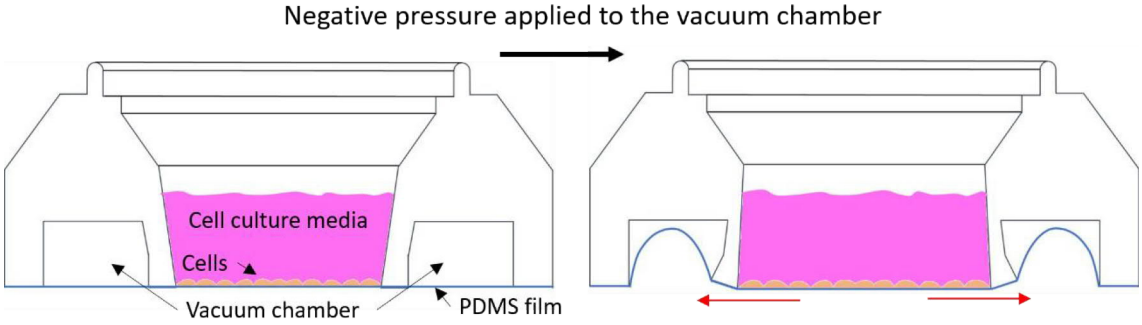

Figure 10. *The stretching mechanism is based on applying negative pressure to the vacuum chamber. This deforms the film and the inner wall and expands the cell culture chamber equiaxially.*

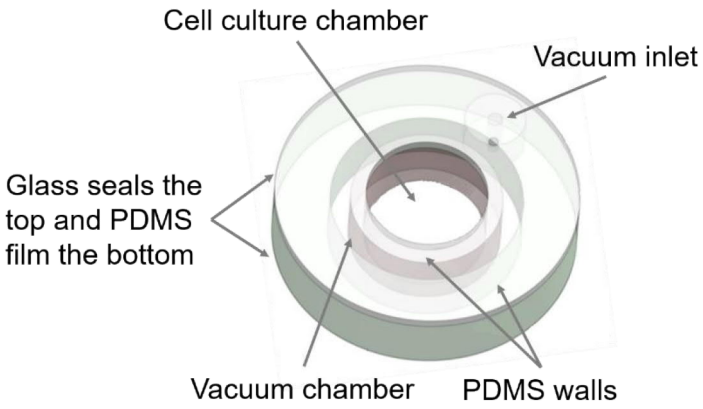

Figure 11. *Previous version of the stretching device* (Kreutzer *et al.*, 2019).

The previous version of the stretching device was compiled of a separate outer wall, inner wall, glass lid, vacuum inlet and PDMS film in the bottom (Figure 11). Each part had to be separately manufactured by hand and then assembled. The PDMS parts were punched from a PDMS disk, and holes had to be drilled to the glass slips. Pieces were assembled together and attached to the PDMS film by oxygen plasma treatment. This was laborious and time consuming and especially the symmetry was challenging to achieve. The maximum stretch reached with this device was 10 % (Kreutzer *et al.*, 2014).

The current version of the device is a step toward better repeatability and faster manufacturing of the stretching device. The procedure will be described in Section 3.1. The advantage of this version is that the entire body of the device can be casted from a single mold. Only the inlet hole has to be stamped and the PDMS film plasma bonded to the bottom. Nevertheless, the new version was designed so that that it would function similarly as the previous device. Therefore, it has the same basic structure and working principle, but the shape is slightly different.

2.2.3 Polydimethylsiloxane

PDMS is a silicone elastomer that is commonly used in stretching devices. It is a relatively cheap material that can be easily processed by soft lithography and replica molding. (Jo *et al.*, 2000; Sui *et al.*, 2006; Slaughter and Stevens, 2014) It is chemically inert, thermally stable in biological temperatures (-70−250 °C), transparent and non-fluorescent (Ghannam and Esmail, 1998). It is also biocompatible, has low toxicity to cells and is permeable to gases. It can be sterilized with steam autoclavation, ultra violet (UV) light or with 70 % ethanol without significantly altering its properties. (Mata, Fleischman and Roy, 2005; Eddington, Puccinelli and Beebe, 2006)

The gas permeability of PDMS can be considered an advantage or disadvantage according to application. It can be utilized for example to control the O_2 and CO_2 concentrations in a cell culture, but on the down side it enables media to evaporate, which can be detrimental to cells or cause bubbles in microfluidic systems. PDMS has also been shown to leach un-crosslinked oligomers into media, and to absorb small molecules such as growth factors from the media. Nevertheless, PDMS is a widely used material in cell culture that does not have many competitors. (Sackmann, Fulton and Beebe, 2014)

PDMS has a siloxane backbone with methyl-groups as substituents as illustrated in Figure 12. The flexibility of the siloxane backbone and long chain lengths create the elasticity of PDMS. Without crosslinking PDMS is held together only by weak intermolacular dispersion foces between methyl groups. These forces allow chains to move past each other making PDMS viscoelastic. However, PDMS can be crosslinked to stabilize its structure. (Owen, 2001)

Four different types of crosslinking reactions exist for PDMS: peroxide-induced free radical reactions, condensation reactions, platinum utilizing hydrosilylation addition reactions, and the hydridosilane/silanol reaction. (Owen, 2001) Out of these the peroxide-induced reactions and platinum addition reactions are the most common (Heiner, Stenberg and Persson, 2003).

The PDMS used in this thesis, SYLGARD™ 184, (Dow Corning Corporation) utilizes the platinum addition reaction. The base consists of dimethylsiloxane oligomers with vinyl-terminated end groups, a platinum catalyst, and silica filler. The curing agent contains the cross-linking agent (dimethylmethylhydrogen siloxane), and an inhibitor (tetramethyl tetravinyl cyclotetrasiloxane). The vinyl and silicon hydride groups undergo a hydrosilylation reaction and form Si-C bonds thus creating crosslinks (Figure 13). The base and the curing agent are recommended to be mixed in a 10:1 ratio. (Lee *et al.*, 2004) However, mechanical properties of PDMS can be modified by adjusting the base:curing agent ratio. For example, increasing the curing agent concentration from 10 % to 14.3 % increased the tensile strength from 7.6 MPa to 10.8 MPa. (Mata, Fleischman and Roy, 2005)

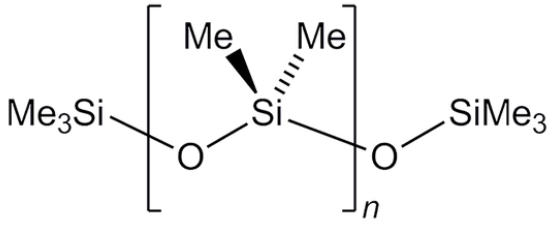

Figure 12. *Repeating unit of PDMS* (American Chemical Society, 2014).

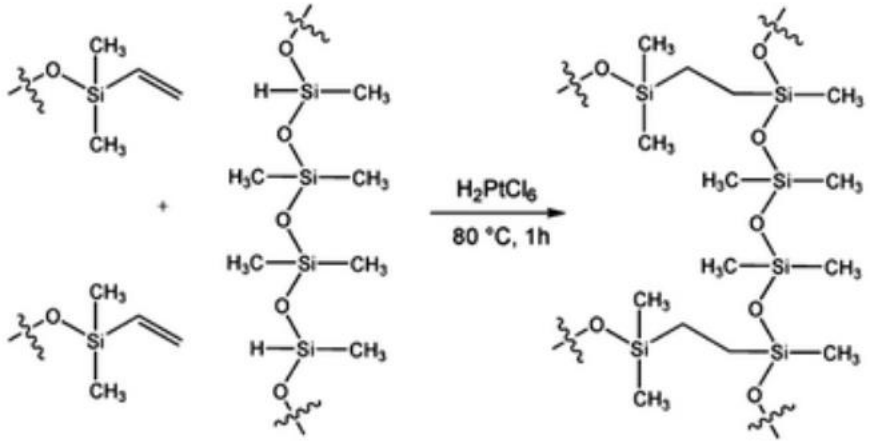

Figure 13. *The platinum based hydrosilylation reaction of PDMS* (Wisser *et al.*, 2015).

Due to its non-polar chemical structure PDMS is hydrophobic. This can be a problem in microfluidics and in cell culture applications as it can disturb cell adhesion, decrease the wettability of surfaces, make structures prone to trap air bubbles and hamper the filling of microfluidic channels. (Eddington, Puccinelli and Beebe, 2006; Lange *et al.*, 2009) Common ways to increase the hydrophilicity of PDMS include oxygen plasma treatment, ultraviolet (UV) treatment and different hydrophilizing coatings. (Chen and Lahann, 2005; Hemmilä *et al.*, 2012)

UV-treatment causes the molecules on the surface of the PDMS to undergo chain scission. This creates radicals that recombine and form a network with hydrophilic properties. (Efimenko, Wallace and Genzer, 2002) Different molecules such as proteins, poly (ethylene glycol) (PEG), gold nanoparticles, TiO_2 and ionic surfactants such as sodium dodecyl sulfate (SDS) and phosphatidic acid (PA) are commonly used to hydrophilize PDMS. Methods to achieve coatings include chemical vapour deposition, sputtering, layer by layer deposition, silanization, dynamic coating and adsorption. (Wang, Xu and Chen, 2006; Hemmilä *et al.*, 2012; Slaughter and Stevens, 2014)

Oxygen plasma treatment replaces methyl (Si-CH_3) groups with hydrophilic silanol (Si-OH) groups on the surface of the PDMS. (McDonald and Whitesides, 2002) The same oxygen plasma treatment can be used to covalently bond PDMS for example to other PDMS-surfaces or to glass. Both surfaces that are to be bonded are treated with oxygen plasma that creates silanol groups on the surfaces. When the surfaces are pressed against each other the silanol groups condense into irreversible Si-O-Si bonds. Normally, these seals can withstand 2–3.5 bar of air pressure. (Bhattacharya *et al.*, 2005)

Unfortunately, some un-crosslinked chains and residual curing agent always remain in the bulk of cured PDMS. These so called low molecular weight (LMW) chains diffuse to

the surface from the bulk replacing the silanol groups with the original methyl groups. Therefore, the hydrophilicity gained with oxygen plasma treatment disappears in less than an hour. For the same reason bonding must be done quickly after the treatment. (Eddington, Puccinelli and Beebe, 2006)

One way to prevent losing the hydrophilicity gained by oxygen plasma treatment is to functionalize the freshly treated surface. The surface is first silanized, after which functional groups such as poly(ethylene glycol) or proteins can be introduced. This adds desired properties to the surface as well as increases the lifetime of the hydrophilicity.(Sui *et al.*, 2006; Hemmilä *et al.*, 2012) Other option is to diminish the amount of LMW chains. Heating while curing is commonly used to increase evaporation of excess curing agent and to enhance the crosslinking reaction. After this, cured PDMS can be soaked in solvents that create swelling and allow LMW chains to diffuse out, or it can be thermally aged by keeping the cured PDMS in elevated temperatures for a long period of time (e.g. 100 °C for 2–14 days). (Eddington, Puccinelli and Beebe, 2006; Lange *et al.*, 2009)

In addition to removing LMW chains, curing conditions can also be used to modify mechanical properties of PDMS. Temperature and curing time affect for example the Young's modulus, ultimate tensile strength, compressive modulus, ultimate compressive strength and hardness. (Johnston *et al.*, 2014)

3. MATERIALS AND METHODS

This chapter first covers the manufacturing of the stretching devices, followed by a description of experimental procedures and the data analyses used in this thesis. These are divided into four sections: choosing the optimal PDMS film, optimizing the device, characterizing the performance of the device and finally the cell experiments.

3.1 Manufacture of the cell stretching device

The mold was designed with compurer-aided design (CAD) with SOLIDWORKS® 2018. They were 3D-printed at Keijom Oy by using polyjet technology, or machined from polyoxymethylene (POM) at Tampere University workshop. The mold was compiled according to Figure 14 by placing the insert into the bottom part and the lid on top of this compiled mold. The insert is separate in order to eaze the removal of the device after curing: the device is easily removed from the mold by pushing the insert form the bottom of the mold. The lid is an important part of the mold as it creates the base of the device including the vacuum chambers and the surfaces that are later oxygen plasma bonded to the PDMS film. The flow out hole in the lid allows excess PDMS and possible air bubbles to escape from the mold during curing. During castring the flow out hole was covered by placing tape on the back of the lid. This was done to avoid PDMS from flowing out before assembling the mold.

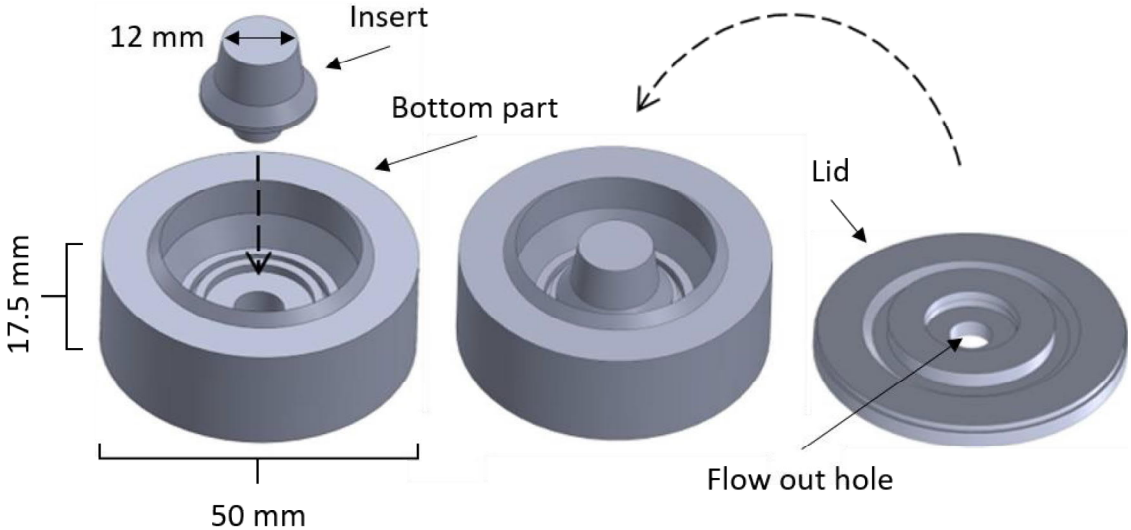

Figure 14. *Parts of the mold. Left: assembly of the bottom mold and insert, center: assembled bottom mold and right: lid. The device is formed upside down in the mold: the insert forms the cell culture chamber, and the lid forms the vacuum chamber and the surfaces that are bonded to the PDMS film.*

The base elastomer (part A) and curing agent (part B) from SYLGARD™ 184 Elastomer Kit (Dow Corning Corporation) were carefully mixed in a ratio of 10 to 1. Vacuum was used to remove bubbles from the mixture before carefully pouring the PDMS into the assembled bottom mold and onto the lid. The PDMS was poured slowly and so that the stream was kept as short as possible to avoid concealing air and creating bubbles. The molds were filled to the brim after which they were again placed into vacuum to remove formed bubbles. Finally, the lid was placed on top of the compiled bottom molds and the pieces of tape were removed to allow excess PDMS and air to escape through the flow out hole. These filled molds were placed into an oven and weights were placed on top to press the lid tightly against the bottom mold. The temperature was set to 60 °C for 10 h.

After curing, the lids were first removed with the help of a scalpel and the devices were carefully pushed out of the molds. Residue PDMS was removed from the inner walls of the cell culture well with a punch and from the outer edges of the device with a scalpel. A G18 injection needle was sharpened into a punch, and used to make a ~0.9 mm Ø hole to the ceiling of the vacuum chamber.

Although a commercial film was chosen for the actual devices, the previously used lab-made PDMS film was also needed for comparison. To make this film, PDMS was prepared as described above, but after degassing the PDMS was poured on a Ø 140 mm plastic plate. The plate was placed in a spinner and spun at 700 rpm for 30 s. This creates a 120 µm thick film. The created film was cured in 60 °C for 10 h.

Prior to bonding, the devices were washed with detergent to remove grease, rinsed with isopropanol and Milli-Q water and finally thoroughly dried. Extra attention was payed to the surfaces that were going to be bonded, because the bonding is easily hampered with grease, dust particles or uneven surfaces.

A Pico Low-pressure plasma system from Diener electronic GmbH + Co. KG was used for plasma treatments. The plasma chamber was filled with oxygen to a pressure of 30 mbar and the plasma was ignited for 15 seconds with a power of 30 W.

The devices with the stabilator rings (see Section 3.3) in place and a sufficient piece of PDMS film were loaded into the plasma device with bondable surfaces facing upwards. After the oxygen plasma bonding program had finished, the devices were carefully lifted and pressed on the film so that the plasma treated surfaces of the device were against the plasma treated film. The device was held gently to prevent deformation while bonding. The freshly bonded parts were left aside for a while to ensure bonding. Finally, the outer walls of the devices were trimmed from extra PDMS film with a scalpel.

Figure 15. *Photograph of a finished device from above and below with the pressure inlet inserted shown on the left, and corresponding CAD-designs on the right.*

After casting, all parts of the molds were first cleaned from PDMS residue, then washed with detergent, rinsed with isopropanol and milli-Q water and finally thoroughly dried with pressurized air.

The finished devices were inspected by inserting negative pressure and positive pressure to the vacuum chamber with a syringe and visually verifying that the vacuum chamber did not leak. With positive pressure inserted, the device could also be inserted in water and inspected for bubble formations. Images of a finished device and of the corresponding CAD-designs are shown in Figure 15.

3.2 Choosing the optimal film

ELASTOSIL® and SILPURAN® PDMS films from Wacker Chemie AG in the thicknesses of 20 µm, 50 µm, 100 µm and 200 µm, and Gloss PDMS film from Specialty Manufacturing inc. in the thicknesses of 125 µm and 254 µm were studied. In addition to the commercial PDMS films, the lab-made 120 µm thick SYLGARD™ 184 PDMS film was studied as comparison.

3.2.1 Optical performance of the films

The optical performance of the films at the microscope were determined by imaging sub-resolution fluorescent beads. The resulting images were analyzed by measuring the full width half maximum value (FWHM) of the fluorescence distribution of the bead. FWHM is a practical method used to determine optical resolution from the intensity profile of the signal. As the name states, the width of the peak at half maximum intensity is calculated (Figure 16). For improved sensitivity the intensity profile is usually fitted to Gaussian distribution before calculating the FWHM. The smaller the FWHM is, the better the resolution and sharper the image. (Demmerle *et al.*, 2015)

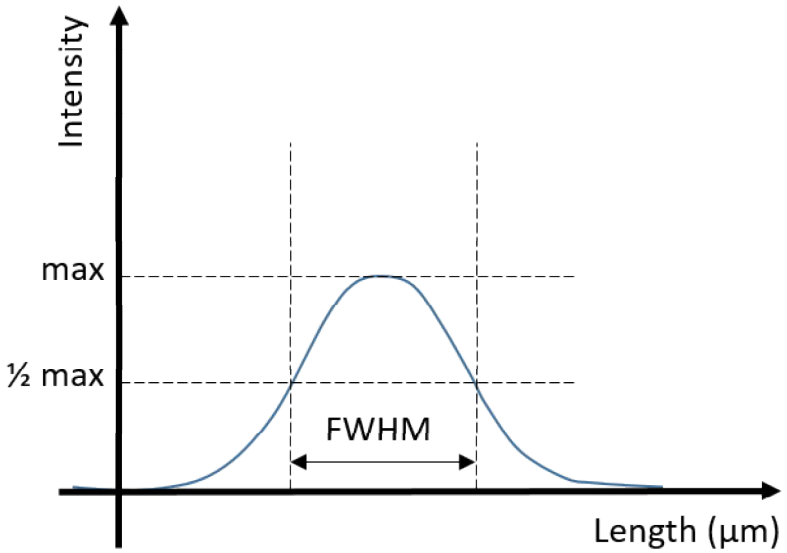

Figure 16. *The FWHM is the width of the peak at half maximum intensity.*

The measurements were done with a Zeiss LSM780 confocal microscope and 0.2 µm Ø fluorescent FluoSpheres™ beads. The opimal excitation wavelength of the beads is 580 nm and emission wavelength 605 nm.

The films that were tested were bonded either to stretching devices or simply to PDMS rings in order to have a media chamber, and to keep films unwrinkled. The beads were diluted 1:50 in MilliQ-water and ~200 µl this solution was pipetted onto the films so that the entire surface was covered. The beads were incubated in room temperature (RT) for ~1 h after which the wells were gently emptied and rinsed with MilliQ-water. After this, the films were allowed to dry.

The excitation wavelength was set to 561 nm and the emission to 615 nm. A 40x/1.20 water immersion objective (C-Apochromat 40x/1.20 W Korr M27) was used, and MilliQ-water was pipetted also into to the media chambers on top of the films to resemble media. Slices were taken every ~200 nm so that the entire bead was covered in z-direction. The total depth of imaging varied a lot. With thinner films more slices were needed, as the film was not necessarily straight, and therefore the range of focus had to be wider to fit all beads. The number of slices varied from 26 (with glass) to 155 (with a PDMS film).

For each studied film, a z-stack was taken from two spots of the film. The spots were chosen from different parts of the film so that they had numerous beads in the field of view (FOV) without the beads being in clumps. The laser power (%) and the detector master gain were adjusted so that the beads were not overexposed but as bright as possible. Marienfeld High Precision cover glass (thickness 170 µm) was used as a control.

Images were analyzed with ImageJ and Matlab. ImageJ was used to create orthogonal views of beads and to plot the intensity profile of each bead. As the data analysis was laborious, the z-direction intensity profiles of five different beads per stack were collected into Excel instead of analyzing all beads from the FOV. The data was normalized with the maximum intensity value of each bead, and the average of these normalized z-direction intensity profiles was calculated. Matlab was used to fit this profile into Gaussian distribution and to calculate the FWHM value. As there were two stacks per each film, two FWHM values were gained for each film. The control cover glass was imaged and analyzed similarly as the films.

3.2.2 Autofluorescence of the films

Autofluorescence scans were done with FLS-1000 (Edinburgh Instruments, UK) spectrofluorometer, where an excitation-emission scan could be programmed. The excitation wavelengths were scanned in 10 nm steps starting from 350 nm up to 650 nm. This is the spectrum usually used in fluorescent dyes. For each excitation wavelength, the emission was scanned in 2 nm steps with a 20 nm offset from the excitation wavelength until 850 nm.

A sample from ELASTOSIL®, SILPURAN®, Gloss and lab-made PDMS film were analyzed. Also, the PDMS film from a commercial Flexcell® device, Marienfeld High Precision cover glass, Menzel-Gläser cover glass, Menzel-Gläser microscope slide, and several polystyrene petri dish plastics were measured. Flexcell® was measured as a positive control, as it had shown disturbing background in the past when used under a fluorescent microscope. The glasses and petri dish plastics were measured for comparison, as cells are commonly imaged on these surfaces.

3.2.3 Biocompatibility of the films

In order to compare the suitability of different PDMS films to cell culture, stretching devices with different films were prepared. ELASTOSIL®, SILPURAN®, Gloss and lab-made PDMS film were studied and Marienfeld High Precision cover glass was used as a positive control. The samples were coated with collagen I. Cells were grown on these coated samples and their morphology was studied. The coating, cell seeding, incubation and imaging was done similarly as for the controls in Section 3.5. Occludin-emerald expressing Madin-Darby Canine Kidney (MDCK) epithelial cells were used in the studies. The fluorescence rising from the occludin-emerald allowed the detection of cell-cell junctions. As epithelial cells adhere tightly to adjacent cells, occuldin-emerald shows the boarders of cells

3.3 Optimization of the device

In initial experiments, the PDMS films were seen to get in contact with the walls of the vacuum chamber, thus preventing the film from further stretching. This was seen as a saturation of stretching, and as the maximum stretching being less than the 10 % reached with the previous version of the device. The approaches used included i) an expansion of the vacuum chamber to prevent the film from touching the roof of the vacuum chamber, and ii) a stabilator ring which was intended to prevent the outer walls of the device from caving in when the pressure decreases. Both modifications were aimed to improve the performance of the device

Three different versions of the device were tested for each film. One device had a 3 mm high vacuum chamber, the second a 3 mm vacuum chamber with a stabilator ring and the third a 4 mm vacuum chamber with a stabilator ring (Figure 17). Stretching was determined with the same procedure as will be described in Section 3.4.

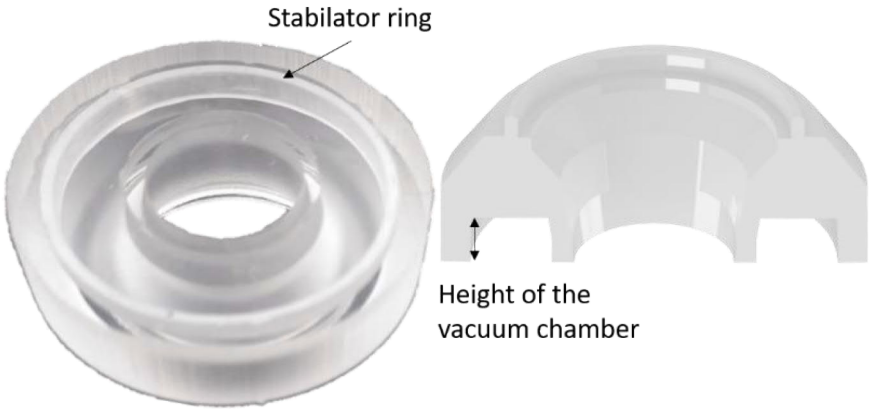

Figure 17. *The stabilator ring (shown in the device on the left) was placed inside the vacuum chamber to support the outer wall of the vacuum chamber. The height of the vacuum chamber is depicted on the right.*

3.4 Characterization of stretching

In order to visualize stretching, 1 µm Ø Dragon Green fluorescent polystyrene microbeads (Bangs Laboratories, Inc.) were adsorbed to the PDMS film of the cell culture chamber in the studied devices. A 1:50 dilution of the beads was prepared in MilliQ water and pipetted on the devices. They were incubated in RT for approximately 1 h, then gently rinsed with MilliQ water and dried.

Imaging was done with Zeiss Axio Scope with 10x/0.25 magnification (A-Plan 10x/0.25 Ph 1). Excitation was done with 450–490 nm light and emission was gathered from 500–550 nm range. The first image was taken at -4 mbar pressure. This small negative pressure was applied instead of 0 mbar in order to straighten the film. After this, the pressure

was decreased in 75 mbar steps until -350 mbar. The pressure was controlled with a custom-made device that utilizes a microcontroller based electro-pneumatic transducer (Kreutzer *et al.*, 2014).

During imaging, a chosen bead was centralized in each FOV throughout the image sequence (Figure 18a). This prevents beads from escaping the FOV, and allows more trajectories to be analyzed. In order to determine how much z-displacement occurs when the device is stretched, the z-coordinate from the microscope was documented at each measurement point. The centralizing of the bead as well as image focusing was done manually.

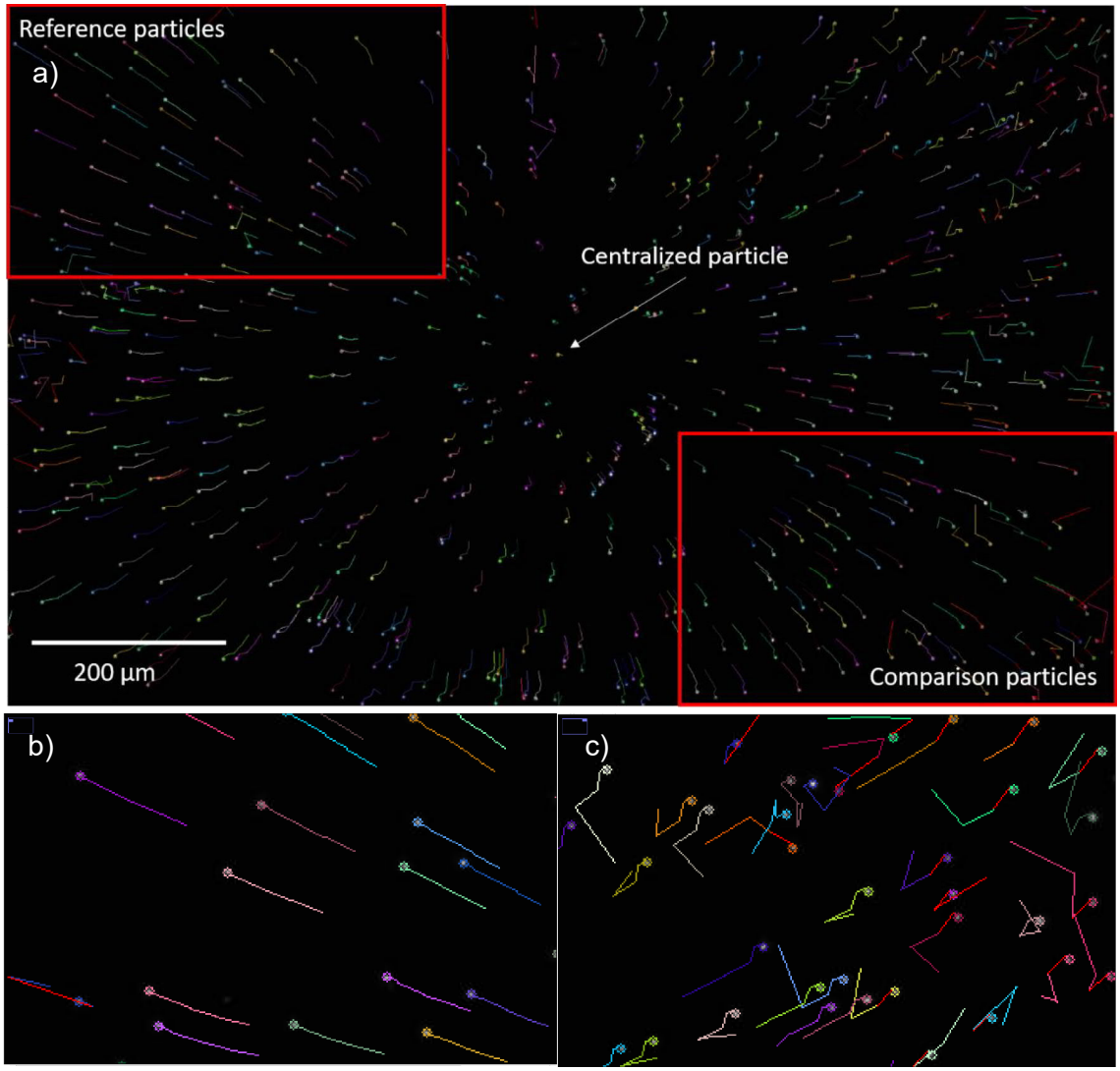

Figure 18. *A) The trajectories for all recognized particles. Reference particles and comparison particles were chosen from opposing corners to maximize difference in x- and y-coordinates. B) Example of successful tracking and c) example of unsuccessful tracking.*

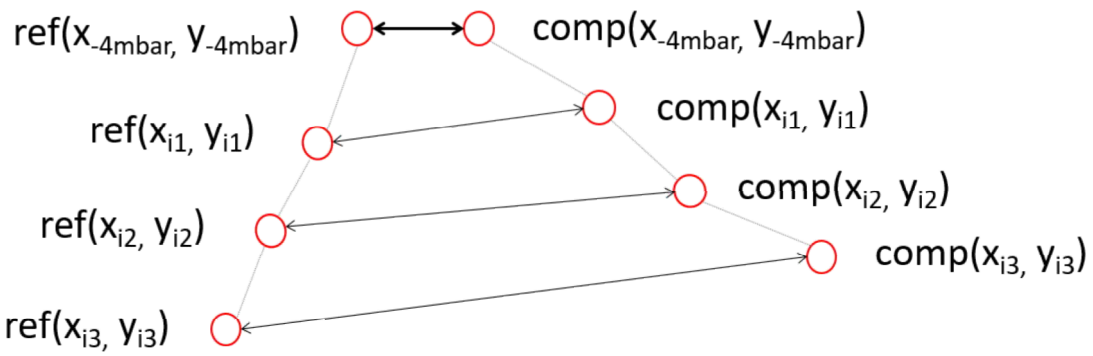

Figure 19. *Stretching was determined by comparing the distance between a reference particle and comparison particle at measurement point to their initial distance at -4 mbar (thicker arrow).*

Particle Tracker 2D/3D plugin (Mosaic) was used to track the trajectories of the beads in the image sequences. The diameter of the beads was set to three pixels and other parameters were adjusted so that as many beads as possible were detected without false readings from the background.

With Particle Tracker, all trajectories can be visualized, and the x- and y-coordinates for a chosen trajectory can be displayed. For each analysis, ten trajectories were chosen. Only trajectories where the particle was correctly tracked in each frame were chosen. Also, the trajectories were chosen so that they were at least several hundred pixels away from each other in both x- and y-directions to minimize error as shown in Figure 18.

The coordinates of the ten trajectories were transferred to an Excel table that calculates the relative stretch and standard deviation between the trajectories. The ten tracked particles were divided into five reference and five comparison trajectories so that the comparison particles were far as possible from the reference particles to avoid error (Figure 18).

Each reference particle was compared to each comparison particle, summing up to 25 calculations. The stretching was determined by calculating the absolute distance between the reference particle and comparison particle at each measurement point, and comparing that to their absolute distance at -4 mbar as described in Figure 19.

The coordinates were used to calculate the distance between the reference and comparison particle. The change in distance was calculated by comparing to the initial distance. The following equation (1) was used:

$$\left(\frac{\sqrt{\left(X_{ref,i}-X_{comp,i}\right)^2+\left(Y_{ref,i}-Y_{comp,i}\right)^2}}{\sqrt{\left(X_{ref,-4mbar}-X_{comp,-4mbar}\right)^2+\left(Y_{ref,-4mbar}-Y_{comp,-4mbar}\right)^2}}-1\right)*100\% \qquad (1),$$

where $X_{ref,i}$, $Y_{ref,i}$, $X_{comp,i}$ and $Y_{comp,i}$ mean the x- and y-coordinate of the reference particle and comparison particle at measurement point i and $X_{ref,-4\ mbar}$, $Y_{ref,-4\ mbar}$, $X_{comp,-4\ mbar}$ and $Y_{comp,-4\ mbar}$ the x- and y-coordinates at the first measurement point (-4 mbar). Standard deviations were calculated for the 25 measurements.

3.5 Cell experiments

The aim of the cell experiments was to study the effect of compression on epithelial cells with the characterized device. Two MDCK epithelial cell lines were used. One cell line expressed occludin (a cell-cell junction protein located on the cell membrane) tagged with emerald fluorescent protein, and thus allowed cell morphology to be visualized. The other expressed a fluorescent calcium indicator, and therefore enabled calcium fluxes to be seen.

3.5.1 Experimental setup

The stretching device was placed in a custom-made mini-incubator (Figure 20) and topped with a glass lid (Figure 21) to prevent evaporation of media. The device was connected to the pressure device.

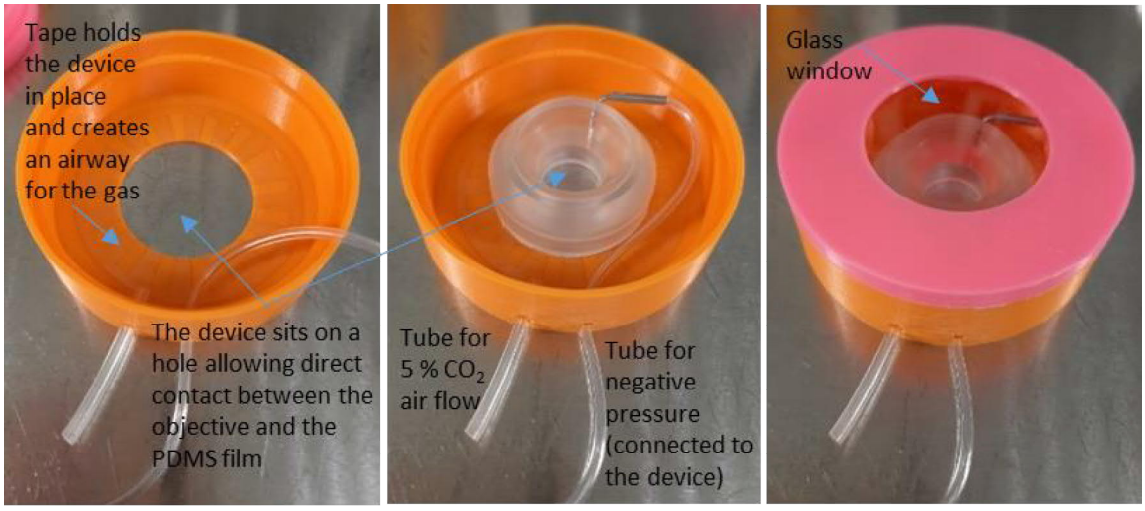

Figure 20. *The custom-made mini-incubator for the stretching device.*

Figure 21. *A glass lid is placed on top of the device to prevent the evaporation of media.*

For cell experiments, an additional pressure battery was connected between the stretching device and the pressure device (Figure 22). It allows the stretching device to be temporarily disconnected from the pressure device, and guarantees that regardless of possible small leaking, the pressure will be maintained. This is necessary as the system has to be transported from cell culture to the microscope without losing pressure. To ensure standard conditions were maintained also during imaging, 5 % CO_2 air was applied to the mini-incubator with 7 ml/min flow rate. During the cell culture period the mini-incubator was in a standard incubator, so no additional gas flow was needed.

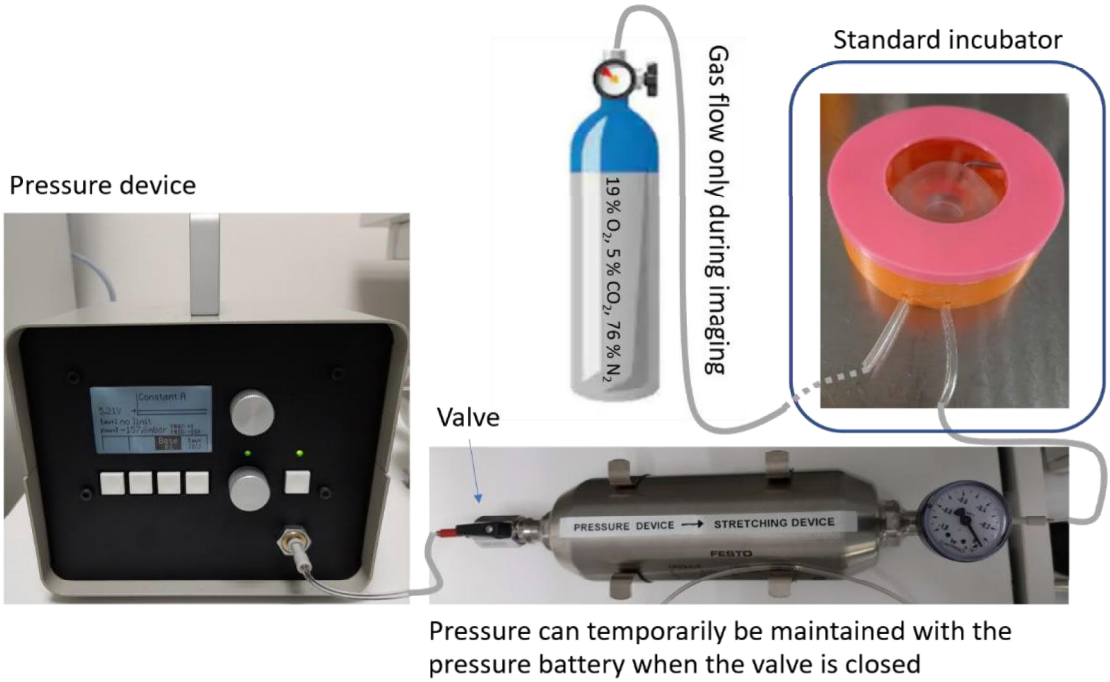

Figure 22. *The set-up for cell experiments. The stretching device was kept in a standard incubator during cell culture. During this time, it was connected to the pressure device via the pressure battery. The stretching device could be transported to the microscope when the valve on the pressure battery was closed. At the microscope, the pressure device was reconnected, and the gas flow was initiated.*

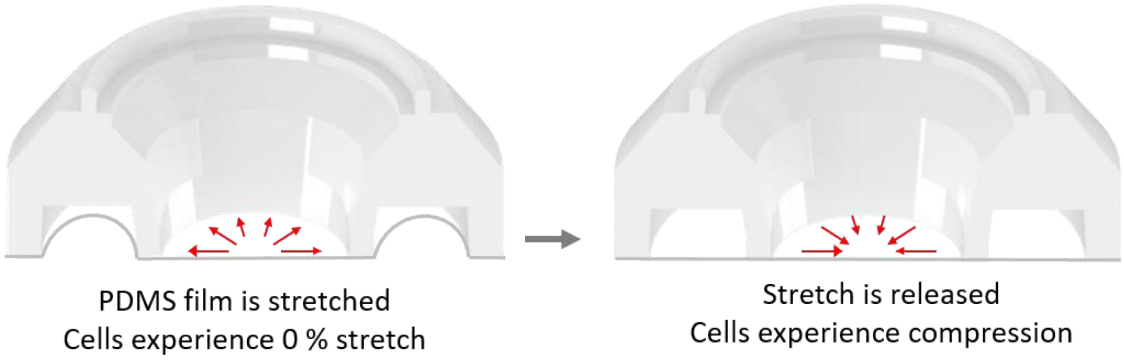

Figure 23. *Schematic of the compression test.*

During cell culture, the pressure was held at -400 mbar which creates 8.6 % strain. This acted as the 0 % stretch state for the cells, that attached to the membrane once it was already stretched. After the incubation period, the stretching was decreased to -4 mbar in a controlled manner, thus causing the cell culture area to decrease by 15 % (Figure 23).

For both cell lines one compression experiment was performed, as the imaging setup allowed only one sample to be imaged at a time. In addition, compression controls and material controls were analyzed for MDCK cells expressing occludin-emerald. The compression controls were stretching devices where no strain was applied. This way the effect of compression could be seen. In addition, cells were grown on glass slips to control the possible effect PDMS had on cells.

3.5.2 Compression's effect on the cytoskeleton

MDCK cells with occludin genetically tagged with emerald was used to study the morphology and cell-cell adhesions. Emerald is a derivative of green fluorescent protein (GFP) and occludin is a tight junction protein.

The devices and glass lids were autoclaved and the mini-incubator and its tubing were thoroughly wiped with 70 % ethanol before use. Devices and glass controls were coated with collagen to improve cell adhesion. Collagen I (rat tail, Gibco, A10483-01) was diluted to 0.1 mg/ml in 0.02 N acetic acid and mixed by vortexing. Enough solution was pipeted to cover the entire surface that was being coated. The coating solution was incubated for 40 min in RT under UV-light to sterilize the un-sterile collagen. This step simultaneously acted as an additional sterilization step for the device, glass lid, mini-incubator and tubing. Excess collagen and acetic acid were removed by rinsing twice with phosphate-buffered saline (PBS). The devices were left in PBS to prevent the coating from drying while cells were prepared.

Approximately 1.4 x 10^5 cells were seeded on the ~1.13 cm^2 cell culture area of the devices. Cells were trypsinized from the cell culture bottle and diluted to the correct concentration in the growth medium; minimum essential medium (MEM, Gibco) supplemented with 10% fetal bovine serum (FBS, Gibco), and 0.25 mg/ml G418 selection antibody (Roche Diagnostics, 892 µg/mg).

Once the cells were plated, ~8.6 % static stretch was initiated. Control devices were placed on petri dishes and no stretching was applied. Cells were grown in an incubator in standard conditions (37 °C, 5 % CO_2) for six days.

For imaging, the imaging chamber of the Zeiss LSM 780 inverted confocal microscope was heated to 37 °C. Imaging was done with a 25x/0.8 objective with water immersion (LD LCI Plan-Apochromat 25x/0.8 Imm Corr DIC M27). The emerald labeled occludin was excited with 488 nm wavelength and emission was detected from 490-607 nm. Simultaneously, also brightfield image was recorded. ~15 um stacks were taken in 30 nm slices to cover the height of the cells. Controls were imaged similarly, but with a 63x/1.20 water immersion objective (C-Apochromat 63x/1.20 W Korr M27).

The stretching sample was first imaged in stretching, i.e. in the 0 % compression (-400 mbar, ~8.6 %), from three locations on the device. Then the stretching was released to apply compression. A -4 mbar stretch was maintained even in compression to keep the film straight. The same locations were attempted to be imaged every 30 min for 4 h from the compressed sample. Unfortunately, as the film compressed the locations changed during the first time points and the imaging locations were therefore random. Controls were likewise imaged from three locations, but as they were only imaged for one time point, and imaging was therefore faster, no gas flow was applied.

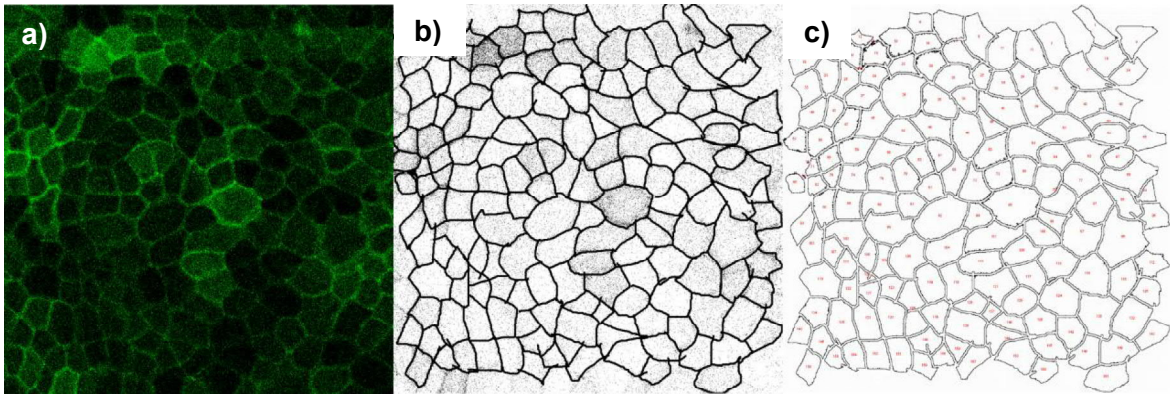

Figure 24. *Example of image analysis. A) the raw image on the left, b) enhanced binary image and c) the cells detected and analyzed by Analyze Particles tool.*

ImageJ was used to analyze cross-sectional areas of cells. An image with optimal focus was chosen from the stack of the fluorescent channel. The image was made binary, and the threshold was adjusted to improve the contrast of cell outlines. The paintbrush tool was used to enhance boundaries, and cross-section areas were analyzed with Analyze Particles tool (Figure 24). The average areas and standard deviations were calculated in Excel.

3.5.3 Compression's effect on calcium signaling

MDCK cells expressing jRGECO1a (modified red intensiometric genetically encoded Ca^{2+}-indicators for optical imaging) were used to study calcium activity. The cell line has the fluorescent calcium indicator genetically encoded and therefore enabled live-cell detection of calcium.

Because of problems with cell attachment, fibronectin was used instead of collagen. Fibronectin was diluted to 10 µg/ml in PBS and mixed gently. Coatings were incubated for 45 minutes under UV-light. After this cell seeding and other aspects of the experiment were done as described in Section 3.5.2. Instead of taking confocal stacks, live video was recorded before and after applying compression. For controls, live video was recorded from the static samples. The frame time was 1.56 s and 121 frames were taken using 561 nm excitation and emission was detected from 569-712 nm. 63x/1.20 magnification (C-Apochromat 63x/1.20 W Korr M27) was used.

From each video, ten regions of interest (ROI) with visible calcium activity were chosen. The ROIs were defined with a freehand selector in ImageJ, and the mean grey value for each ROI was calculated through the entire image sequence. In addition, the mean grey value of the entire FOV was calculated and used to normalize the mean values of ROIs. The normalized values were plotted as graphs.

4. RESULTS

This chapter presents the results gained from all the performed experiments. Each section contains also a short analysis of the results and of the possible error sources. A more detailed discussion will be presented in Chapter 5. The results are divided in a similar manner as in Chapter 3: choosing the optimal PDMS film, optimization of the device, characterization and cell experiments.

4.1 Choosing the PDMS film

Initially both SILPURAN® and ELASTOSIL® films were studied. However, ELASTOSIL® was left out as it is merely a non-medical grade version of SILPURAN®, and for cell culture applications a medical grade material is preferred. Also, the thinnest SILPURAN® films (20 µm and 50 µm) were left out due to difficulty in handling the films. Therefore, results contain only SILPURAN® in 200 µm and 100 µm thicknesses and Gloss in 125 µm and 254 µm thicknesses along with the lab-made 120 µm thick PDMS film.

4.1.1 Optical properties

The bead axial FWHM values for samples from several different imaging sessions, and the average of all values and standard deviations are presented in Table 1. The High Precision cover glass had the smallest values, which was expected. The FWHM values of the different films were relatively similar. Both PDMS type and its thickness had an effect. This makes sense, as microscopes are optimized for the refractive index of glass and for the 170 µm coverslip thickness. As PDMS has a smaller refractive index than glass (1.5 for glass and 1.4 for PDMS (*Refractive Index Database*, 2020)), slightly thicker PDMS films will behave better. SILPURAN® 200 µm and Gloss 254 µm had the FWHMs closest to the positive glass control.

Table 1: *Axial FWHM values of the PDMS film samples. High Precision cover glass was used as positive control. Values in grey deviate from the other results and are ignored in the average.*

Sample	FWHM values (µm)					
	Imaging session					
	1	2	3	4	Average	St. Dev.
Marienfeld High Precision cover glass 170 µm	1.038 1.038	1.349 1.349	1.349	0.934 1.038 0.519	1.077	0.264
Lab-made PDMS 120 µm	2.387 2.387	3.529 3.425	2.698 2.387		2.802	0.490
Gloss 254 µm	1.142 1.038	2.283 2.906	2.595	2.595 2.283 1.972	2.102	0.639
Gloss 125 µm		3.010 3.217 2.906	3.044	1.349	2.705	0.685
SILPURAN® 200 µm	2.283 2.076	1.868 1.972	1.920	1.661 1.868 1.557	1.901	0.212
SILPURAN® 100 µm	5.501 2.491	3.114 3.114	3.114		2.958	0.270
SILPURAN® 50 µm	3.217 2.906				3.062	0.156
SILPURAN® 20 µm	3.010 2.179				2.595	0.415
ELASTOSIL® 200 µm	2.698 2.179				2.439	0.259
ELASTOSIL® 100 µm	2.802 2.283				2.543	0.259

There is variation in FWHM-values depending on the measurement session and on the thickness of the PDMS film. Although the results might be partly explained by the refractive indexes, the measurement setup might also cause error. The movement of the objective as it scans the sample might have caused the PDMS films to move along with it. This would automatically cause the z-directional intensity plot to spread, and the FWHM to be larger. This would affect the thinner films more, as they are most susceptible for deformation. As glass is stiff, the movement of the objective does not affect it and therefore the aforementioned error does not apply to glass.

If the PDMS films were fixed and no z-directional movement was allowed, the FWHM values might be even smaller. However, these values tell of the functional optical resolution of these PDMS films in this device, as in this device the z-directional movement cannot be completely eliminated.

4.1.2 Autofluorescence

As can be seen in Figure 25, the emission scan for quartz barely differs from the baseline, and in glass samples the signal is extremely weak. In polystyrene and PDMS samples the signal is higher. In all of these samples the shapes of the 3D plots are similar. There is some emission at 390-450 nm wavelengths when the sample is excited in the near-UV range, but at higher excitation wavelengths the signals drop. In all other samples the z-axes is similar, but for FlexCell® the range had to be increased to fit the plot.

According to Elina Vuorimaa-Laukkanen, University Lecturer in Chemistry in Tampere University even the highest signals rise only from weak fluorescence emission, and might be partly caused by scattering. Furthermore, the polystyrene samples and PDMS samples have similar emissions. Cells are often imaged directly on the polystyrene culture plates, so they can be considered another negative control. As the autofluorescence is not higher than in the commonly used polystyrene plates, it can be considered low enough.

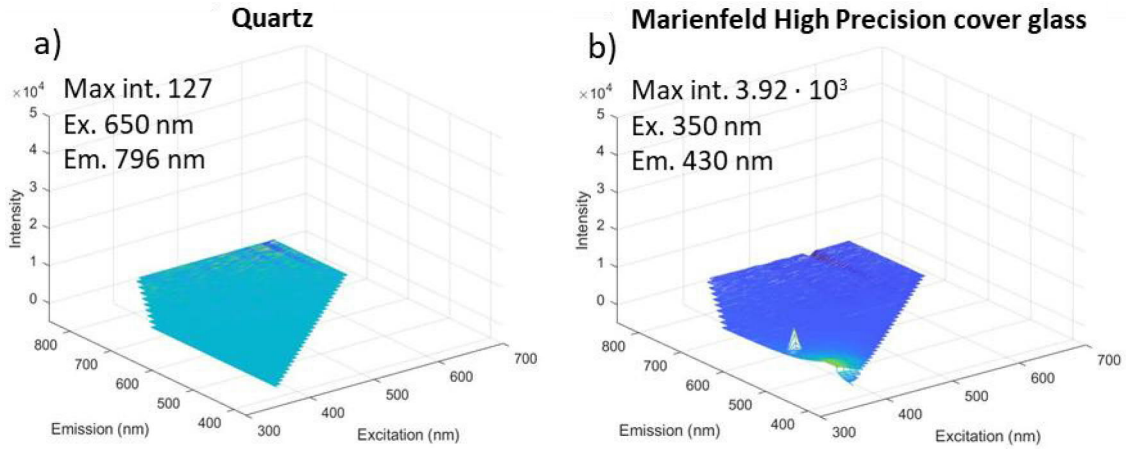

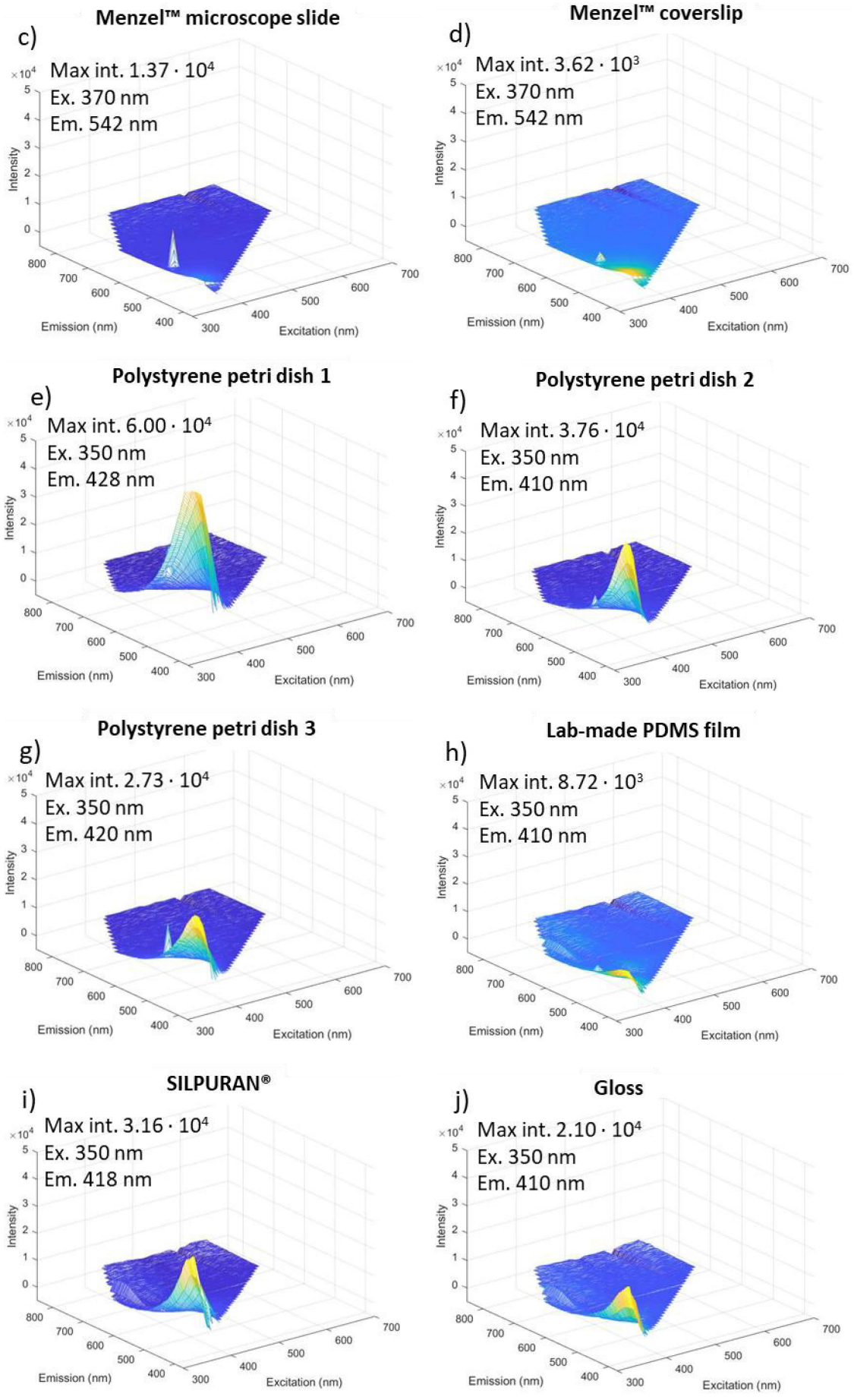
Menzel™ microscope slide
c)
Max int. 1.37 · 10⁴
Ex. 370 nm
Em. 542 nm
Menzel™ coverslip
d)
Max int. 3.62 · 10³
Ex. 370 nm
Em. 542 nm
Polystyrene petri dish 1
e)
Max int. 6.00 · 10⁴
Ex. 350 nm
Em. 428 nm
Polystyrene petri dish 2
f)
Max int. 3.76 · 10⁴
Ex. 350 nm
Em. 410 nm
Polystyrene petri dish 3
g)
Max int. 2.73 · 10⁴
Ex. 350 nm
Em. 420 nm
Lab-made PDMS film
h)
Max int. 8.72 · 10³
Ex. 350 nm
Em. 410 nm
SILPURAN®
i)
Max int. 3.16 · 10⁴
Ex. 350 nm
Em. 418 nm
Gloss
j)
Max int. 2.10 · 10⁴
Ex. 350 nm
Em. 410 nm
Intensity
Emission (nm)
Excitation (nm)

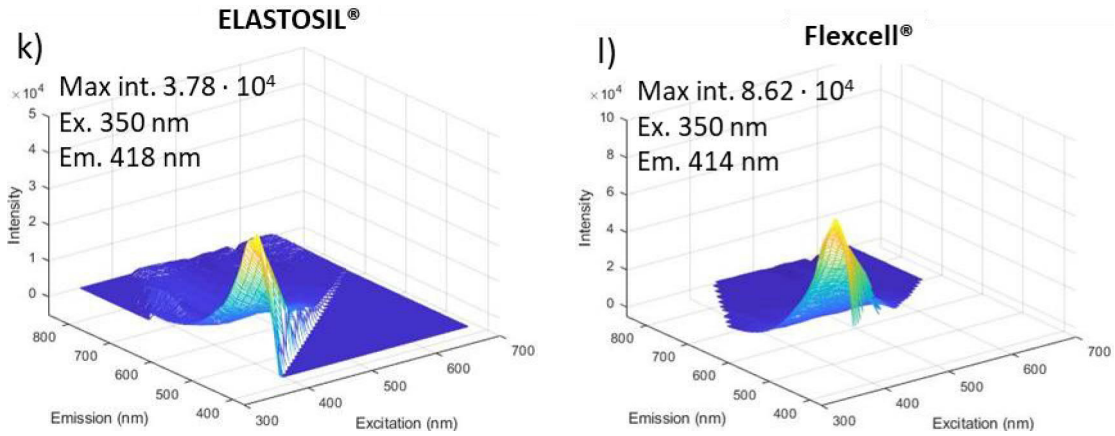

Figure 25. *3D-plots of emission intensities from a) quartz, b) Marienfield High Precision cover glass, c) Menzel™ microscope slide, d) Menzel™ coverslip, three polystyrene cell culture plastics (e-g), h) lab-made PDMS film, i) SILPURAN® film, j) Gloss film, K) ELASTOSIL® film and l) the PDMS film from FlexCell®. Note the different z-axis range for FlexCell®. The maximum intensity value (Max int.) and its corresponding excitation (Ex.) and emission (Em.) wavelengths are marked in each plot.*

As can be seen from the emission plots, the lab-made PDMS seems to have the lowest emission peak of the different PDMS films. Nevertheless, the emissions of SILPURAN®, ELASTOSIL® and Gloss are in the same scale as, and all PDMS samples have low emission intensity. FlexCell®, which had shown problems in the past, had a higher yet not concerning intensity. More detailed plots of quartz, SILPURAN®, ELASTOSIL®, Gloss and lab-made PDMS can be seen in Appendix A.

4.1.3 Biocompatibility

The biocompatibility of the different PDMS films was tested by plating MDCK epithelial cells on collagen coated devices. Glass and lab-made PDMS were used as controls. Z-stacks were taken from several locations on two parallel control devices per sample.

As Figure 26 shows, cells are slightly bigger on glass than on the PDMS films. Otherwise, cells look similar on all samples. The only exception is Gloss, where cell-free areas exist. This is probably caused by the collagen coating detaching from the film. Nevertheless, all films are biocompatible and can hold the collagen coating at least partly.

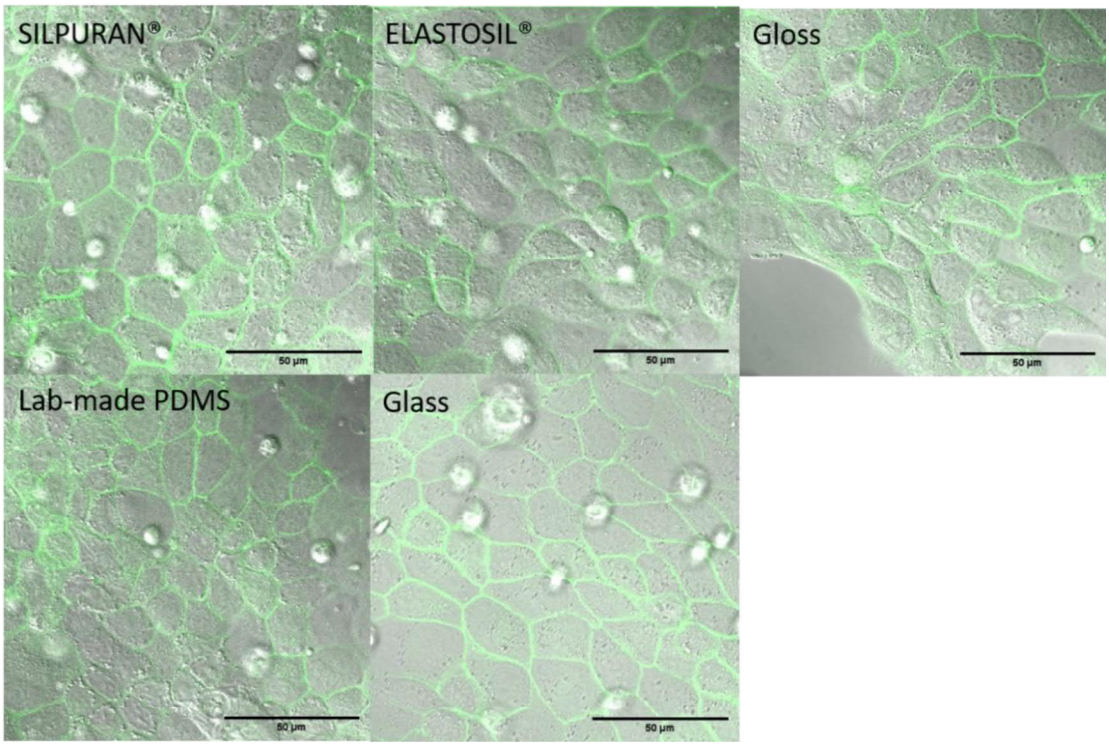

Figure 26. *Biocompatibility test of PDMS films. Scale bar is 50 µm.*

As ELASTOSIL® is not a medical grade product and Gloss shows problems in adhering collagen, SILPURAN® seems to be the most promising PDMS film when considering biocompatibility.

The results from comparing the films are gathered in Table 2, where the best results are highlighted in bold.

Table 2: *A summary of the results from comparing the different commercial PDMS films. The best result for each test is highlighted in bold. Glass is included as a positive control.*

	Resolution (FHWM, µm)	Autofluorescence	Biocompatibility	Other
Glass (control)	1.077	No emission	Excellent	
ELASTOSIL ® 200 µm	2.439	Some emission with near-UV excitation	**Good**	Not medical grade
ELASTOSIL ® 100 µm	2.543			
SILPURAN® 200 µm	**1.901**	Some emission with near-UV excitation	**Good**	**Convenient packaging**
SILPURAN® 100 µm	2.958			
Gloss 254 µm	2.102	**Smallest emission with near-UV excitation**	Some cell-free areas	Problems in adsorbing fluorescent beads
Gloss 125 µm	2.705			

4.1.4 Optimization of the device

Stretching properties of the films were compared with the three different versions of the device: 3 mm vacuum chamber with and without the stabilator ring and 4 mm vacuum chamber with the stabilator ring. The results are shown in Figure 27.

As can be seen from Figure 27A especially for SILPURAN® 100 µm and Gloss 125 µm, the film stops stretching at ~-180 mbar. This was caused by the film touching the ceiling of the vacuum chamber. For Gloss 125 µm the modifications to the device clearly improve stretching as it increases from ~6 % maximum to ~8.5 % maximum.

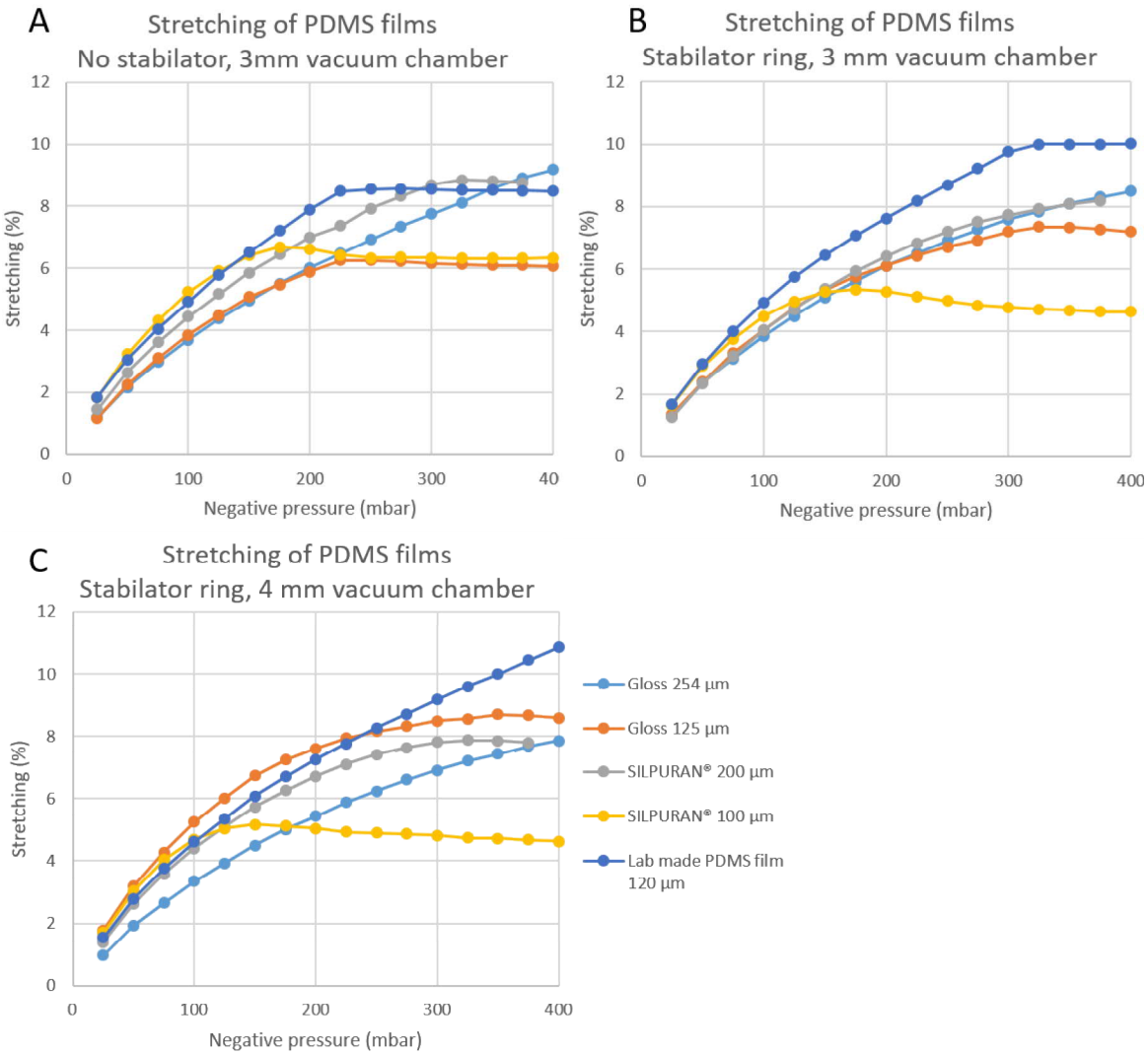

Figure 27. *Stretching of different films (Gloss 254 µm and 125 µm, SILPURAN® 200 µm and 100 µm and the lab-made PDMS film) with A) a 3 mm vacuum chamber without a stabilator ring, B) 3 mm vacuum chamber with a stabilator ring and C) 4 mm vacuum chamber with a stabilator ring. The legend is the same for all plots.*

Interestingly, for SILPURAN® 100 µm this improvement does not occur. Clear improvement can also be seen for the lab-made PDMS. For other films, the changes are smaller, and can partly by caused by variation between devices. The version of the device with a 4 mm vacuum chamber and a stabilator ring was chosen as the best candidate.

All ELASTOSIL® films were rejected already in the beginning, as they were not medical grade. Between SILPURAN® and Gloss, Gloss had cell-free areas in the biocompatibility test whereas SILPURAN® showed no problems. There were also problems in adsorbing fluorescent beads to the surface of Gloss, which would have greatly hampered the characterization process. SILPURAN® also comes in a more user-friendly packaging than Gloss. Therefore, SILPURAN® was chosen over Gloss. Out of the two different thicknesses of SILPURAN®, 200 µm showed significantly better stretching properties than the 100 µm thick film. Therefore the 200 µm thick SILPURAN® was chosen for detailed characterization.

For verification, a device with a 3 mm vacuum chamber and 4 mm vacuum chamber both with and without the stabilator ring were tested with SILPURAN® 200 µm. This time, also the z-displacement data was collected. This data shows that although the height of the vacuum chamber does not have an effect, the stabilator ring does. Without the stabilator ring the film rises up to 300 µm from zero level and has thus significant z-displacment while stretching. On the contrary, and as Figure 28 shows, with the stabilator the film first descends and the rises approximately back to zero level so that the all in all movement is only tens of micrometers. This movement is smaller, which makes focusing easier, and might diminish shear stress.

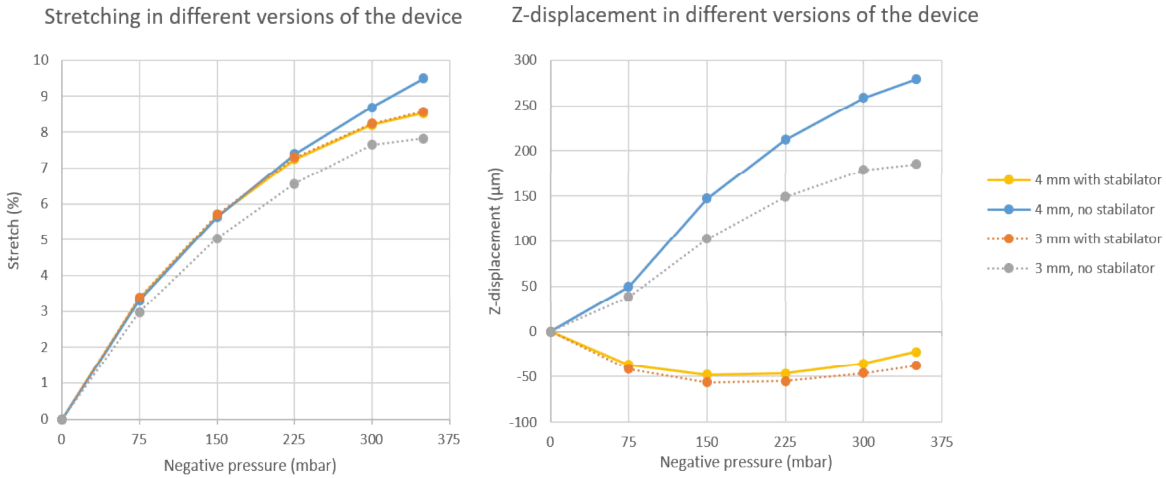

Figure 28. *Comparison of 4 mm vacuum chamber and 3 mm vacuum chamber with and without a stabilator ring for SILPURAN 200®. Stretching is showed on the left and z-displacement on the right.*

Therefore, SILPURAN® 200 µm was chosen as the optimal film, and a device with a 4 mm vacuum chamber and a stabilator ring was chosen as the best version of the device for further studies.

4.2 Characterization of stretching

Equiaxial stretching was characterized in detail with devices with 4 mm vacuum chambers, stabilator rings and SILPURAN® 200 µm film. Repeatability was tested both between different devices and between different measurement times of the same device. Four spots of the device (Figure 29) were measured to verify that stretching was uniform throughout the device, especially between the center and the edges.

Each measurement consisted of 3–5 repetitions. Any abnormal data was then excluded before calculating averages. The measurement step was 75 mbar, and measurements were done from -4 mbar to -350 mbar. The measurements were continued to -350 mbar as stretching was seen to saturate at that point.

As can be seen in Figure 30, the maximum stretching reached with this device is 8.6 ± 0.6 %. The z-displacement, however, varies from device to device, and according to the location on the device. Nevertheless, it follows the same trend in all measured devices and in all spots.

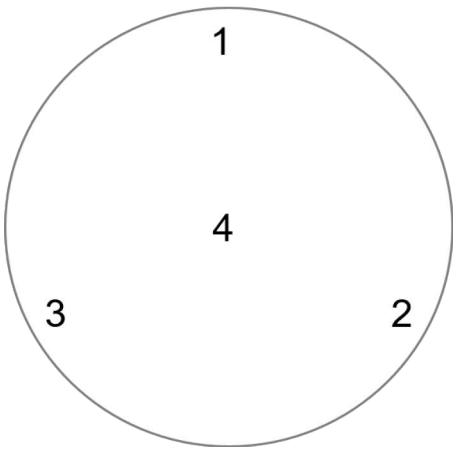

Figure 29. *Measurement points in the cell culture chamber of the device.*

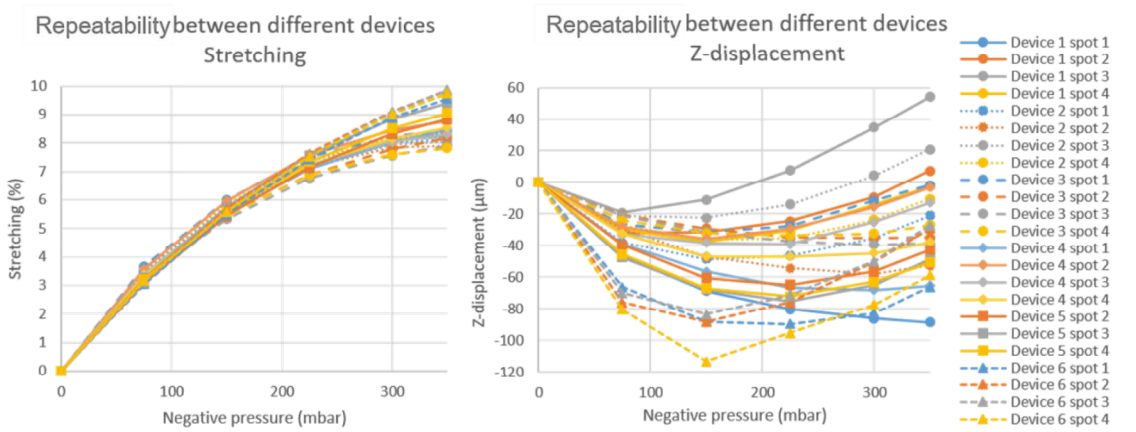

Figure 30. *The stretching (left) and z-displacement (right) measured at four different spots from six different devices. Spot 1 for Device 5 is missing because fluorescent beads were not dispersed well enough on the device. All devices had a 4 mm vacuum chamber and a stabilator ring. The spots are marked with the same colors, and the devices are differentiated by different data point markers and trend line types.*

Even smaller variation of 0.2 %-units can be seen when a single device is measured repeatedly (Figure 31). Between measurement 1 and 2 the device was in 1 Hz cyclic stretching over night, and between measurements 2 and 3 in rest. This does not affect the performance of the device, and makes the repeatability of a single device excellent. A difference in z-displacement is clearly seen between the measurement locations, but even this uneven behavior remains similar in every measurement. Each spot is marked with the same color, and as seen in Figure 31 the same colored lines form clusters.

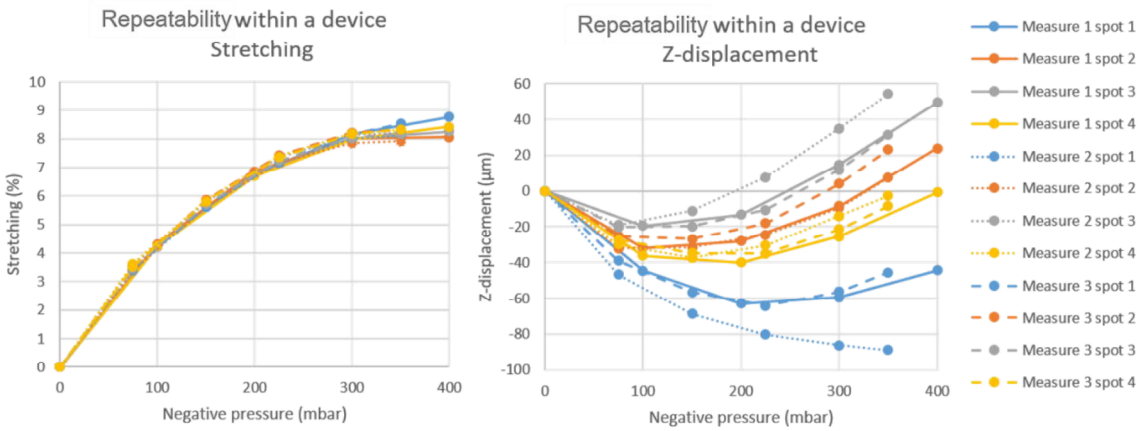

Figure 31. *The stretching (left) and z-displacement (right) measured from four different spots. The measurements were repeated to the same device three times. The spots are marked with same colors and the different measurements are differentiated by different trend line types.*

In the beginning of measurements when the pressure was set to -4 mbar, the device was leveled. This was done by manually finding the focus at eight points on the edges of the device. If the device was not leveled, the microscope sample table was adjusted to minimize the angle. Maximum 50 µm displacement along the diameter was accepted. This leads to 0.239° angle along the axis of the device, which will create 0.0009 % error to x-y-plane measurements.

The other error source in stretching measurements comes from the uneven z-displacement caused by the stretching. The maximum difference in z-displacement between the center and edge within a device is ~50 µm, as can be seen in Figure 29 (Device 1 between the center and locations 1 and 3). Along the axis this displacement would be 100 µm. This combined with the maximum displacement due to the device not being leveled (discussed above) would approximately triple the angle, leading to 0.0078 % error in the x-y-plane. Nevertheless, this error is negligible.

In the case of too dense particles in the image, incorrect tracking is possible as shown in Figure 18. The all in all movement of a particle ranges typically from 15 pixels to 100 pixels depending on its location (particles near the edge of the FOV move more than central ones). Incorrect tracking leading to an error of three pixels (diameter of the particle) can create an error of 10 % if both particles move all in all 15 pixels, and an error of 1 % if both particles move 100 pixels. As the 3-pixel deviation is relatively larger when particles move less, a significantly larger error is created. Therefore, the particles were chosen carefully to avoid incorrect tracking, and particles at the edges of the FOV were preferred.

The standard deviations were calculated for all measurements. They, along with all measurement data, are presented in Appendix B. For most measurements the standard deviation was smaller than 0.1 %-units. However, in some measurements of Device 1, the highest standard deviation was 0.48 %-units.

Finally, the stretching of the device was determined when it was filled with MilliQ-water and topped with a glass lid. This resembles the stretching in cell culture conditions. The results are shown in Figure 32.

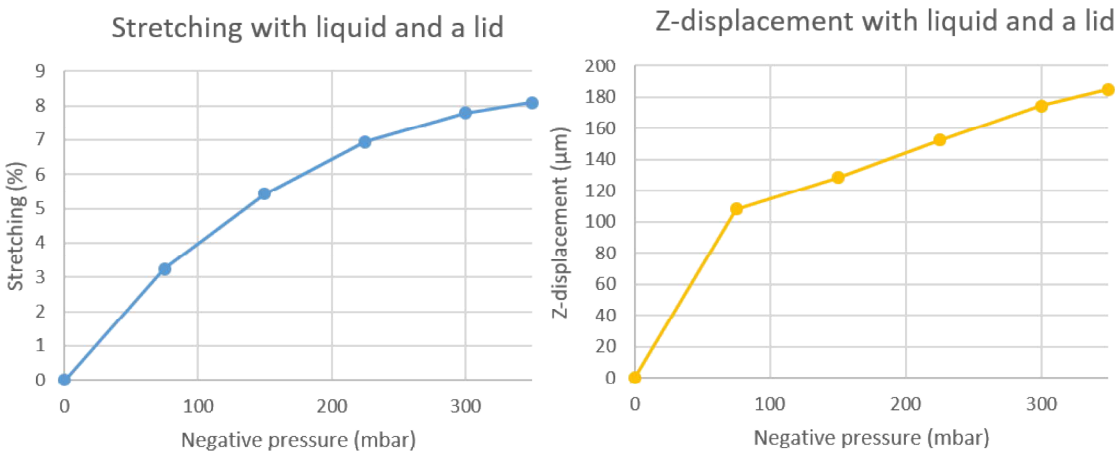

Figure 32. *Stretching and z-displacement of the device in cell culture conditions i.e. when it is filled with liquid to resemble media and topped with a glass lid.*

As can be seen in Figure 32, the stretching is unaffected by the liquid and lid, but z-displacement changes radically. The adding of the lid causes the film to rise upon stretching. The lid is tight so that media would not evaporate. Therefore, as the film stretches, negative pressure builds also in the cell culture chamber, and might cause the PDMS film to rise. This, however was not further investigated.

4.3 Cell compression

Cell compression experiments were performed on two different MDCK epithelial cell lines. MDCK occludin-emerald cells were used to assess the change in cross-sectional area, and MDCK jRGECO1a cells were used to study calcium activity.

4.3.1 Compression's effect on cell morphology

Although the biocompatibility of SILPURAN® was already tested, controls were plated also during cell experiments to verify that cells were acting normally during experiments. Control samples were imaged and cross-sectional areas of cells were calculated from images. As Figure 33 shows, cells are viable and have formed a dense epithelial sheet on both control types. The collagen coating therefore seems to adsorb to the SILPURAN® film, and the PDMS does not affect cell behavior. Average cross-sectional areas of cells were determined from three locations from a SILPURAN® sample and glass sample. On glass the average cross-sectional cell area was 204.63 ± 84 µm^2 and 182.57 ± 67 µm^2 on SILPURAN®. The data is fully shown in Appendix C.

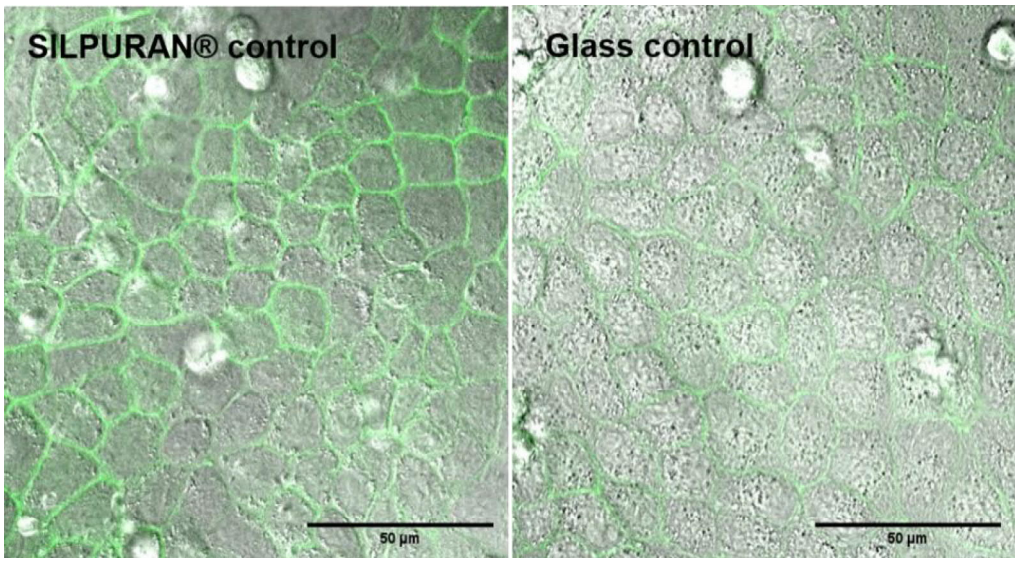

Figure 33. *Cells grown on SILPURAN® to see whether the PDMS film affect cells, and positive control of cells grown on Marienfeld High Precision cover glass. Scale bar is 50 µm.*

For the compression test, the cells were imaged before compression and after compression every 30 minutes. Example images from each time point from imaging location 3 are shown in Figure 34. The cells look similar as on the control samples, although slightly smaller. There are also more dead cells in the compression test sample than on the controls. This might be explained by a larger initial cell amount. Cell areas were determined for each time point from three to five locations and averages were calculated (Table 3). The values are presented in detail in Appendix C.

Table 3: *Average cross-sectional cell area (µm^2) and standard deviation for each time point of the compression test on MDCK occludin-emerald cells.*

Time point	Average cross-sectional area (µm^2)	St. Dev
Before compression	129.48	53.39
0 h	100.87	38.48
0.5 h	73.02	27.43
1 h	78.72	21.91
1.5 h	62.60	22.08
2 h	61.40	23.39
2.5 h	75.58	25.84
3 h	75.99	29.18
3.5 h	74.03	27.62
4 h	78.19	38.83

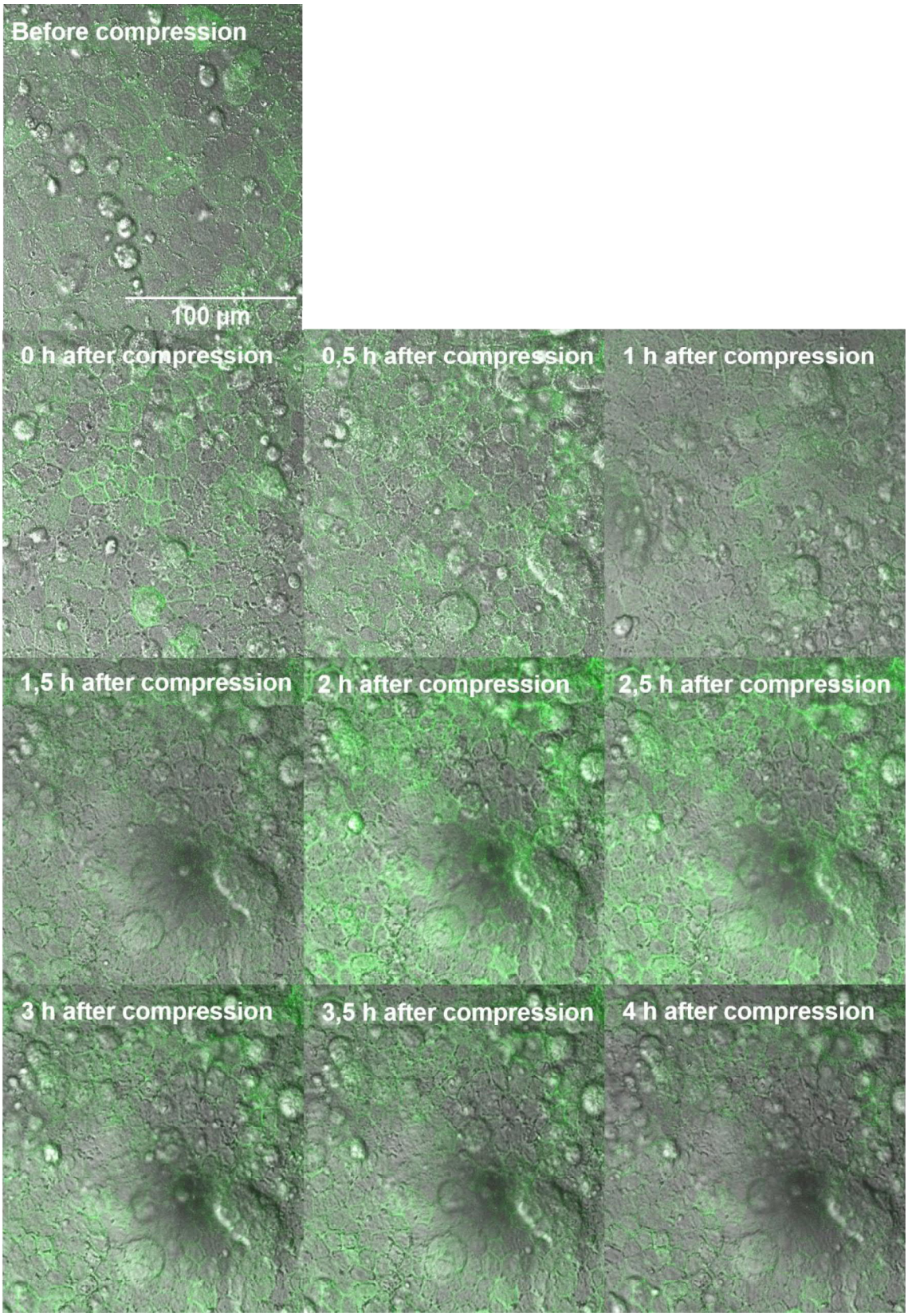

Figure 34. *Stacked fluorescent image and brightfield image of each timepoint of the compression test. The 100 µm scale bar is the same in all images.*

The plan was to take z-stacks from same fields of view in all time points. Then, the change in cross-sectional area of individual cells could have been determined, which would have produced more accurate and informative data. Additionally, the height of the cells could have been determined from the z-stack allowing inspection of cell volumes. Unfortunately, neither of these were able to be carried out. Z-stacks could not be taken due to a malfunction in the microscope software. Instead, images were manually taken from several stage positions. The same locations could not be maintained during compression simply because of the movement caused by compression. In order to maintain the location, automized control and a software to recognize locations would have been required. Therefore, average cross-sectional cell areas were determined instead of inspecting the change in volume of individual cells. The average cell areas for each time point are presented in Appendix C.

There is a lot of variation in cross-sectional cell areas as can be seen from the large standard deviations in Figure 35. The average might therefore not give a realistic picture of the cell population. However, Figure 36 shows that despite large standard deviations, the majority of cells have similar cross-sectional areas in each time point. The curves for "0 h" after compression and especially the curve for "Before compression" are shifted to the right. This means that a higher percentage of cells in these time points belong to the sections of larger cross-sectional areas. The rest of the time points are clustered at smaller cross-sectional areas. Figure 36 therefore follows the same trend as Figure 35.

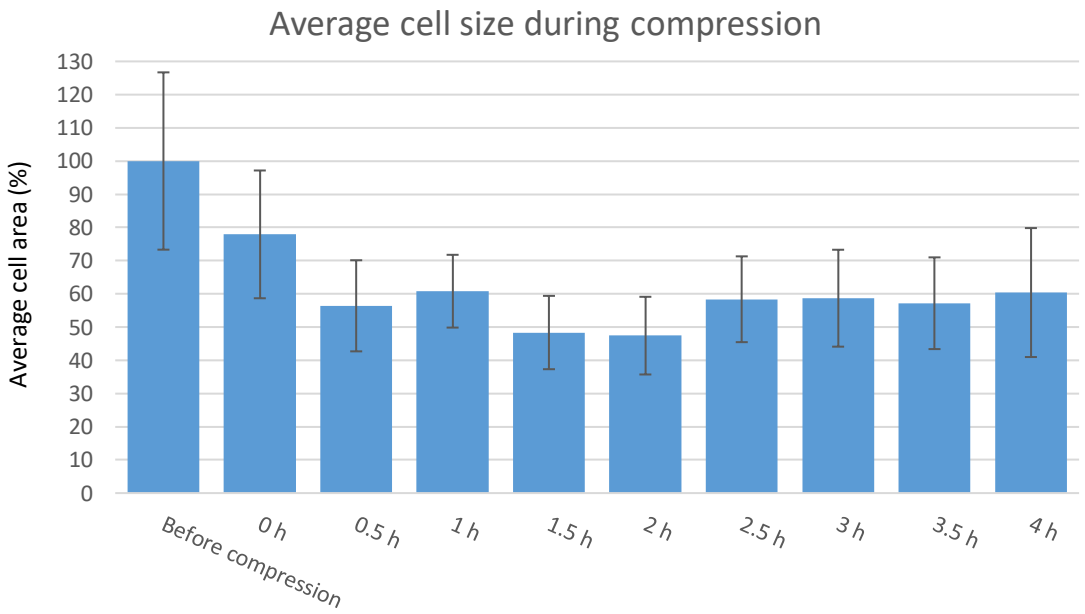

Figure 35. *The change in average cell area directly after compression (0 h) and every 30 minutes for 4 hours. The average cell area before compression was used as reference.*

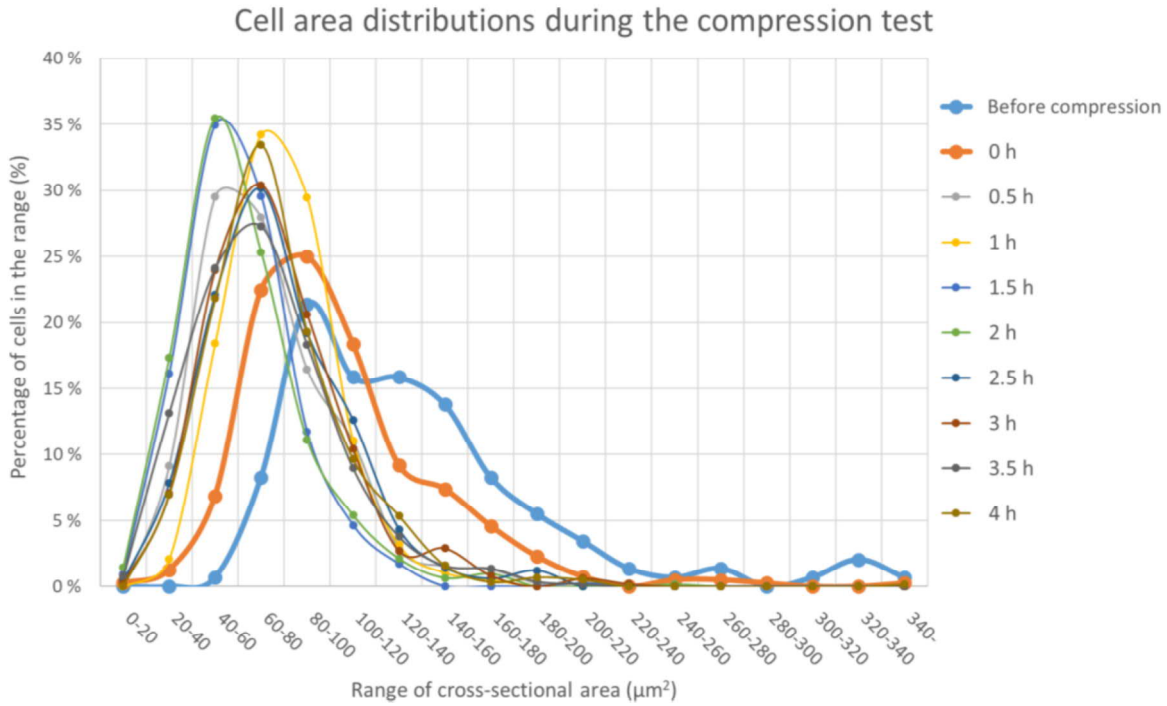

Figure 36. *All cross-sectional cell areas for each time point were pooled and sorted into 20 µm² ranges. The percentage of cells in each cross-sectional area range were plotted for each time point. The plots for "Before compression" and "0 h" (in bold) are shifted towards the right in comparison to the other time points, suggesting that in these time points a higher fraction of cells in have larger cross-sectional areas.*

Because the cell edges were traced by hand and no replica measurements were done, the data can only be considered indicative. Nevertheless, it is clear that cell areas decrease due to compression (Figures 35 and 36). Decrease in cross-sectional cell area occurs during the first hour after compression and remains unchanged for the rest of the experiment.

Interestingly, it seems that the cross-sectional cell areas decrease more than the compression created by the device. According to the average cross-sectional cell areas (Figure 35), directly after compression cells are compressed ~22 %, after which the cell area settles to about 40-50 % of the original average area. These values are significantly larger than the 15 % decrease in area created by the device. This indicates that cells are not only passively compressed, but actively reorganize their shape and become very tightly packed. If z-stacks would have been taken, this would have probably been seen as an intense growth in the height of cells.

4.3.2 Compression's effect on calcium signaling

Three videos before compression and three videos after compression were analyzed. The graphs are shown in Figure 37. In the figure, "Before compression 3" and "After compression 1" are taken of the same cells and same ROIs. A video was taken also during compression, but the video was unusable as the focus shifted significantly.

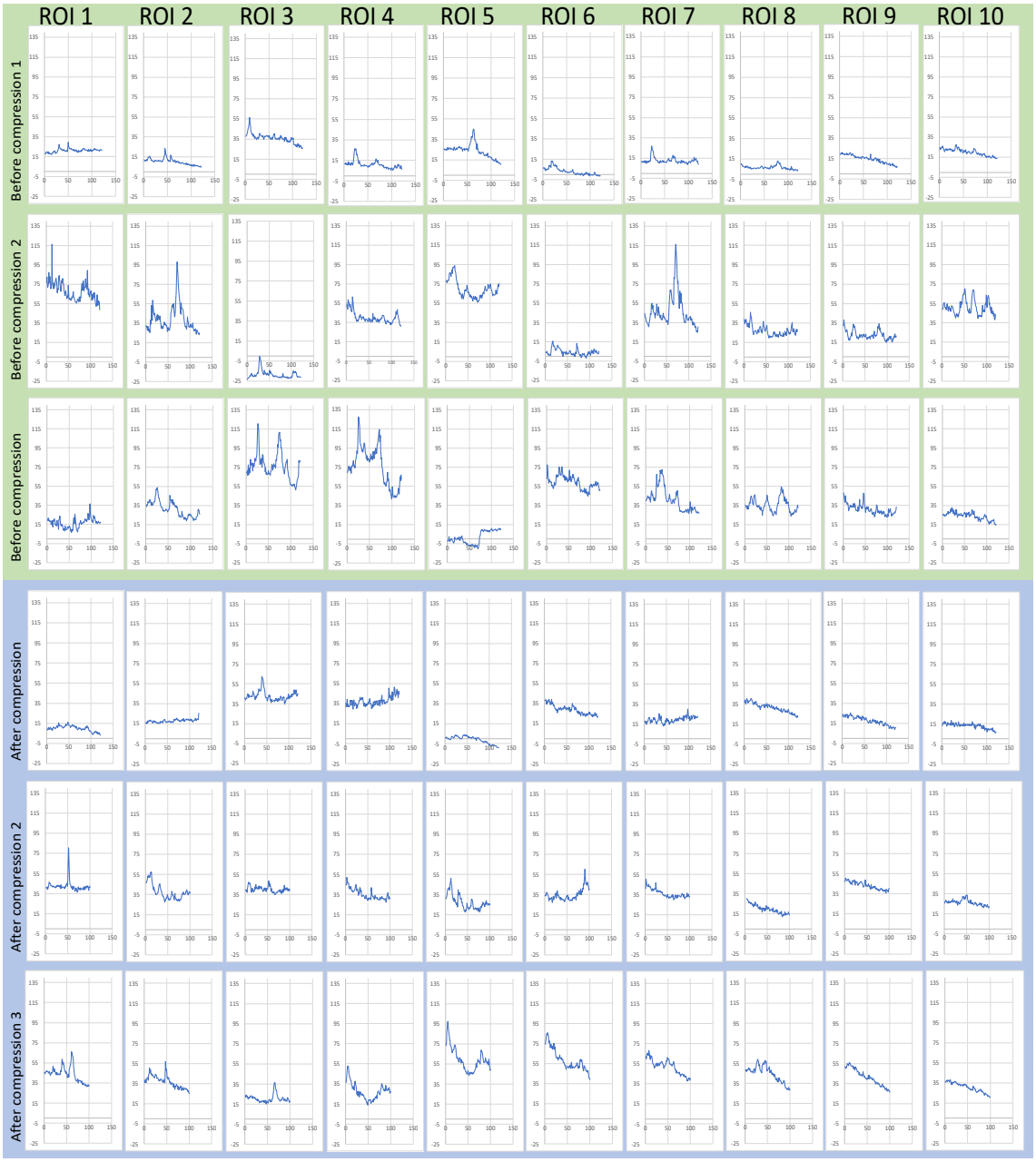

Figure 37. *Three spots were imaged before compression and three spots after compression. For each spot, 10 ROIs were chosen and their normalized intensities were plotted. The same spots and identical ROIs were imaged for "Before compression 3" and "After compression 1", other spots were random.*

The compression caused problems in maintaining the focus during imaging especially after compression. Right after compression the PDMS film was still in small movement, and once it has settled, the less stretched film shifted easily when the objective was moved. This can be seen as an uneven and decreasing baseline especially in “After compression 3”. Because of this, the final 21 frames were excluded from some of the ROIs.

Nevertheless, it seems that there is more calcium activity before compression than after compression. Before compression there are more peaks and they are clearer, whereas after compression most of the intensities remain close to baseline and peaks are smaller.

This is especially evident when comparing “Before compression 3” and “After compression 1”, where the same exact spots are recorded before and after compression. Before compression there are very clear peaks especially in ROI 1 and ROI 2, and after compression only one small peak can be seen in ROI 3.

Bleaching has only a small effect on the decrease of intensity. In “Before compression 2” the baseline shifts the least and is therefore least affected by the loss of focus. There the difference in mean grey value of the entire FOV decreases only 2.7 units or 6 %. This is so small that it cannot be accounted for the decrese in calcium activity. The calcium indicator jRGECO1a itself suffers from photoactivation with 488 nm excitation, which might cause false positives (Akerboom *et al.*, 2013; Wu *et al.*, 2013). However, with the 561 nm exctitation used here, this problem is avoided.

The fact that ROIs were manually chosen could cause some error. The clearest blinking areas were attempted to be chosen from all videos, but from videos taken after compression these clear blinks were much rarer, and even the clearest ones are lower than the blinks before compression. This too indicated that calcium activity indeed decreased after compression. Additionally, and similarly as in Section 4.3.1, the experiment was only performed once without replicas, making the results inexact.

To summarize both cell compression tests, the results show that the cell stretching device can be used to apply compression on living cells. The device performed reliably and was usable despite the complete test setup (Figure 22) not being very compact in size. Cells were viable and formed dense epithelial sheets during the cell culture periods. They were viable and attached to the substrate during cell culture, and remained so also for four hours after compression with occludin-emerald cells. MDCK jRGECO1a cells were only imaged for 30 minutes after compression, but they too remained viable and attached during this time.

The compression caused epithelial cells to be packed tightly as showed in Figure 35. Average cross-sectional area decreased to ~60% of the initial. This loss in space is probably the cause of the lowered calcium activity. As the cells have no room to change their shape or to migrate, they become more passive.

5. DISCUSSION

The SILPURAN®, ELASTOSIL®, Gloss and lab-made PDMS films were compared for their optical resolution, autofluorescence, biocompatibility and stretching. Differences between PDMS films were small with only stretching properties showing clear variation. The thickness of the film seemed to have an equal effect as the material.

Optical resolution was studied by determining the FWHM values. As microscope systems are optimized for the refractive index of glass and 170 µm thickness of the coverslip, it is logical that the thicker samples had slightly better resolutions. The thickness of the film compensates for the refractive index of PDMS, which is smaller than that of glass (1.5 for lass and 1.4 for PDMS (*Refractive Index Database*, 2020)). All PDMS samples had a slightly larger FWHM in axial direction than glass, but they were in the same range. However, there was variation in results between imaging sessions.

In addition to the refractive index and thickness, also the movement of the film might have affected the results. Glass is stiff and is therefore unaffected by the movement of the objective as it scans the z-stacks. The PDMS films, however, can stretch, and might have slightly moved along with the objective. This would automatically spread the intensity function in z-direction and increase the FWHM. Also, it would effect the thinnest and therefore least stiff PDMS films the most. This hypothesis correlates with the results: the results suggested that the resolution was worse in thinner PDMS films. However, despite these possible errors, the results give information about well these PDMS films behave in this specific device and under conditions where the film is not fixed.

Autofluorescence was low in all samples, but especially in Gloss PDMS film. Here, the different thicknesses were not studied as autofluorescence is a material property. All samples had a peak in emission with near-UV excitation and produced barely any signal with larger wavelengths. The peaks were probably in part emission and in part scattering. The fact that the emission peaks in PDMS films were not greater than in polystyrene control samples tells that the autofluoresce is insignificantly low for standard fluorescence microscopy. The PDMS films were not studied further, and it therefore remains unknown how much of the signal originated from scattering and how much from actual autofluorescence. In the future, however, it would be interesting to study this in more detail. Additionally, the effects of longer exposure to near-UV wavelengths could be studied, as in many cases imaging exposes the sample for tens of minutes whereas here exposure was only seconds.

In addition to the effects of light, also the chemical absorption properties of the films would be interesting to study. It is known that PDMS absorbs small molecules, but the possible variation between samples was not studied in this thesis. This might affect stainability of the films greatly and could account for some of the possible background in fluorescent microscopy.

The biocompatibility of the different PDMS films was studied only superficially. The films were coated with collagen I and seeded with MDCK occludin-emerald cells. There was no clear difference between the samples and the positive control (Marienfield High Precision Glass). Cells formed a dense epithelial sheet, cells were flat and attached to the bottom and viability was high. On Gloss there were some cell-free zones, but otherwise the cells did not differ from other samples. The cell-free zones were probably not caused by the interactions between cells and the film, but by the capability of Gloss to adsorb and hold the collagen coating. Therefore, the actual biocompatibility of the different PDMS films was not studied. Nevertheless, the study reveals that all samples are bioinert and mostly adsorb the coating well. Although the test does not tell much of the interplay between cells and the PDMS films, it does tell of the usability of the films in cell culture. If coatings are not well adsorbed, covalent bonding must be used. Although protocols exist (Leivo *et al.*, 2017), the procedure is much more inconvenient that simple adsorption.

The clearest difference in films was seen in how well they performed in the stretching device. The original design of the device was optimized for the lab-made PDMS film, so it is not surprising that the lab-made film performed best also in this new version of the device. Despite this, a commercial film was chosen as it makes production of devices more efficient.

While the other films behaved relatively similarly with the final optimized version of the device, the 100 µm thick SILPURAN® had the poorest performance. This was caused by excess stretching of the film, which caused the film to be pressed against the walls of the vacuum chamber. This hampered further movement of the film and prevented stretching. The same effect was seen also in other films, but to a lesser extent, and therefore only causing the stretching to not be linear. Interestingly, there was no clear correlation between stretching properties and thickness of the film. SILPURAN® 200 µm performed significantly better than SILPURAN® 100 µm, whereas Gloss 125 µm performed better than Gloss 254 µm in the final optimized version of the device. Therefore, both the thickness and the material properties determine how well each film performs in this stretching device.

As discussed, the stretching was not as linear as had been intended, and it did not reach the 10 % stretch reached by the previous version (Kreutzer *et al.*, 2014). Therefore, some modifications to the device were tested: the vacuum chamber was expanded and a stabilator ring added. The stabilator ring decreases the z-direction movement of the film significantly, which makes focusing easier and decreases fluid shear stress. For SILPURAN® 200 µm, the height of the vacuum chamber had less of an effect. Stretching and z-displacement were similar with both versions of the device. However, the 4 mm vacuum chamber was chosen as it offers some extra space for the film to move in the vacuum chamber.

Unfortunately, the decrease in z-displacement occurred only in testing conditions. When a glass lid and liquid were added to resemble cell culture conditions, z-displacement behaved similarly as without a stabilator ring. The stretching, however, was unaffected by the lid. The purpose of the lid was to prevent media from evaporating, and it was therefore tight. This might have caused negative pressure to build up inside the cell culture chamber during stretching, and might explain the increased z-directional movement of the film.

In order to reach higher stretching and to make it more linear, modifications to the device are still required. As discussed, the geometry of the device is the main cause for the saturation of stretching. When stretched the PDMS film gets too close to the walls of the vacuum chamber, which therefore diminishes the pulling force of the PDMS film.

One solution worth trying is to add a double layer of film to cover the vacuum chamber and a single layer in the cell culture chamber. A double layer would be stiffer, and therefore would diminish the stretching of the film in the vacuum chamber. This would prevent the film from getting in contact with the walls. Meanwhile the central chamber would be more flexible in comparison.

Secondly, the vacuum chamber could be made wider. This would increase the angle between the walls of the vacuum chamber and the stretching film which would therefore increase the pulling force of the PDMS film. However, changing the outer dimensions of the device is not desired, as the current size makes it compatible to other systems and parts made by the research group. Alternatively, the vacuum chamber could be made wider with the expense of the cell culture chamber, but neither this is an ideal solution. Reducing the size of the cell culture chamber would lead to a smaller cell volume, and possibly problems in collecting enough material for typical analyses such as sequencing or western blotting.

Although the mold is a significant improvement to compiling the device from pieces, the production of devices remains inefficient. The main problem are air bubbles appearing into the structure while casting the PDMS. The surfaces of the device that are bonded are at the top of the mold, which is where all air bubbles end up as they rise. If the device was upside down in the mold, possible bubbles would rise to a less critical surface. However, this would require the whole mold to be designed and compiled differently. Furthermore, for the mass production point of view, the possibilities of injection molding should also be investigated.

All in all, the device is capable of producing 8.6 ± 0.6 % stretching. The stretching saturates as the negative pressure increases, thus making it unlinear. Repeatability of stretching is good from device to device and excellent within a device: standard deviation was 0.6 %-units from device to device, and 0.2 %-units within a device. The device is therefore reliable and applicable for cell culture. However, only crude adjustment of the stretching is possible: the device cannot reliably be used to compare, for example, the effects of 7 % and 8 % stretching. On the other hand, in many cell culture applications such precise control is not necessary.

The device is very multi-functional, as it can be used to apply static stretching, static compression or cyclic stretching. Microscope imaging is easy and the microscope can get as close as 200 µm from the cells. Thanks to this small working distance, objectives with high magnification and numerical aperture can be used. This is a major advantage of the device when compared to other similar devices, where such proximity is not possible. However, the movement of the film causes problems in maintaining the FOV and focus. The loss of focus could be decreased by diminishing the z-displacement, but as the film stretches the maintainment of the FOV is not possible without additional software.

The device is completely made of PDMS, a bioinert material that can easily be coated for enhanced cellular adhesion. Furthermore, the device is actuated with negative pressure, and therefore does not have any electronic components. The pressure controller can be kept at a long distance from the cell culture media, thus making it safer.

The device was successfully used in cell culture. The 15 % decrease in area created by the device causes average cell cross-sectional cell area to decrease to ~60 % of the initial. This indicates that cells were not only passively compressed, but actively rearranged their cytoskeleton.

The height of the cells could not be determined in this study, but it most likely increased as a consequence of compression. Wyatt *et al. (2020)* saw that the volume of epithelial

cells remains constant even under compression. This is seen as an increase in height of the cells as the cross-sectional area decreases.

It seems strange that cells compressed more than they were forced to. It would have been equally expected that cells would have compensated the decreased living space by, for example, actively delaminating cells (Marinari *et al.*, 2012). The details of the reaction of cells to the compression can only be speculated with the gained data. However, cells survived the experiment and clearly reacted to the compression by decreasing their cross-sectional area.

With calcium imaging there were unexpected problems with cell viability. The collagen coating seemed to detach, and consequently led to cell death. Fibronectin was therefore used instead of collagen with improved results. It is possible that the MDCK jRGECO1a cell line was more more delicate than the occludin-emerald cell line.

Compression seemed to reduce calcium activity. Before compression there were multiple peaks in intensity and the peaks were high. These peaks indicate calcium fluxes which are a sign of calcium signaling. After compression there were less peaks and they were smaller, thus indicationg less calcium activity. This is probably caused by the decreased living space. As cells do not have space to migrate or to change their shape, they become more passive. Conversely, when cells have more space, cells change their shape and migrate, which can be seen as calcium activity. (Jones and Nauli, 2012) This supports the results from studying cross-sectional cell areas. Cells become tightly packed, which causes calcium activity to decrease.

In summary, the device and the custom made mini-incubator proved functional for cell culture. The device can be used to apply compression on cell populations, and the mini-incubator ensures that a stable 5 % CO_2 air environment can be maintained even during extended imaging. Although the device requires optimization, it can be reliably used in cell culture. In addition to the device itself, the entire setup requires improvements. A platform that allows the use of six devices at once exists, and should be tested. Furthermore, the setup could be more compact and a holder could be developed to facilitate transportation.

6. CONCLUSIONS

The aim of the thesis was to characterize the new version of a stretching device. Four different PDMS films from three different manufacturers in various thicknesses were compared out of which SILPURAN® 200 µm was chosen. Furthermore, several versions of the device were tested and the version with a 4 mm vacuum chamber and a stabilator ring was chosen.

The device reaches 8.6 ± 0.6 % strain with good repeatability from device to device (0.6 %-unit standard deviation), and excellent repeatability within a single device (0.2 %-unit standard deviation). Compression caused epithelial cells to become tightly packed which was seen as significant decrease in cross-sectional area. Decrease in cross-sectional cell area was greater then the areal compression of the device, thus suggesting active remodeling of the cell cytoskeletons instead of a mere passive response. As a consequence of diminished living space, calcium activity decreased.

The device can be used in cell culture to mechanically stimulate cells. However, the device requires further development in order to reach higher and more linear stretching and to make production of the devices more efficient.

7. REFERENCES

Akerboom, J., Carreras Calderón, N., Tian, L., Wabnig, S., Prigge, M., Tolö, J., Gordus, A., Orger, M. B., Severi, K. E., Macklin, J. J., Patel, R., Pulver, S. R., Wardill, T. J., Fischer, E., Schüler, C., Chen, T.-W., *et al.* (2013) 'Genetically encoded calcium indicators for multi-color neural activity imaging and combination with optogenetics', *Frontiers in molecular neuroscience*. Frontiers Media S.A., 6, p. 2. doi: 10.3389/fnmol.2013.00002.

American Chemical Society (2014) *Polydimethylsiloxane*. Available at: https://www.acs.org/content/acs/en/molecule-of-the-week/archive/p/polydimethylsiloxane.html (Accessed: 3 October 2019).

Anderson, D. E. and Johnstone, B. (2017) 'Dynamic Mechanical Compression of Chondrocytes for Tissue Engineering: A Critical Review', *Frontiers in bioengineering and biotechnology*. Frontiers Media S.A., 5, p. 76. doi: 10.3389/fbioe.2017.00076.

Anishkin, A., Loukin, S. H., Teng, J. and Kung, C. (2014) 'Feeling the hidden mechanical forces in lipid bilayer is an original sense', *Proceedings of the National Academy of Sciences of the United States of America*. 2014/05/21. National Academy of Sciences, 111(22), pp. 7898–7905. doi: 10.1073/pnas.1313364111.

Benavides Damm, T. and Egli, M. (2014) 'Calcium's Role in Mechanotransduction during Muscle Development', *Cellular Physiology and Biochemistry*, 33(2), pp. 249–272. doi: 10.1159/000356667.

Bhattacharya, S., Datta, A., Berg, J. M. and Gangopadhyay, S. (2005) 'Studies on surface wettability of poly(dimethyl) siloxane (PDMS) and glass under oxygen-plasma treatment and correlation with bond strength', *Journal of Microelectromechanical Systems*, 14(3), pp. 590–597. doi: 10.1109/JMEMS.2005.844746.

Birla, R. (2014) *Introduction to Tissue Engineering*. 1st edn. New Jersey: John Wiley & Sons, Ltd.

Boyle, S. T., Kular, J., Nobis, M., Ruszkiewicz, A., Timpson, P. and Samuel, M. S. (2018) 'Acute compressive stress activates RHO/ROCK-mediated cellular processes', *Small GTPases*. Taylor & Francis, pp. 1–17. doi: 10.1080/21541248.2017.1413496.

Chen, C.-H., Kuo, C.-Y. and Chen, J.-P. (2018) 'Effect of Cyclic Dynamic Compressive Loading on Chondrocytes and Adipose-Derived Stem Cells Co-Cultured in Highly Elastic Cryogel Scaffolds', *International journal of molecular sciences*. MDPI, 19(2), p. 370. doi: 10.3390/ijms19020370.

Chen, H.-Y. and Lahann, J. (2005) 'Fabrication of Discontinuous Surface Patterns within Microfluidic Channels Using Photodefinable Vapor-Based Polymer Coatings', *Analytical Chemistry*. American Chemical Society, 77(21), pp. 6909–6914. doi: 10.1021/ac050964e.

Deguchi, S., Kudo, S., Matsui, T. S., Huang, W. and Sato, M. (2015) 'Piezoelectric actuator-based cell microstretch device with real-time imaging capability', *AIP Advances*. American Institute of Physics, 5(6), p. 67110. doi: 10.1063/1.4922220.

Demmerle, J., Wegel, E., Schermelleh, L. and Dobbie, I. (2015) 'Assessing Resolution in Super-Resolution Imaging.', *Methods (San Diego, Calif.)*, 88, pp. 3–10. doi: 10.1016/j.ymeth.2015.07.001.

Eddington, D. T., Puccinelli, J. P. and Beebe, D. J. (2006) 'Thermal aging and reduced hydrophobic recovery of polydimethylsiloxane', *Sensors and Actuators B: Chemical*, 114(1), pp. 170–172. doi: https://doi.org/10.1016/j.snb.2005.04.037.

Efimenko, K., Wallace, W. E. and Genzer, J. (2002) 'Surface Modification of Sylgard-184 Poly(dimethyl siloxane) Networks by Ultraviolet and Ultraviolet/Ozone Treatment', *Journal of Colloid and Interface Science*, 254(2), pp. 306–315. doi: https://doi.org/10.1006/jcis.2002.8594.

Flexcell® International Corporation (2018) *User Manual - Flexcell Dynamic Culture System*. Available at: https://www.flexcellint.com/product/fx6000t (Accessed: 15 November 2019).

Flexcell® International Corporation (2020) *Cell Culture Compression Systems*. Available at: https://www.flexcellint.com/category/compression (Accessed: 15 November 2019).

Ghannam, M. T. and Esmail, M. N. (1998) 'Rheological Properties of Poly(dimethylsiloxane)', *Industrial & Engineering Chemistry Research*. American Chemical Society, 37(4), pp. 1335–1340. doi: 10.1021/ie9703346.

Heiner, J., Stenberg, B. and Persson, M. (2003) 'Crosslinking of siloxane elastomers', *Polymer Testing*. Elsevier, 22(3), pp. 253–257. doi: 10.1016/S0142-9418(02)00081-8.

Hemmilä, S., Cauich-Rodríguez, J. V, Kreutzer, J. and Kallio, P. (2012) 'Rapid, simple, and cost-effective treatments to achieve long-term hydrophilic PDMS surfaces', *Applied Surface Science*, 258(24), pp. 9864–9875. doi: https://doi.org/10.1016/j.apsusc.2012.06.044.

Heo, Y. J., Kan, T., Iwase, E., Matsumoto, K. and Shimoyama, I. (2013) 'Stretchable cell culture platforms using micropneumatic actuators', *Micro & Nano Letters*, 8(12), pp. 865–868. doi: 10.1049/mnl.2013.0476.

Huang, Y. and Nguyen, N.-T. (2013) 'A polymeric cell stretching device for real-time imaging with optical microscopy', *Biomedical Microdevices*, 15(6), pp. 1043–1054. doi: 10.1007/s10544-013-9796-2.

Huh, D., Matthews, B. D., Mammoto, A., Montoya-Zavala, M., Hsin, H. Y. and Ingber, D. E. (2010) 'Reconstituting Organ-Level Lung Functions on a Chip', *Science*, 328(5986), pp. 1662 LP – 1668. doi: 10.1126/science.1188302.

Iwadate, Y. and Yumura, S. (2009) 'Cyclic stretch of the substratum using a shape-memory alloy induces directional migration in Dictyostelium cells', *BioTechniques*. Future Science, 47(3), pp. 757–767. doi: 10.2144/000113217.

Jo, B.-H., Van Lerberghe, L. M., Motsegood, K. M. and Beebe, D. J. (2000) 'Three-dimensional micro-channel fabrication in polydimethylsiloxane (PDMS) elastomer', *Journal of Microelectromechanical Systems*, 9(1), pp. 76–81. doi: 10.1109/84.825780.

Johnston, I. D., McCluskey, D. K., Tan, C. K. L. and Tracey, M. C. (2014) 'Mechanical characterization of bulk Sylgard 184 for microfluidics and microengineering', *Journal of Micromechanics and Microengineering*. IOP Publishing, 24(3), p. 35017. doi: 10.1088/0960-1317/24/3/035017.

Jones, T. J. and Nauli, S. M. (2012) 'Mechanosensory Calcium Signaling BT - Calcium Signaling', in Islam, M. S. (ed.). Dordrecht: Springer Netherlands, pp. 1001–1015. doi: 10.1007/978-94-007-2888-2_46.

Kamble, H., Barton, M. J., Jun, M., Park, S. and Nguyen, N.-T. (2016) 'Cell stretching devices as research tools: engineering and biological considerations', *Lab on a Chip*. The Royal Society of Chemistry, 16(17), pp. 3193–3203. doi: 10.1039/C6LC00607H.

Kamble, H., Vadivelu, R., Barton, M., Shiddiky, M. J. A. and Nguyen, N.-T. (2018) 'Pneumatically actuated cell-stretching array platform for engineering cell patterns in vitro', *Lab on a Chip*. The Royal Society of Chemistry, 18(5), pp. 765–774. doi: 10.1039/C7LC01316G.

Kreutzer, J., Ikonen, L., Hirvonen, J., Pekkanen-Mattila, M., Aalto-Setälä, K. and Kallio, P. (2014) 'Pneumatic cell stretching system for cardiac differentiation and culture', *Medical*

Engineering & Physics, 36(4), pp. 496–501. doi: https://doi.org/10.1016/j.medengphy.2013.09.008.

Kreutzer, J., Viehrig, M., Pölönen, R.-P., Zhao, F., Ojala, M., Aalto-Setälä, K. and Kallio, P. (2019) 'Pneumatic unidirectional cell stretching device for mechanobiological studies of cardiomyocytes', *Biomechanics and Modeling in Mechanobiology*. doi: 10.1007/s10237-019-01211-8.

Lan, B., Mitchel, J. A., O'Sullivan, M. J., Park, C. Y., Kim, J. H., Cole, W. C., Butler, J. P. and Park, J.-A. (2018) 'Airway epithelial compression promotes airway smooth muscle proliferation and contraction', *American journal of physiology. Lung cellular and molecular physiology*. 2018/08/02. American Physiological Society, 315(5), pp. L645–L652. doi: 10.1152/ajplung.00261.2018.

Lange, J. J., Collinson, M. M., Culbertson, C. T. and Higgins, D. A. (2009) 'Single-Molecule Studies of Oligomer Extraction and Uptake of Dyes in Poly(dimethylsiloxane) Films', *Analytical Chemistry*. American Chemical Society, 81(24), pp. 10089–10096. doi: 10.1021/ac902250p.

Lee, D., Erickson, A., You, T., Dudley, A. T. and Ryu, S. (2018) 'Pneumatic microfluidic cell compression device for high-throughput study of chondrocyte mechanobiology', *Lab on a chip*, 18(14), pp. 2077–2086. doi: 10.1039/c8lc00320c.

Lee, J. N., Jiang, X., Ryan, D. and Whitesides, G. M. (2004) 'Compatibility of Mammalian Cells on Surfaces of Poly(dimethylsiloxane)', *Langmuir*. American Chemical Society, 20(26), pp. 11684–11691. doi: 10.1021/la048562+.

Leivo, J., Virjula, S., Vanhatupa, S., Kartasalo, K., Kreutzer, J., Miettinen, S. and Kallio, P. (2017) 'A durable and biocompatible ascorbic acid-based covalent coating method of polydimethylsiloxane for dynamic cell culture', *Journal of the Royal Society, Interface*. The Royal Society, 14(132), p. 20170318. doi: 10.1098/rsif.2017.0318.

Li, N., Li, Q., Zhou, X. D., Kolosov, V. P. and Perelman, J. M. (2012) 'Chronic mechanical stress induces mucin5AC expression in human bronchial epithelial cells through ERK dependent pathways', *Molecular Biology Reports*, 39(2), pp. 1019–1028. doi: 10.1007/s11033-011-0827-x.

Lim, C.-G., Jang, J. and Kim, C. (2018) 'Cellular machinery for sensing mechanical force', *BMB reports*. 2018/12/31. Korean Society for Biochemistry and Molecular Biology, 51(12), pp. 623–629. doi: 10.5483/BMBRep.2018.51.12.237.

Marinari, E., Mehonic, A., Curran, S., Gale, J., Duke, T. and Baum, B. (2012) 'Live-cell delamination counterbalances epithelial growth to limit tissue overcrowding', *Nature*, 484(7395), pp. 542–545. doi: 10.1038/nature10984.

Martino, F., Perestrelo, A. R., Vinarský, V., Pagliari, S. and Forte, G. (2018) 'Cellular Mechanotransduction: From Tension to Function', *Frontiers in physiology*. Frontiers Media S.A., 9, p. 824. doi: 10.3389/fphys.2018.00824.

Mata, A., Fleischman, A. J. and Roy, S. (2005) 'Characterization of Polydimethylsiloxane (PDMS) Properties for Biomedical Micro/Nanosystems', *Biomedical Microdevices*, 7(4), pp. 281–293. doi: 10.1007/s10544-005-6070-2.

McDonald, J. C. and Whitesides, G. M. (2002) 'Poly(dimethylsiloxane) as a Material for Fabricating Microfluidic Devices', *Accounts of Chemical Research*. American Chemical Society, 35(7), pp. 491–499. doi: 10.1021/ar010110q.

Occhetta, P., Mainardi, A., Votta, E., Vallmajo-Martin, Q., Ehrbar, M., Martin, I., Barbero, A. and Rasponi, M. (2019) 'Hyperphysiological compression of articular cartilage induces an osteoarthritic phenotype in a cartilage-on-a-chip model', *Nature Biomedical Engineering*, 3(7), pp. 545–557. doi: 10.1038/s41551-019-0406-3.

Owen, M. J. (2001) 'Elastomers: Siloxane', *Encyclopedia of Materials: Science and Technology*. Elsevier, pp. 2480–2482. doi: 10.1016/B0-08-043152-6/00448-4.

Pavesi, A., Adriani, G., Rasponi, M., Zervantonakis, I. K., Fiore, G. B. and Kamm, R. D. (2015) 'Controlled electromechanical cell stimulation on-a-chip', *Scientific Reports*, 5(1), p. 11800. doi: 10.1038/srep11800.

Refractive Index Database (2020) *RefractiveIndex.com*. Available at: https://refractiveindex.info/ (Accessed: 5 March 2020).

Sackmann, E. K., Fulton, A. L. and Beebe, D. J. (2014) 'The present and future role of microfluidics in biomedical research', *Nature*, 507(7491), pp. 181–189. doi: 10.1038/nature13118.

Schürmann, S., Wagner, S., Herlitze, S., Fischer, C., Gumbrecht, S., Wirth-Hücking, A., Prölß, G., Lautscham, L. A., Fabry, B., Goldmann, W. H., Nikolova-Krstevski, V., Martinac, B. and Friedrich, O. (2016) 'The IsoStretcher: An isotropic cell stretch device to study mechanical biosensor pathways in living cells', *Biosensors and Bioelectronics*, 81, pp. 363–372. doi: https://doi.org/10.1016/j.bios.2016.03.015.

Shyer, A. E., Tallinen, T., Nerurkar, N. L., Wei, Z., Gil, E. S., Kaplan, D. L., Tabin, C. J. and Mahadevan, L. (2013) 'Villification: how the gut gets its villi', *Science (New York, N.Y.)*. 2013/08/29, 342(6155), pp. 212–218. doi: 10.1126/science.1238842.

Sidhaye, J. and Norden, C. (2017) 'Concerted action of neuroepithelial basal shrinkage and active epithelial migration ensures efficient optic cup morphogenesis', *eLife*. eLife Sciences Publications, Ltd, 6, p. e22689. doi: 10.7554/eLife.22689.

Slaughter, G. and Stevens, B. (2014) 'A cost-effective two-step method for enhancing the hydrophilicity of PDMS surfaces', *BioChip Journal*, 8(1), pp. 28–34. doi: 10.1007/s13206-014-8105-3.

Sophia Fox, A. J., Bedi, A. and Rodeo, S. A. (2009) 'The basic science of articular cartilage: structure, composition, and function', *Sports health*. SAGE Publications, 1(6), pp. 461–468. doi: 10.1177/1941738109350438.

STREX Cell Strain Instrument User Manual (2020). Available at: https://strexcell.com/product-manuals/ (Accessed: 15 November 2019).

Sui, G., Wang, J., Lee, C.-C., Lu, W., Lee, S. P., Leyton, J. V, Wu, A. M. and Tseng, H.-R. (2006) 'Solution-Phase Surface Modification in Intact Poly(dimethylsiloxane) Microfluidic Channels', *Analytical Chemistry*. American Chemical Society, 78(15), pp. 5543–5551. doi: 10.1021/ac060605z.

Sun, Z., Costell, M. and Fässler, R. (2019) 'Integrin activation by talin, kindlin and mechanical forces', *Nature Cell Biology*, 21(1), pp. 25–31. doi: 10.1038/s41556-018-0234-9.

Tomakidi, P., Schulz, S., Proksch, S., Weber, W. and Steinberg, T. (2014) 'Focal adhesion kinase (FAK) perspectives in mechanobiology: implications for cell behaviour', *Cell and Tissue Research*, 357(3), pp. 515–526. doi: 10.1007/s00441-014-1945-2.

Tremblay, D., Chagnon-Lessard, S., Mirzaei, M., Pelling, A. E. and Godin, M. (2014) 'A microscale anisotropic biaxial cell stretching device for applications in mechanobiology', *Biotechnology letters*. 2013/10/16. Springer Netherlands, 36(3), pp. 657–665. doi: 10.1007/s10529-013-1381-5.

Tschumperlin, D. J., Shively, J. D., Swartz, M. A., Silverman, E. S., Haley, K. J., Raab, G. and Drazen, J. M. (2002) 'Bronchial epithelial compression regulates MAP kinase signaling and HB-EGF-like growth factor expression', *American Journal of Physiology-Lung Cellular and*

Molecular Physiology. American Physiological Society, 282(5), pp. L904–L911. doi: 10.1152/ajplung.00270.2001.

Tse, J. M., Cheng, G., Tyrrell, J. A., Wilcox-Adelman, S. A., Boucher, Y., Jain, R. K. and Munn, L. L. (2012) 'Mechanical compression drives cancer cells toward invasive phenotype', *Proceedings of the National Academy of Sciences of the United States of America*. 2011/12/27. National Academy of Sciences, 109(3), pp. 911–916. doi: 10.1073/pnas.1118910109.

Uto, K., Tsui, J. H., DeForest, C. A. and Kim, D.-H. (2017) 'Dynamically Tunable Cell Culture Platforms for Tissue Engineering and Mechanobiology', *Progress in polymer science*. 2016/09/17, 65, pp. 53–82. doi: 10.1016/j.progpolymsci.2016.09.004.

Wang, A.-J., Xu, J.-J. and Chen, H.-Y. (2006) 'Proteins modification of poly(dimethylsiloxane) microfluidic channels for the enhanced microchip electrophoresis', *Journal of Chromatography A*, 1107(1), pp. 257–264. doi: https://doi.org/10.1016/j.chroma.2005.12.040.

Wisser, F. M., Schumm, B., Mondin, G., Grothe, J. and Kaskel, S. (2015) 'Precursor strategies for metallic nano- and micropatterns using soft lithography', *Journal of Materials Chemistry C*. The Royal Society of Chemistry, 3(12), pp. 2717–2731. doi: 10.1039/C4TC02418D.

Wu, J., Liu, L., Matsuda, T., Zhao, Y., Rebane, A., Drobizhev, M., Chang, Y.-F., Araki, S., Arai, Y., March, K., Hughes, T. E., Sagou, K., Miyata, T., Nagai, T., Li, W.-H. and Campbell, R. E. (2013) 'Improved orange and red Ca^{2}± indicators and photophysical considerations for optogenetic applications', *ACS chemical neuroscience*. 2013/03/19. American Chemical Society, 4(6), pp. 963–972. doi: 10.1021/cn400012b.

Wu, M.-H., Wang, H.-Y., Liu, H.-L., Wang, S.-S., Liu, Y.-T., Chen, Y.-M., Tsai, S.-W. and Lin, C.-L. (2011) 'Development of high-throughput perfusion-based microbioreactor platform capable of providing tunable dynamic tensile loading to cells and its application for the study of bovine articular chondrocytes', *Biomedical Microdevices*, 13(4), pp. 789–798. doi: 10.1007/s10544-011-9549-z.

Wyatt, T. P. J., Fouchard, J., Lisica, A., Khalilgharibi, N., Baum, B., Recho, P., Kabla, A. J. and Charras, G. T. (2020) 'Actomyosin controls planarity and folding of epithelia in response to compression', *Nature Materials*, 19(1), pp. 109–117. doi: 10.1038/s41563-019-0461-x.

APPENDIX A: DETAILED EXCITATION-EMISSION PLOTS

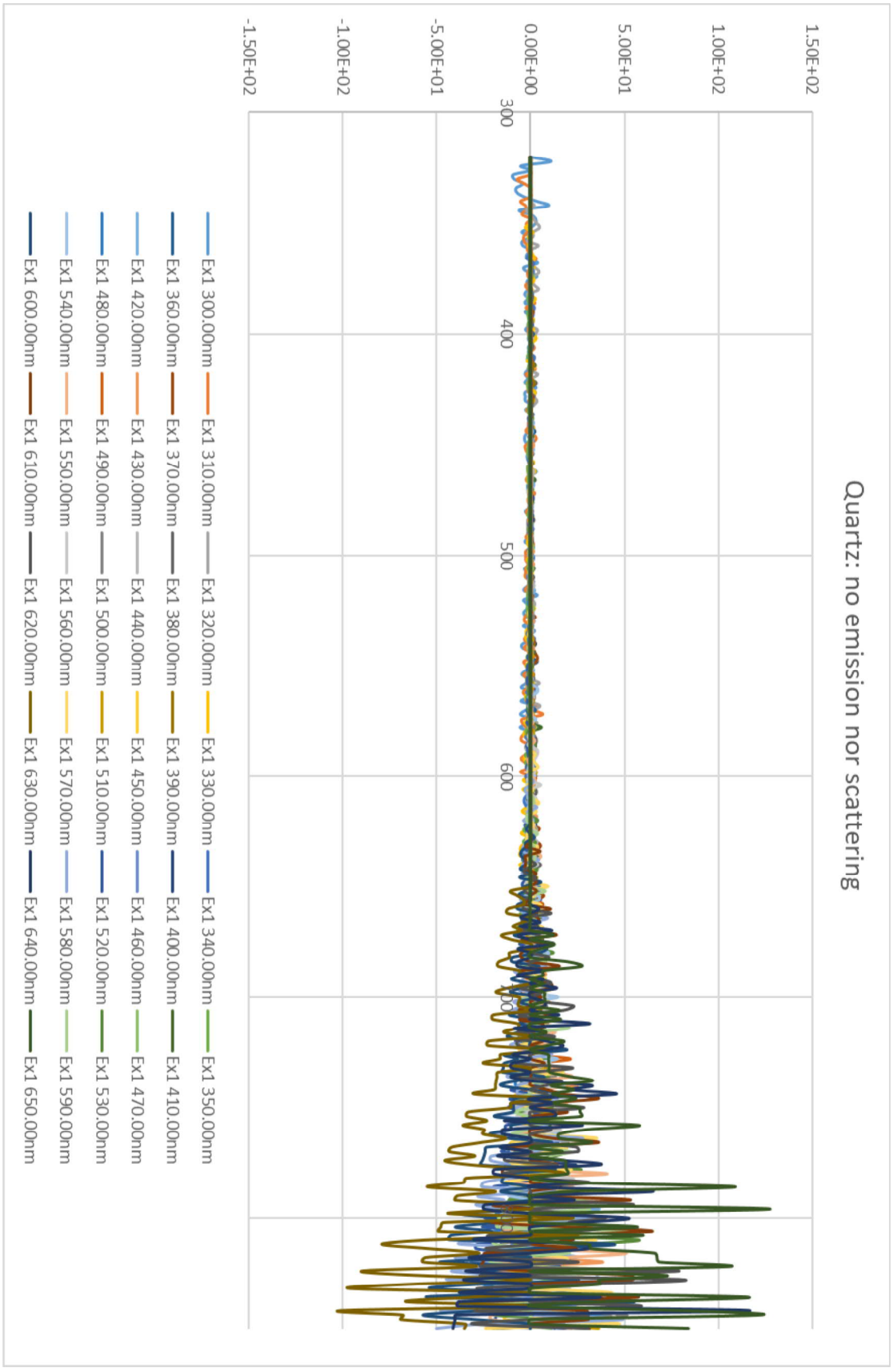

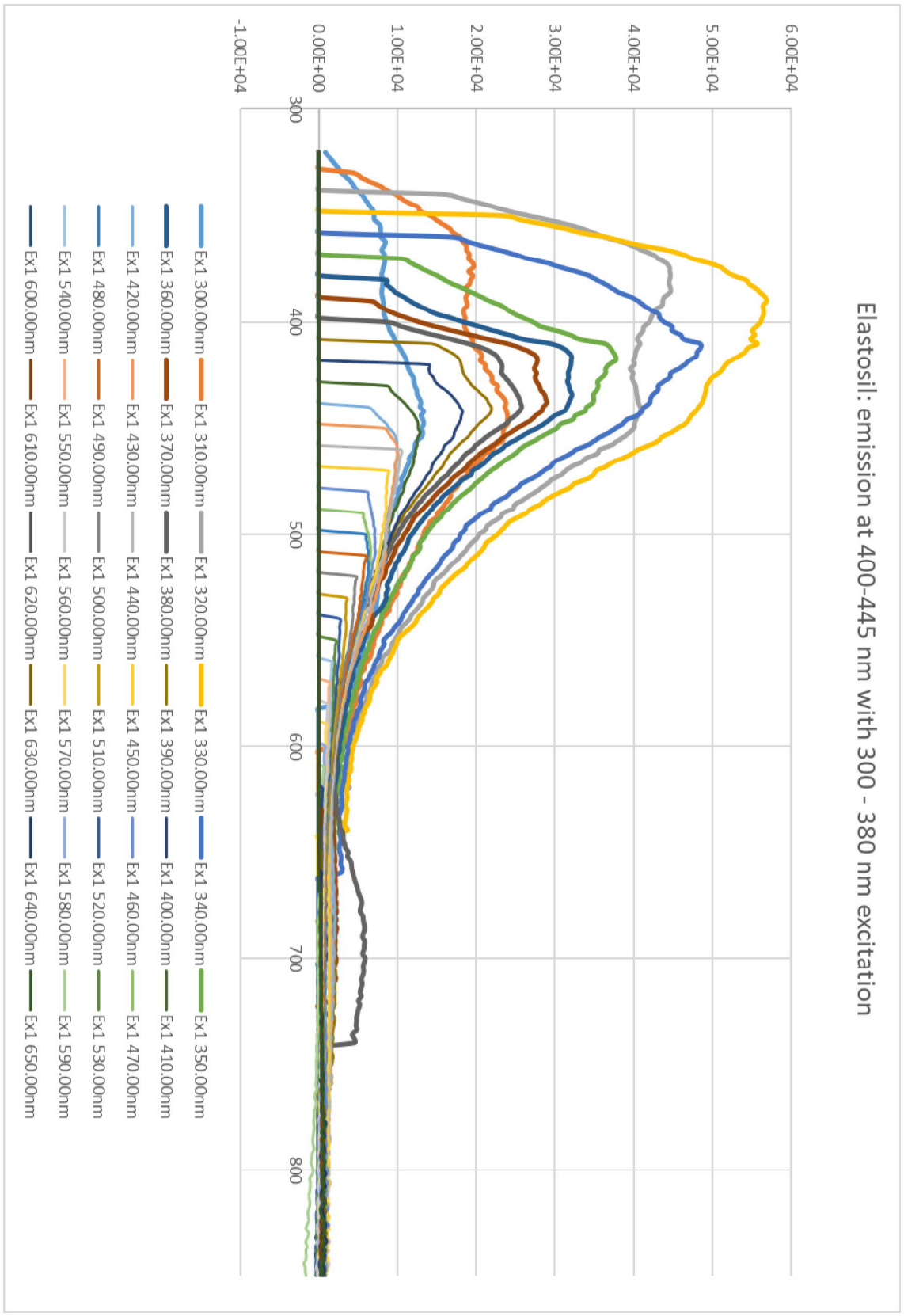
Elastosil: emission at 400-445 nm with 300 - 380 nm excitation
6.00E+04
5.00E+04
4.00E+04
3.00E+04
2.00E+04
1.00E+04
0.00E+00
-1.00E+04
300
400
500
600
700
800
Ex1 300.00nm
Ex1 310.00nm
Ex1 320.00nm
Ex1 330.00nm
Ex1 340.00nm
Ex1 350.00nm
Ex1 360.00nm
Ex1 370.00nm
Ex1 380.00nm
Ex1 390.00nm
Ex1 400.00nm
Ex1 410.00nm
Ex1 420.00nm
Ex1 430.00nm
Ex1 440.00nm
Ex1 450.00nm
Ex1 460.00nm
Ex1 470.00nm
Ex1 480.00nm
Ex1 490.00nm
Ex1 500.00nm
Ex1 510.00nm
Ex1 520.00nm
Ex1 530.00nm
Ex1 540.00nm
Ex1 550.00nm
Ex1 560.00nm
Ex1 570.00nm
Ex1 580.00nm
Ex1 590.00nm
Ex1 600.00nm
Ex1 610.00nm
Ex1 620.00nm
Ex1 630.00nm
Ex1 640.00nm
Ex1 650.00nm

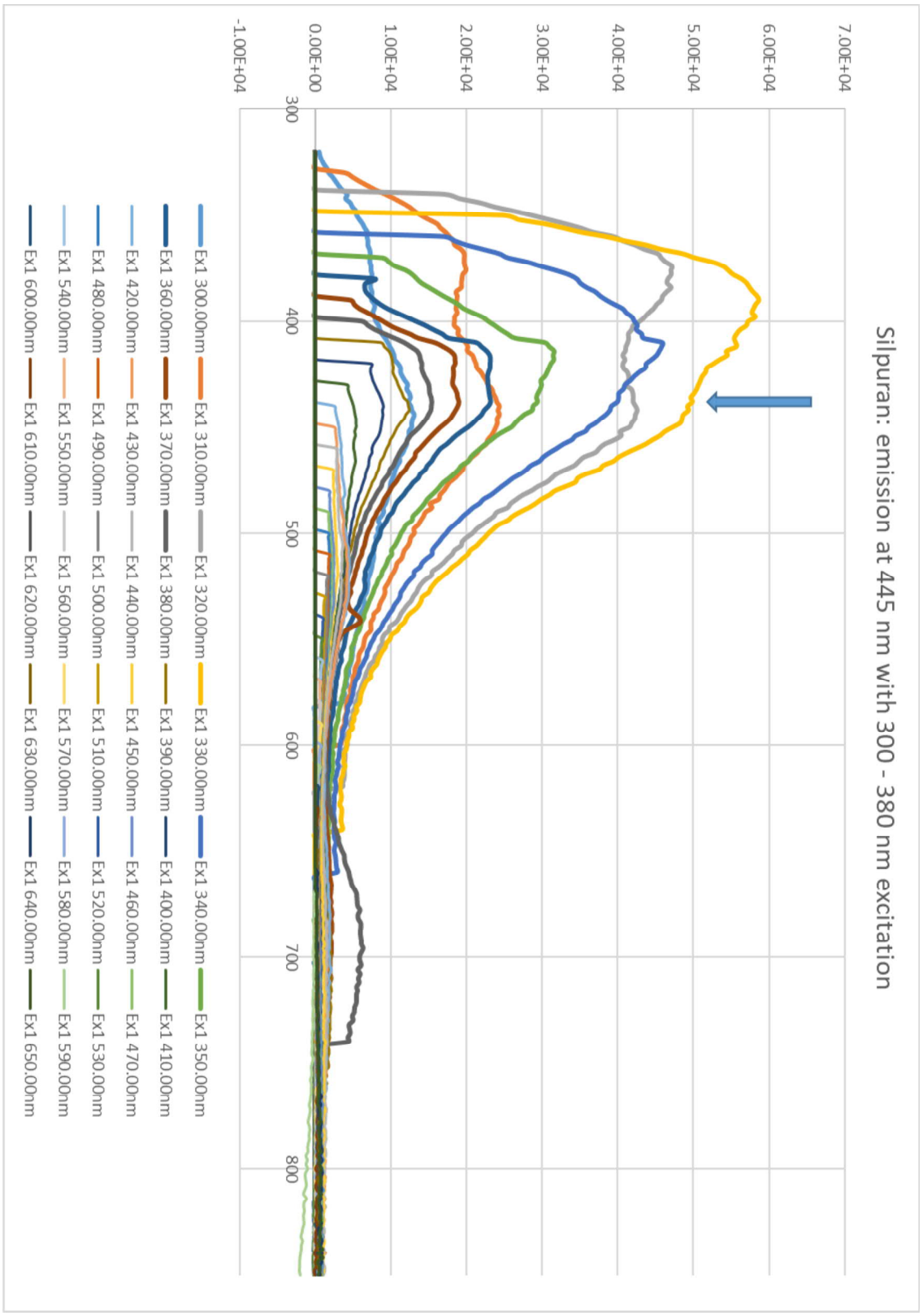
Silpuran: emission at 445 nm with 300 - 380 nm excitation
7.00E+04
6.00E+04
5.00E+04
4.00E+04
3.00E+04
2.00E+04
1.00E+04
0.00E+00
-1.00E+04
300
400
500
600
700
800
Ex1 300.00nm
Ex1 310.00nm
Ex1 320.00nm
Ex1 330.00nm
Ex1 340.00nm
Ex1 350.00nm
Ex1 360.00nm
Ex1 370.00nm
Ex1 380.00nm
Ex1 390.00nm
Ex1 400.00nm
Ex1 410.00nm
Ex1 420.00nm
Ex1 430.00nm
Ex1 440.00nm
Ex1 450.00nm
Ex1 460.00nm
Ex1 470.00nm
Ex1 480.00nm
Ex1 490.00nm
Ex1 500.00nm
Ex1 510.00nm
Ex1 520.00nm
Ex1 530.00nm
Ex1 540.00nm
Ex1 550.00nm
Ex1 560.00nm
Ex1 570.00nm
Ex1 580.00nm
Ex1 590.00nm
Ex1 600.00nm
Ex1 610.00nm
Ex1 620.00nm
Ex1 630.00nm
Ex1 640.00nm
Ex1 650.00nm

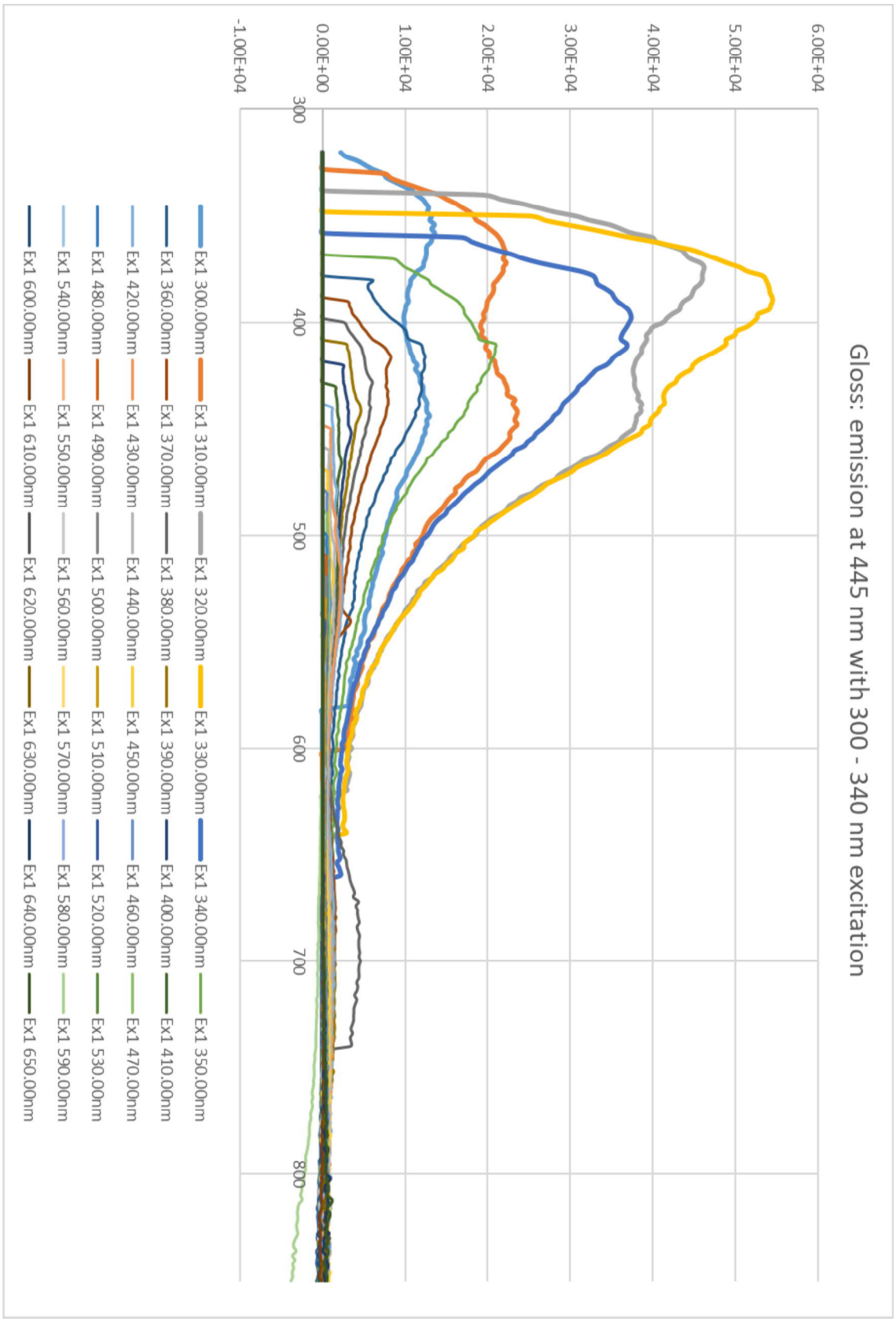
Gloss: emission at 445 nm with 300 - 340 nm excitation
6.00E+04
5.00E+04
4.00E+04
3.00E+04
2.00E+04
1.00E+04
0.00E+00
-1.00E+04
300
400
500
600
700
800
Ex1 300.00nm
Ex1 310.00nm
Ex1 320.00nm
Ex1 330.00nm
Ex1 340.00nm
Ex1 350.00nm
Ex1 360.00nm
Ex1 370.00nm
Ex1 380.00nm
Ex1 390.00nm
Ex1 400.00nm
Ex1 410.00nm
Ex1 420.00nm
Ex1 430.00nm
Ex1 440.00nm
Ex1 450.00nm
Ex1 460.00nm
Ex1 470.00nm
Ex1 480.00nm
Ex1 490.00nm
Ex1 500.00nm
Ex1 510.00nm
Ex1 520.00nm
Ex1 530.00nm
Ex1 540.00nm
Ex1 550.00nm
Ex1 560.00nm
Ex1 570.00nm
Ex1 580.00nm
Ex1 590.00nm
Ex1 600.00nm
Ex1 610.00nm
Ex1 620.00nm
Ex1 630.00nm
Ex1 640.00nm
Ex1 650.00nm

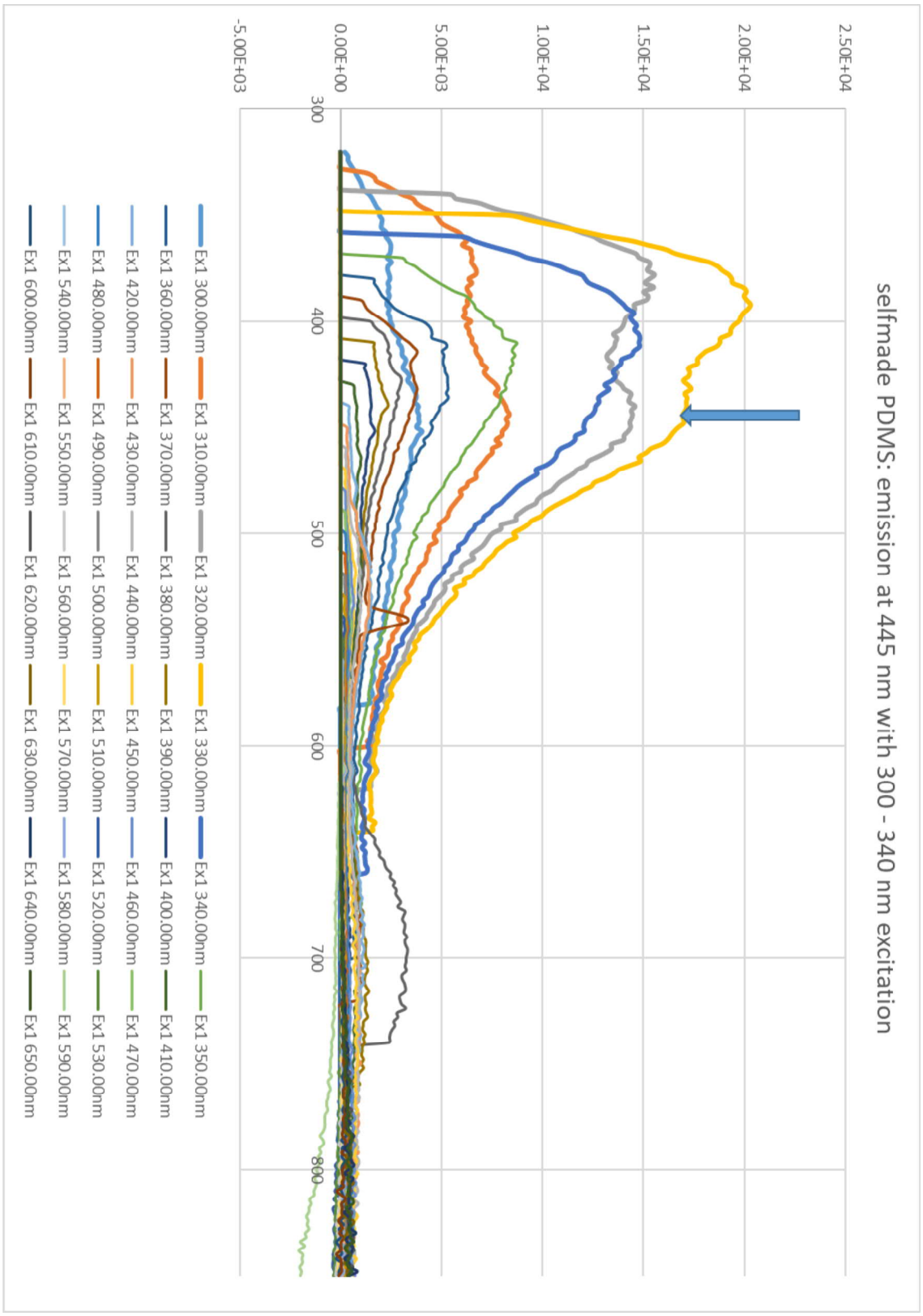
selfmade PDMS: emission at 445 nm with 300 - 340 nm excitation
2.50E+04
2.00E+04
1.50E+04
1.00E+04
5.00E+03
0.00E+00
-5.00E+03
300
400
500
600
700
800
Ex1 300.00nm
Ex1 310.00nm
Ex1 320.00nm
Ex1 330.00nm
Ex1 340.00nm
Ex1 350.00nm
Ex1 360.00nm
Ex1 370.00nm
Ex1 380.00nm
Ex1 390.00nm
Ex1 400.00nm
Ex1 410.00nm
Ex1 420.00nm
Ex1 430.00nm
Ex1 440.00nm
Ex1 450.00nm
Ex1 460.00nm
Ex1 470.00nm
Ex1 480.00nm
Ex1 490.00nm
Ex1 500.00nm
Ex1 510.00nm
Ex1 520.00nm
Ex1 530.00nm
Ex1 540.00nm
Ex1 550.00nm
Ex1 560.00nm
Ex1 570.00nm
Ex1 580.00nm
Ex1 590.00nm
Ex1 600.00nm
Ex1 610.00nm
Ex1 620.00nm
Ex1 630.00nm
Ex1 640.00nm
Ex1 650.00nm

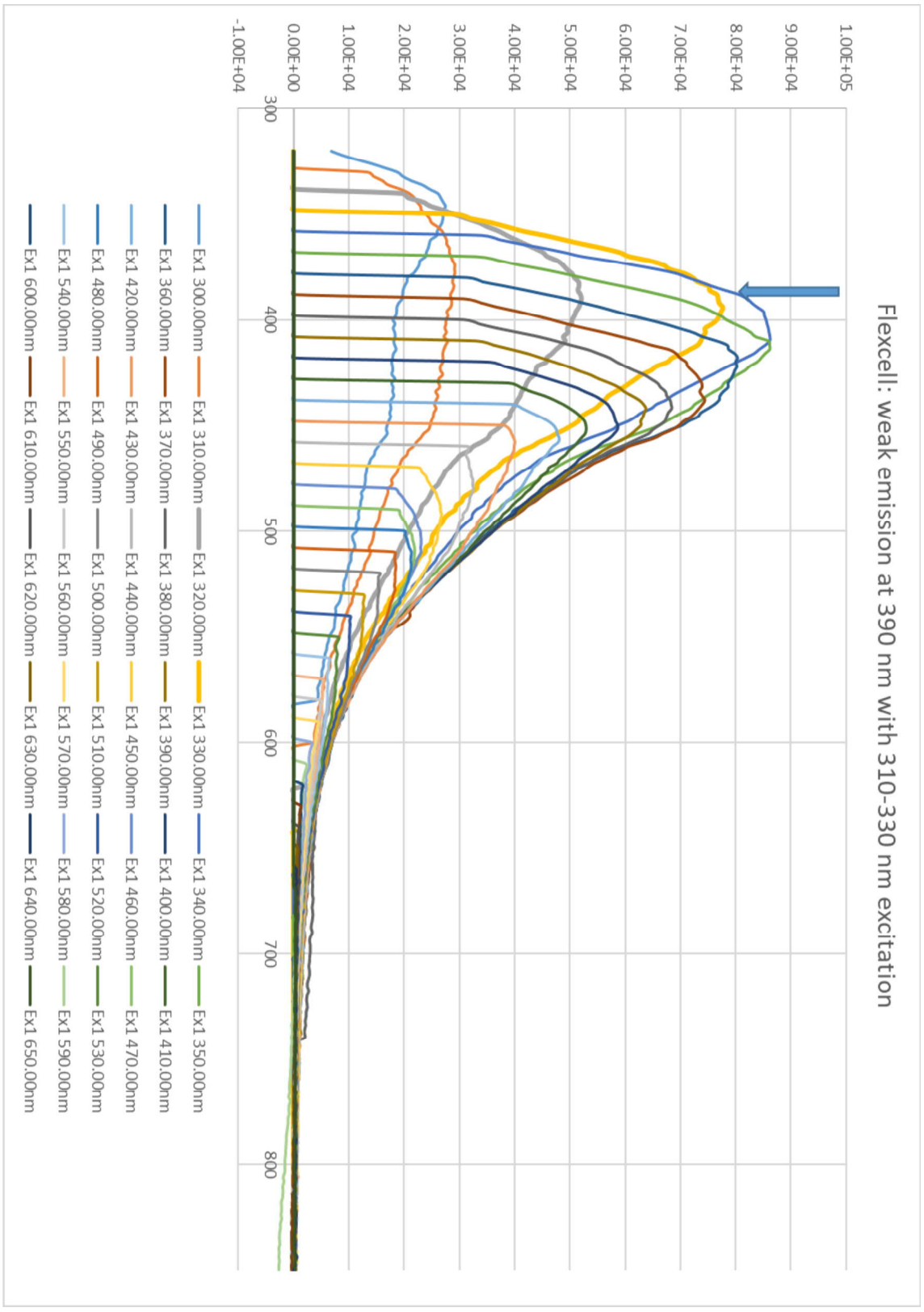
Flexcell: weak emission at 390 nm with 310-330 nm excitation
1.00E+05
9.00E+04
8.00E+04
7.00E+04
6.00E+04
5.00E+04
4.00E+04
3.00E+04
2.00E+04
1.00E+04
0.00E+00
-1.00E+04
300
400
500
600
700
800
Ex1 300.00nm
Ex1 310.00nm
Ex1 320.00nm
Ex1 330.00nm
Ex1 340.00nm
Ex1 350.00nm
Ex1 360.00nm
Ex1 370.00nm
Ex1 380.00nm
Ex1 390.00nm
Ex1 400.00nm
Ex1 410.00nm
Ex1 420.00nm
Ex1 430.00nm
Ex1 440.00nm
Ex1 450.00nm
Ex1 460.00nm
Ex1 470.00nm
Ex1 480.00nm
Ex1 490.00nm
Ex1 500.00nm
Ex1 510.00nm
Ex1 520.00nm
Ex1 530.00nm
Ex1 540.00nm
Ex1 550.00nm
Ex1 560.00nm
Ex1 570.00nm
Ex1 580.00nm
Ex1 590.00nm
Ex1 600.00nm
Ex1 610.00nm
Ex1 620.00nm
Ex1 630.00nm
Ex1 640.00nm
Ex1 650.00nm

APPENDIX B: CHARACTERIZATION DATA

Device 1 measurement 1

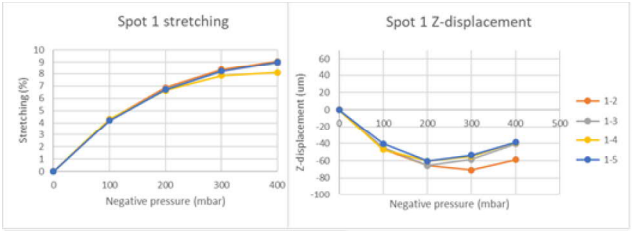

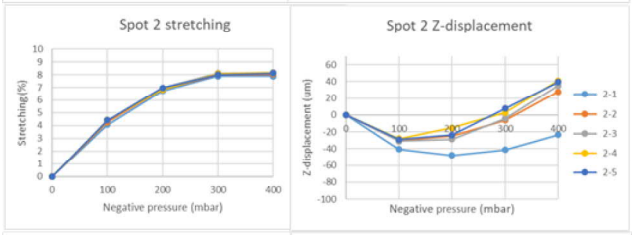

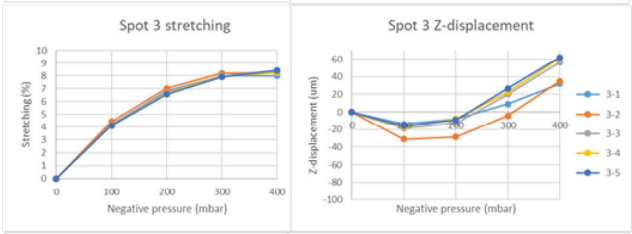

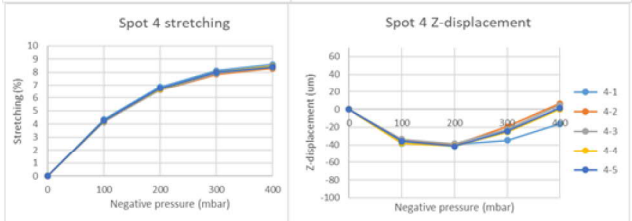

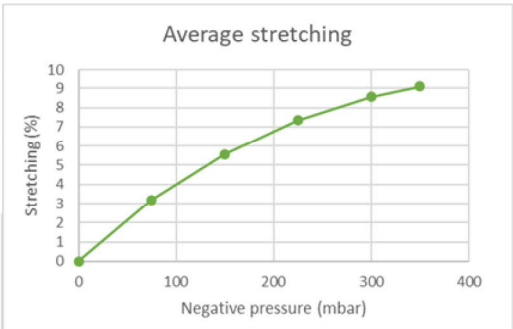

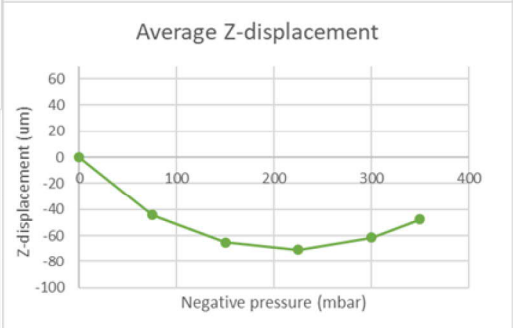

Spot 1 measure 1				Spot 1 measure 2				Spot 1 measure 3				Spot 1 measure 4				Spot 1 measure 5			
Pressure	Stretch	St. Dev.	Z	Pressure	Stretch	St. Dev.	Z	Pressure	Stretch	St. Dev.	Z	Pressure	Stretch	St. Dev.	Z	Pressure	Stretch	St. Dev.	Z
0-100				0-100	4.28	0.04	-46.33	0-100	4.25	0.09	-44.47	0-100	4.31	0.28	-47.07	0-100	4.20	0.08	-40.33
0-200				0-200	6.86	0.04	-65.29	0-200	6.75	0.10	-65.69	0-200	6.64	0.46	-60.52	0-200	6.71	0.08	-60.37
0-300				0-300	8.36	0.04	-70.79	0-300	8.20	0.11	-58.33	0-300	7.84	0.46	-54.78	0-300	8.21	0.07	-53.53
0-400				0-400	9.05	0.08	-58.81	0-400	8.92	0.12	-40.44	0-400	8.10	0.46	-38.75	0-400	8.98	0.07	-38.65
Spot 2 measure 1				Spot 2 measure 2				Spot 2 measure 3				Spot 2 measure 4				Spot 2 measure 5			
Pressure	Stretch	St. Dev.	Z	Pressure	Stretch	St. Dev.	Z	Pressure	Stretch	St. Dev.	Z	Pressure	Stretch	St. Dev.	Z	Pressure	Stretch	St. Dev.	Z
0-100	4.27	0.44	-40.79	0-100	4.26	0.41	-30.55	0-100	4.41	0.03	-31.22	0-100	4.41	0.02	-28.01	0-100	4.41	0.01	-29.09
0-200	6.94	0.45	-47.87	0-200	6.83	0.41	-25.24	0-200	6.97	0.05	-28.69	0-200	6.83	0.02	-15.16	0-200	6.98	0.03	-23.64
0-300	8.09	0.46	-41.43	0-300	7.99	0.42	-6.20	0-300	8.12	0.05	-4.28	0-300	8.08	0.04	2.83	0-300	7.99	0.03	7.68
0-400	8.10	0.47	-23.59	0-400	8.03	0.43	27.66	0-400	8.17	0.03	35.09	0-400	8.14	0.02	41.16	0-400	8.12	0.02	39.50
Spot 3 measure 1				Spot 3 measure 2				Spot 3 measure 3				Spot 3 measure 4				Spot 3 measure 5			
Pressure	Stretch	St. Dev.	Z	Pressure	Stretch	St. Dev.	Z	Pressure	Stretch	St. Dev.	Z	Pressure	Stretch	St. Dev.	Z	Pressure	Stretch	St. Dev.	Z
0-100	4.21	0.03	-13.79	0-100	4.44	0.03	-31.22	0-100	4.17	0.26	-18.79	0-100	4.13	0.40	-17.32	0-100	4.12	0.07	-15.79
0-200	6.80	0.02	-8.04	0-200	7.02	0.04	-28.69	0-200	6.68	0.29	-12.77	0-200	6.62	0.41	-7.67	0-200	6.56	0.23	-8.84
0-300	7.99	0.06	8.92	0-300	8.19	0.04	-4.28	0-300	8.00	0.25	20.23	0-300	7.93	0.41	22.64	0-300	7.90	0.21	26.63
0-400	7.99	0.13	32.29	0-400	8.26	0.09	35.09	0-400	8.43	0.06	56.34	0-400	8.23	0.42	61.32	0-400	8.40	0.18	62.12
Spot 4 measure 1				Spot 4 measure 2				Spot 4 measure 3				Spot 4 measure 4				Spot 4 measure 5			
Pressure	Stretch	St. Dev.	Z	Pressure	Stretch	St. Dev.	Z	Pressure	Stretch	St. Dev.	Z	Pressure	Stretch	St. Dev.	Z	Pressure	Stretch	St. Dev.	Z
0-100	4.34	0.03	-38.31	0-100	4.20	0.28	-34.92	0-100	4.16	0.14	-33.45	0-100	4.24	0.06	-37.87	0-100	4.27	0.06	-35.67
0-200	6.86	0.04	-39.41	0-200	6.60	0.30	-39.65	0-200	6.61	0.14	-38.44	0-200	6.67	0.06	-41.03	0-200	6.73	0.06	-41.46
0-300	8.13	0.03	-34.89	0-300	7.83	0.29	-19.39	0-300	7.91	0.15	-22.46	0-300	7.99	0.05	-25.43	0-300	8.00	0.05	-24.36
0-400	8.60	0.06	-16.22	0-400	8.30	0.29	6.44	0-400	8.38	0.15	4.53	0-400	8.46	0.04	0.12	0-400	8.39	0.05	1.49

Device 1 measurement 2

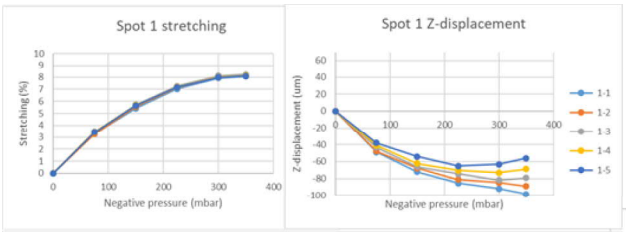

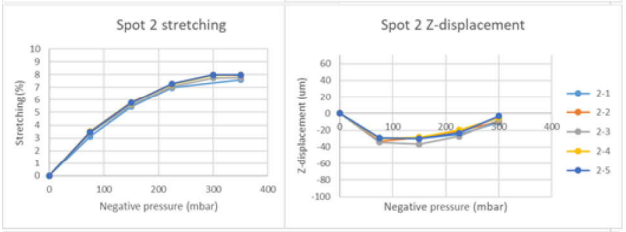

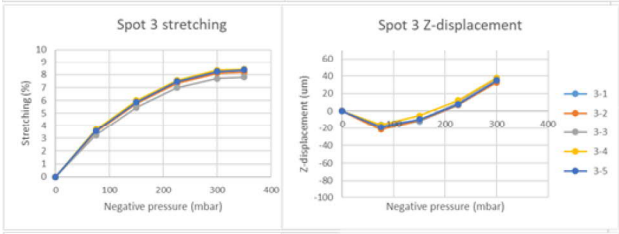

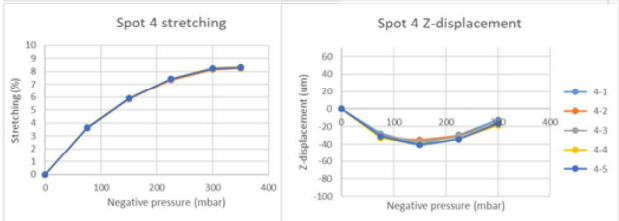

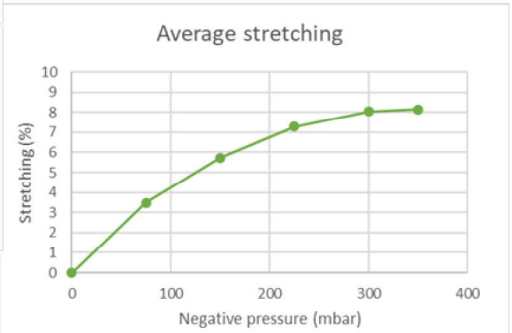

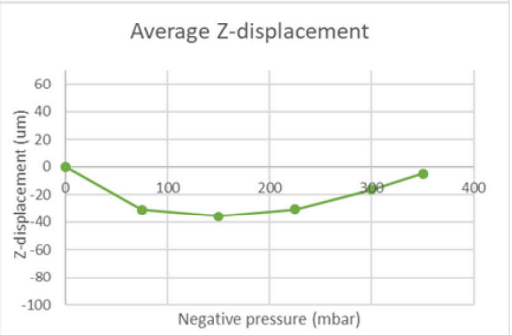

Spot 1 measure 1				Spot 1 measure 2				Spot 1 measure 3				Spot 1 measure 4				Spot 1 measure 5			
Pressure	Stretch	St. Dev.	Z	Pressure	Stretch	St. Dev.	Z	Pressure	Stretch	St. Dev.	Z	Pressure	Stretch	St. Dev.	Z	Pressure	Stretch	St. Dev.	Z
0-75	3.30	0.31	-48.77	0-75	3.27	0.47	-47.85	0-75	3.47	0.03	-43.21	0-75	3.45	0.03	-41.07	0-75	3.43	0.19	-38.16
0-150	5.44	0.38	-71.90	0-150	5.57	0.44	-67.77	0-150	5.72	0.04	-66.07	0-150	5.67	0.04	-62.16	0-150	5.66	0.13	-53.97
0-225	7.04	0.39	-85.24	0-225	7.16	0.45	-81.17	0-225	7.27	0.05	-74.11	0-225	7.19	0.05	-70.19	0-225	7.18	0.13	-65.20
0-300	7.93	0.39	-91.76	0-300	8.02	0.46	-84.82	0-300	8.11	0.08	-81.78	0-300	8.00	0.07	-72.83	0-300	7.98	0.13	-63.30
0-350	8.06	0.39	-96.27	0-350	8.17	0.47	-88.88	0-350	8.23	0.11	-79.00	0-350	8.11	0.09	-68.74	0-350	8.09	0.13	-56.11
Spot 2 measure 1				Spot 2 measure 2				Spot 2 measure 3				Spot 2 measure 4				Spot 2 measure 5			
Pressure	Stretch	St. Dev.	Z	Pressure	Stretch	St. Dev.	Z	Pressure	Stretch	St. Dev.	Z	Pressure	Stretch	St. Dev.	Z	Pressure	Stretch	St. Dev.	Z
0-75	3.13	0.48	-29.09	0-75	3.51	0.04	-32.89	0-75	3.40	0.26	-34.34	0-75	3.49	0.04	-29.74	0-75	3.48	0.03	-29.36
0-150	5.45	0.46	-29.63	0-150	5.76	0.05	-28.75	0-150	5.56	0.33	-36.69	0-150	5.73	0.06	-28.16	0-150	5.75	0.04	-30.07
0-225	6.98	0.46	-24.86	0-225	7.28	0.07	-21.13	0-225	7.06	0.35	-27.40	0-225	7.24	0.08	-19.61	0-225	7.27	0.06	-23.40
0-300	7.61	0.47	-10.87	0-300	7.97	0.08	-9.20	0-300	7.75	0.36	-7.69	0-300	7.96	0.09	-5.34	0-300	7.99	0.08	-3.32
0-350			5.06	0-350	7.97	0.07	7.90	0-350	7.76	0.35	9.44	0-350	7.97	0.07	12.70	0-350	7.97	0.07	13.24
Spot 3 measure 1				Spot 3 measure 2				Spot 3 measure 3				Spot 3 measure 4				Spot 3 measure 5			
Pressure	Stretch	St. Dev.	Z	Pressure	Stretch	St. Dev.	Z	Pressure	Stretch	St. Dev.	Z	Pressure	Stretch	St. Dev.	Z	Pressure	Stretch	St. Dev.	Z
0-75	3.63	0.10	-19.59	0-75	3.51	0.44	-21.58	0-75	3.24	0.07	-15.83	0-75	3.69	0.07	-15.97	0-75	3.60	0.10	-18.80
0-150	5.85	0.12	-11.75	0-150	5.76	0.46	-10.63	0-150	5.45	0.45	-10.56	0-150	5.99	0.09	-5.44	0-150	5.87	0.14	-9.55
0-225	7.42	0.12	6.86	0-225	7.32	0.47	6.89	0-225	7.00	0.45	9.10	0-225	7.56	0.10	12.06	0-225	7.46	0.15	7.71
0-300	8.22	0.12	34.41	0-300	8.13	0.48	32.61	0-300	7.70	0.46	37.43	0-300	8.34	0.08	37.67	0-300	8.26	0.12	34.84
0-350	8.30	0.12	55.26	0-350	8.17	0.48	52.47	0-350	7.80	0.46	55.26	0-350	8.41	0.05	57.30	0-350	8.38	0.07	52.48
Spot 4 measure 1				Spot 4 measure 2				Spot 4 measure 3				Spot 4 measure 4				Spot 4 measure 5			
Pressure	Stretch	St. Dev.	Z	Pressure	Stretch	St. Dev.	Z	Pressure	Stretch	St. Dev.	Z	Pressure	Stretch	St. Dev.	Z	Pressure	Stretch	St. Dev.	Z
0-75	3.60	0.12	-27.99	0-75	3.61	0.06	-32.37	0-75	3.64	0.05	-29.59	0-75	3.65	0.06	-33.04	0-75	3.63	0.05	-31.16
0-150	5.85	0.11	-39.58	0-150	5.82	0.07	-35.01	0-150	5.86	0.05	-37.11	0-150	5.88	0.06	-40.33	0-150	5.88	0.06	-40.73
0-225	7.36	0.12	-29.46	0-225	7.35	0.07	-30.57	0-225	7.41	0.05	-31.29	0-225	7.43	0.06	-34.09	0-225	7.43	0.06	-34.22
0-300	8.17	0.12	-12.31	0-300	8.15	0.07	-14.88	0-300	8.22	0.05	-14.48	0-300	8.25	0.07	-18.53	0-300	8.23	0.07	-16.63
0-350	8.27	0.12	0.41	0-350	8.25	0.09	-4.29	0-350	8.33	0.06	-4.24	0-350	8.34	0.08	-5.69	0-350	8.33	0.07	-3.58

Device 1 measurement 3

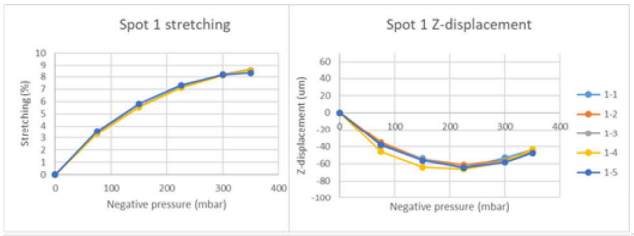

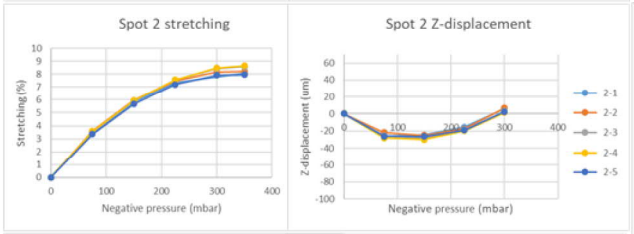

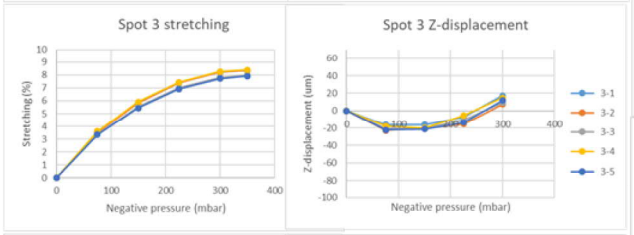

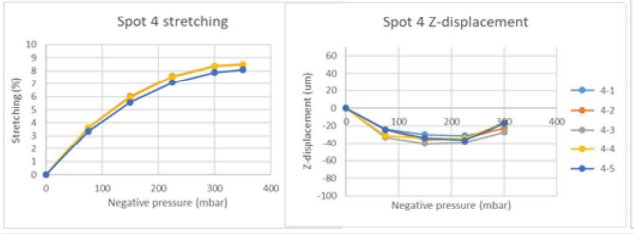

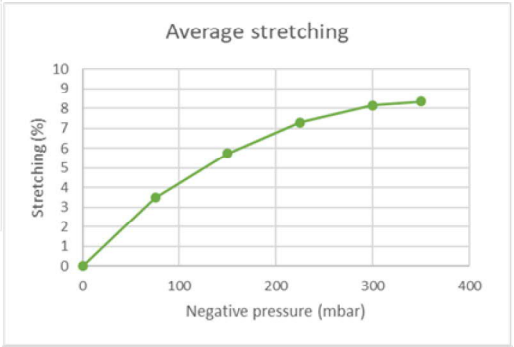

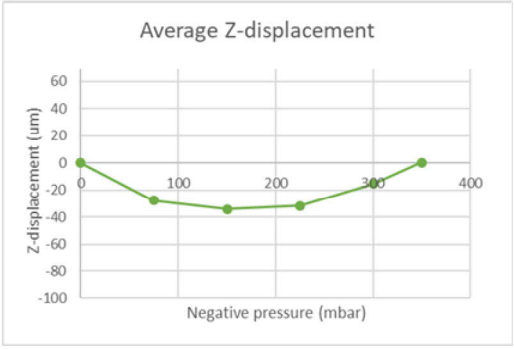

Spot 1 measure 1				Spot 1 measure 2				Spot 1 measure 3				Spot 1 measure 4				Spot 1 measure 5			
Pressure	Stretch	St. Dev.	Z	Pressure	Stretch	St. Dev.	Z	Pressure	Stretch	St. Dev.	Z	Pressure	Stretch	St. Dev.	Z	Pressure	Stretch	St. Dev.	Z
0-75	3.43	0.07	-36.34	0-75	3.41	0.05	-35.25	0-75	3.43	0.06	-39.02	0-75	3.34	0.09	-33.94	0-75	3.57	0.05	-38.21
0-150	5.62	0.10	-53.77	0-150	5.59	0.06	-54.40	0-150	5.59	0.13	-54.10	0-150	5.54	0.09	-53.90	0-150	5.81	0.07	-56.00
0-225	7.19	0.10	-64.02	0-225	7.15	0.07	-61.27	0-225	7.17	0.14	-64.84	0-225	7.11	0.10	-61.96	0-225	7.31	0.08	-64.63
0-300	8.18	0.10	-53.06	0-300	8.18	0.07	-55.88	0-300	8.19	0.14	-56.79	0-300	8.12	0.11	-54.92	0-300	8.16	0.10	-58.43
0-350	8.59	0.10	-43.66	0-350	8.59	0.08	-46.24	0-350	8.60	0.14	-47.04	0-350	8.54	0.11	-44.29	0-350	8.33	0.14	-47.37
Spot 2 measure 1				Spot 2 measure 2				Spot 2 measure 3				Spot 2 measure 4				Spot 2 measure 5			
Pressure	Stretch	St. Dev.	Z	Pressure	Stretch	St. Dev.	Z	Pressure	Stretch	St. Dev.	Z	Pressure	Stretch	St. Dev.	Z	Pressure	Stretch	St. Dev.	Z
0-75	3.50	0.02	-25.51	0-75	3.61	0.23	-21.52	0-75	3.54	0.01	-25.23	0-75	3.59	0.01	-27.76	0-75	3.36	0.30	-26.02
0-150	5.83	0.02	-24.63	0-150	5.95	0.27	-24.83	0-150	5.92	0.01	-28.31	0-150	5.93	0.02	-29.79	0-150	5.67	0.30	-26.15
0-225	7.35	0.03	-15.24	0-225	7.47	0.28	-17.30	0-225	7.54	0.02	-18.26	0-225	7.56	0.02	-19.55	0-225	7.19	0.30	-18.90
0-300	8.08	0.02	6.00	0-300	8.16	0.28	6.85	0-300	8.44	0.04	2.78	0-300	8.48	0.03	1.60	0-300	7.92	0.31	2.54
0-350	8.10	0.02	25.10	0-350	8.21	0.28	26.01	0-350	8.58	0.07	22.57	0-350	8.65	0.04	19.90	0-350	7.96	0.31	22.23
Spot 3 measure 1				Spot 3 measure 2				Spot 3 measure 3				Spot 3 measure 4				Spot 3 measure 5			
Pressure	Stretch	St. Dev.	Z	Pressure	Stretch	St. Dev.	Z	Pressure	Stretch	St. Dev.	Z	Pressure	Stretch	St. Dev.	Z	Pressure	Stretch	St. Dev.	Z
0-75	3.54	0.04	-16.42	0-75	3.51	0.04	-22.05	0-75	3.36	0.06	-20.61	0-75	3.61	0.04	-17.90	0-75	3.35	0.10	-22.44
0-150	5.83	0.05	-16.17	0-150	5.83	0.04	-20.39	0-150	5.53	0.08	-20.64	0-150	5.92	0.05	-20.16	0-150	5.43	0.13	-21.36
0-225	7.39	0.04	-7.30	0-225	7.40	0.03	-15.72	0-225	6.99	0.08	-10.43	0-225	7.44	0.04	-5.39	0-225	6.92	0.13	-13.76
0-300	8.22	0.03	17.17	0-300	8.21	0.03	7.19	0-300	7.79	0.05	9.36	0-300	8.25	0.03	14.56	0-300	7.72	0.12	11.64
0-350	8.34	0.05	36.14	0-350	8.34	0.06	26.44	0-350	7.97	0.03	29.79	0-350	8.38	0.05	33.28	0-350	7.92	0.13	30.87
Spot 4 measure 1				Spot 4 measure 2				Spot 4 measure 3				Spot 4 measure 4				Spot 4 measure 5			
Pressure	Stretch	St. Dev.	Z	Pressure	Stretch	St. Dev.	Z	Pressure	Stretch	St. Dev.	Z	Pressure	Stretch	St. Dev.	Z	Pressure	Stretch	St. Dev.	Z
0-75	3.61	0.02	-23.86	0-75	3.65	0.04	-24.44	0-75	3.33	0.19	-32.90	0-75	3.65	0.03	-31.10	0-75	3.36	0.05	-24.50
0-150	5.94	0.02	-29.91	0-150	6.00	0.04	-35.79	0-150	5.58	0.18	-40.40	0-150	5.93	0.03	-33.73	0-150	5.57	0.05	-33.73
0-225	7.55	0.02	-31.15	0-225	7.58	0.04	-34.17	0-225	7.07	0.18	-38.89	0-225	7.52	0.03	-34.39	0-225	7.08	0.04	-36.65
0-300	8.34	0.03	-22.79	0-300	8.38	0.02	-22.44	0-300	7.86	0.18	-27.45	0-300	8.35	0.02	-16.43	0-300	7.89	0.03	-17.33
0-350	8.47	0.04	-17.12	0-350	8.51	0.02	-9.73	0-350	8.06	0.19	-13.36	0-350	8.49	0.02	-2.14	0-350	8.10	0.02	0.84

Device 2

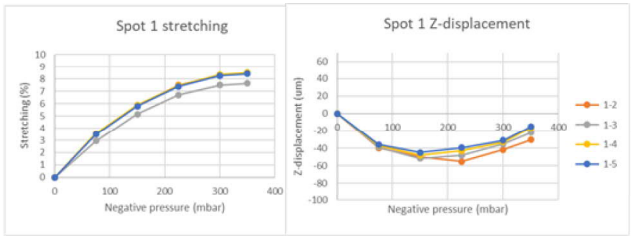

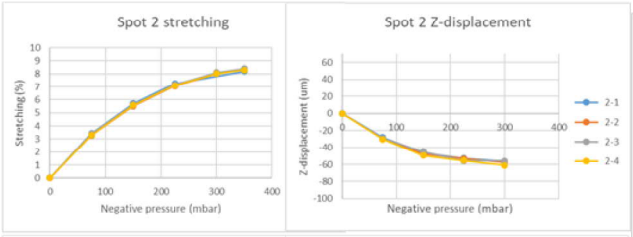

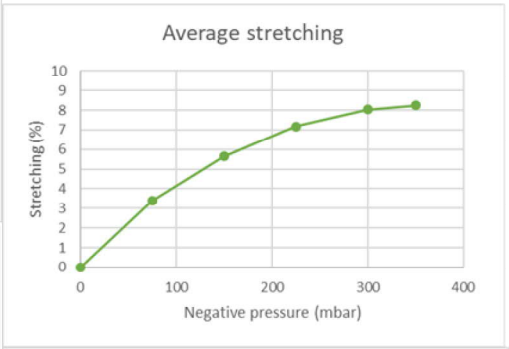

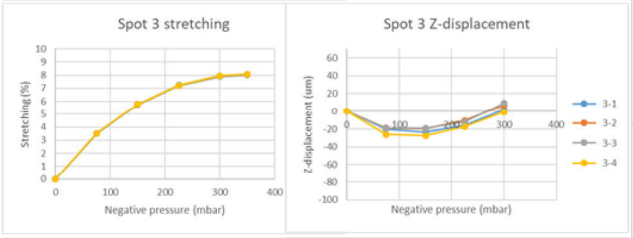

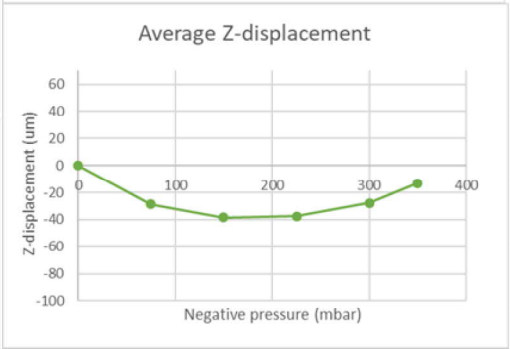

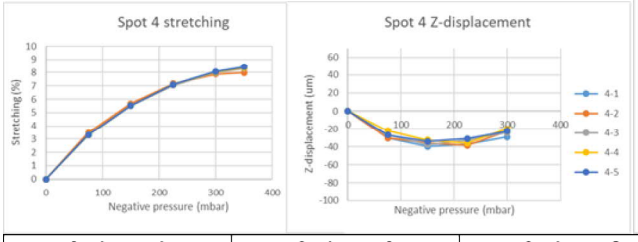

Spot 1 measure 1				Spot 1 measure 2				Spot 1 measure 3				Spot 1 measure 4				Spot 1 measure 5			
Pressure	Stretch	St. Dev.	Z	Pressure	Stretch	St. Dev.	Z	Pressure	Stretch	St. Dev.	Z	Pressure	Stretch	St. Dev.	Z	Pressure	Stretch	St. Dev.	Z
0-75				0-75	3.52	0.05	-39.89	0-75	2.95	1.08	-38.91	0-75	3.55	0.02	-37.11	0-75	3.50	0.06	-35.90
0-150				0-150	5.86	0.09	-49.69	0-150	5.15	1.17	-51.79	0-150	5.88	0.04	-48.17	0-150	5.80	0.11	-44.97
0-225				0-225	7.49	0.12	-55.24	0-225	6.69	1.19	-48.36	0-225	7.46	0.06	-43.21	0-225	7.39	0.15	-39.38
0-300				0-300	8.31	0.14	-41.88	0-300	7.50	1.20	-35.28	0-300	8.34	0.08	-33.12	0-300	8.24	0.18	-31.11
0-350				0-350	8.45	0.16	-30.40	0-350	7.64	1.20	-22.25	0-350	8.50	0.10	-16.72	0-350	8.41	0.20	-15.18

Spot 2 measure 1				Spot 2 measure 2				Spot 2 measure 3				Spot 2 measure 4				Spot 2 measure 5			
Pressure	Stretch	St. Dev.	Z	Pressure	Stretch	St. Dev.	Z	Pressure	Stretch	St. Dev.	Z	Pressure	Stretch	St. Dev.	Z	Pressure	Stretch	St. Dev.	Z
0-75	3.44	0.02	-28.08	0-75	3.29	0.17	-29.81	0-75	3.41	0.05	-28.91	0-75	3.30	0.23	-30.31	0-75			
0-150	5.71	0.12	-46.88	0-150	5.51	0.18	-47.67	0-150	5.62	0.06	-45.23	0-150	5.57	0.22	-49.66	0-150			
0-225	7.25	0.13	-52.85	0-225	7.07	0.18	-53.22	0-225	7.18	0.03	-55.79	0-225	7.10	0.23	-55.65	0-225			
0-300	8.19	0.13	-56.45	0-300	8.02	0.18	-57.54	0-300	8.11	0.03	-56.07	0-300	8.03	0.24	-61.15	0-300			
0-350	8.43	0.06	-51.24	0-350	8.34	0.19	-53.20	0-350	8.41	0.06	-53.66	0-350	8.31	0.25	0.00	0-350			

Spot 3 measure 1				Spot 3 measure 2				Spot 3 measure 3				Spot 3 measure 4				Spot 3 measure 5			
Pressure	Stretch	St. Dev.	Z	Pressure	Stretch	St. Dev.	Z	Pressure	Stretch	St. Dev.	Z	Pressure	Stretch	St. Dev.	Z	Pressure	Stretch	St. Dev.	Z
0-75	3.50	0.02	-20.24	0-75	3.50	0.02	-18.77	0-75	3.49	0.02	-19.32	0-75	3.53	0.02	-26.29	0-75			
0-150	5.75	0.03	-23.72	0-150	5.77	0.03	-19.62	0-150	5.73	0.04	-19.23	0-150	5.77	0.03	-27.42	0-150			
0-225	7.24	0.05	-16.21	0-225	7.23	0.04	-10.36	0-225	7.19	0.06	-12.13	0-225	7.23	0.04	-17.47	0-225			
0-300	7.94	0.06	2.00	0-300	7.95	0.05	7.04	0-300	7.90	0.06	9.39	0-300	7.95	0.05	-1.11	0-300			
0-350	8.05	0.06	20.26	0-350	8.06	0.05	25.32	0-350	8.02	0.06	22.19	0-350	8.07	0.05	15.56	0-350			

Spot 4 measure 1				Spot 4 measure 2				Spot 4 measure 3				Spot 4 measure 4				Spot 4 measure 5			
Pressure	Stretch	St. Dev.	Z	Pressure	Stretch	St. Dev.	Z	Pressure	Stretch	St. Dev.	Z	Pressure	Stretch	St. Dev.	Z	Pressure	Stretch	St. Dev.	Z
0-75	3.33	0.02	-30.16	0-75	3.48	0.05	-30.37	0-75	3.30	0.01	-26.58	0-75	3.31	0.02	-22.09	0-75	3.33	0.03	-26.97
0-150	5.55	0.04	-39.85	0-150	5.68	0.06	-36.06	0-150	5.51	0.02	-37.58	0-150	5.52	0.04	-32.64	0-150	5.53	0.04	-34.07
0-225	7.12	0.07	-37.05	0-225	7.17	0.07	-38.36	0-225	7.04	0.04	-32.71	0-225	7.10	0.07	-36.01	0-225	7.10	0.07	-31.05
0-300	8.08	0.10	-29.19	0-300	7.88	0.07	-22.63	0-300	7.99	0.07	-24.27	0-300	8.03	0.10	-19.81	0-300	8.07	0.10	-22.56
0-350	8.43	0.12	-15.19	0-350	8.00	0.05	-7.94	0-350	8.31	0.09	-11.35	0-350	8.36	0.13	-6.32	0-350	8.43	0.11	-11.39

Device 3

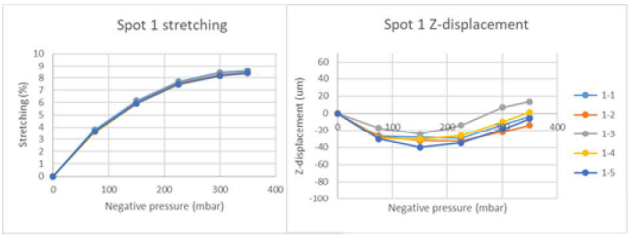

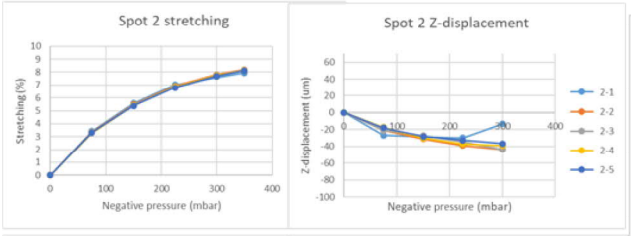

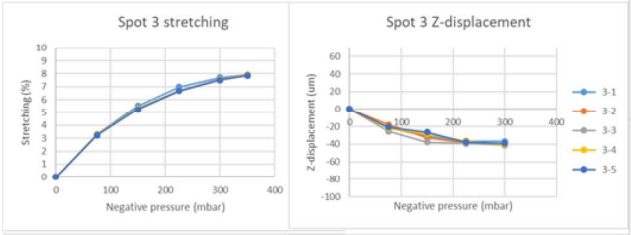

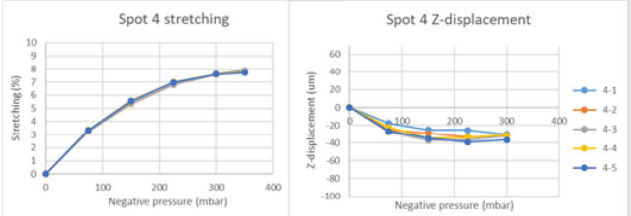

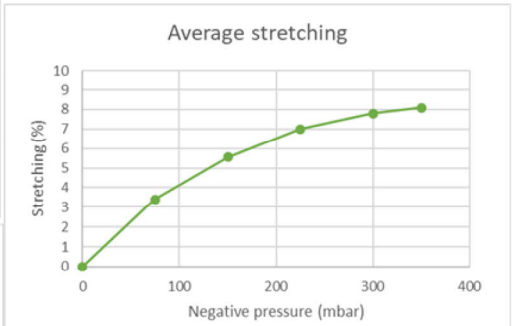

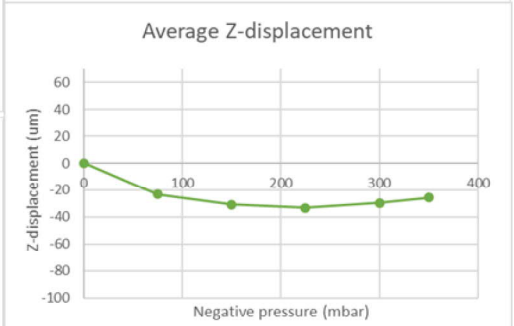

Spot 1 measure 1				Spot 1 measure 2				Spot 1 measure 3				Spot 1 measure 4				Spot 1 measure 5			
Pressure	Stretch	St. Dev.	Z	Pressure	Stretch	St. Dev.	Z	Pressure	Stretch	St. Dev.	Z	Pressure	Stretch	St. Dev.	Z	Pressure	Stretch	St. Dev.	Z
0-75	3.81	0.02	-26.74	0-75	3.66	0.01	-27.43	0-75	3.62	0.01	-17.09	0-75	3.58	0.01	-29.83	0-75	3.64	0.01	-30.43
0-150	6.15	0.02	-28.40	0-150	5.99	0.01	-32.36	0-150	5.92	0.01	-24.39	0-150	5.94	0.01	-30.77	0-150	5.94	0.01	-40.09
0-225	7.68	0.02	-29.71	0-225	7.52	0.02	-32.62	0-225	7.46	0.02	-14.04	0-225	7.46	0.02	-26.26	0-225	7.47	0.02	-34.77
0-300	8.43	0.02	-13.47	0-300	8.26	0.03	-22.09	0-300	8.15	0.03	6.75	0-300	8.17	0.02	-9.88	0-300	8.18	0.02	-19.01
0-350	8.58	0.02	-3.76	0-350	8.44	0.02	-13.99	0-350	8.36	0.03	13.44	0-350	8.40	0.02	1.33	0-350	8.40	0.02	-6.19
Spot 2 measure 1				Spot 2 measure 2				Spot 2 measure 3				Spot 2 measure 4				Spot 2 measure 5			
Pressure	Stretch	St. Dev.	Z	Pressure	Stretch	St. Dev.	Z	Pressure	Stretch	St. Dev.	Z	Pressure	Stretch	St. Dev.	Z	Pressure	Stretch	St. Dev.	Z
0-75	3.42	0.04	-26.74	0-75	3.37	0.04	-20.79	0-75	3.34	0.05	-21.06	0-75	3.31	0.05	-17.50	0-75	3.33	0.05	-18.00
0-150	5.56	0.06	-28.40	0-150	5.49	0.06	-31.26	0-150	5.41	0.07	-27.07	0-150	5.40	0.07	-30.27	0-150	5.38	0.07	-28.07
0-225	7.02	0.09	-29.71	0-225	6.91	0.08	-38.99	0-225	6.85	0.08	-34.75	0-225	6.85	0.09	-37.17	0-225	6.79	0.09	-32.80
0-300	7.94	0.08	-13.47	0-300	7.81	0.06	-43.56	0-300	7.76	0.07	-43.61	0-300	7.73	0.08	-39.14	0-300	7.68	0.09	-36.71
0-350	8.31	0.06	-3.76	0-350	8.20	0.05	-45.30	0-350	8.15	0.06	-44.88	0-350	8.12	0.08	-38.63	0-350	8.11	0.08	-41.95
Spot 3 measure 1				Spot 3 measure 2				Spot 3 measure 3				Spot 3 measure 4				Spot 3 measure 5			
Pressure	Stretch	St. Dev.	Z	Pressure	Stretch	St. Dev.	Z	Pressure	Stretch	St. Dev.	Z	Pressure	Stretch	St. Dev.	Z	Pressure	Stretch	St. Dev.	Z
0-75	3.30	0.01	-21.65	0-75	3.23	0.01	-17.71	0-75	3.27	0.01	-25.31	0-75	3.27	0.01	-21.85	0-75	3.23	0.00	-20.54
0-150	5.53	0.03	-31.07	0-150	5.27	0.02	-32.59	0-150	5.34	0.01	-37.58	0-150	5.30	0.01	-28.26	0-150	5.24	0.01	-26.34
0-225	6.99	0.04	-36.29	0-225	6.68	0.02	-38.35	0-225	6.72	0.01	-39.33	0-225	6.69	0.01	-36.36	0-225	6.69	0.01	-37.72
0-300	7.70	0.05	-36.65	0-300	7.52	0.02	-39.76	0-300	7.57	0.01	-41.18	0-300	7.53	0.02	-40.22	0-300	7.51	0.01	-38.81
0-350	7.91	0.04	-34.66	0-350	7.88	0.01	-37.67	0-350	7.94	0.02	-43.26	0-350	7.90	0.02	-41.30	0-350	7.86	0.01	-36.13
Spot 4 measure 1				Spot 4 measure 2				Spot 4 measure 3				Spot 4 measure 4				Spot 4 measure 5			
Pressure	Stretch	St. Dev.	Z	Pressure	Stretch	St. Dev.	Z	Pressure	Stretch	St. Dev.	Z	Pressure	Stretch	St. Dev.	Z	Pressure	Stretch	St. Dev.	Z
0-75	3.27	0.03	-17.62	0-75	3.28	0.03	-25.09	0-75	3.26	0.03	-27.87	0-75	3.37	0.05	-22.32	0-75	3.35	0.04	-26.61
0-150	5.38	0.03	-25.09	0-150	5.36	0.03	-29.11	0-150	5.39	0.04	-37.18	0-150	5.59	0.05	-34.38	0-150	5.56	0.05	-34.88
0-225	6.80	0.01	-25.43	0-225	6.82	0.02	-33.13	0-225	6.81	0.03	-36.57	0-225	6.99	0.03	-33.88	0-225	6.97	0.03	-38.95
0-300	7.63	0.02	-30.12	0-300	7.59	0.02	-31.89	0-300	7.58	0.02	-31.82	0-300	7.60	0.01	-30.91	0-300	7.58	0.01	-36.74
0-350	7.90	0.03	-19.74	0-350	7.88	0.04	-25.21	0-350	7.89	0.02	-30.94	0-350	7.72	0.03	-29.99	0-350	7.71	0.04	-29.20

Device 4

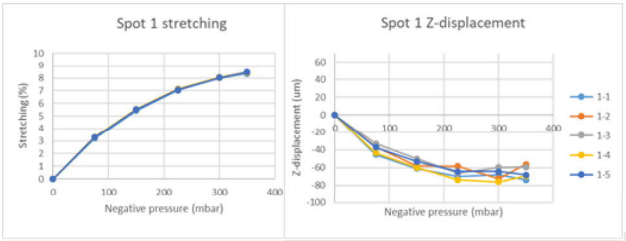

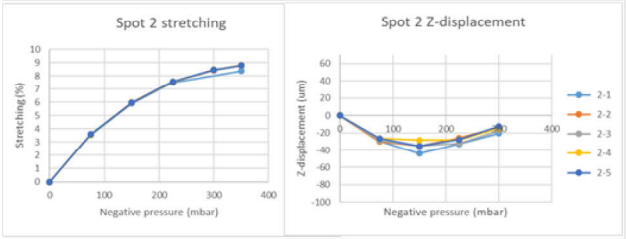

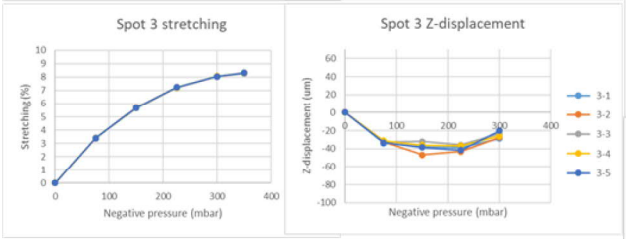

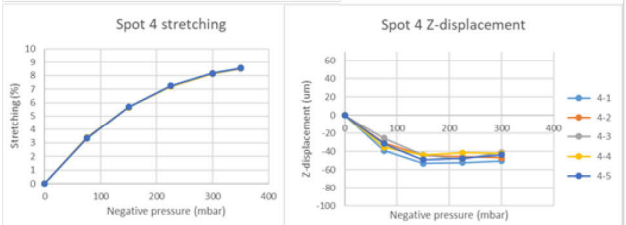

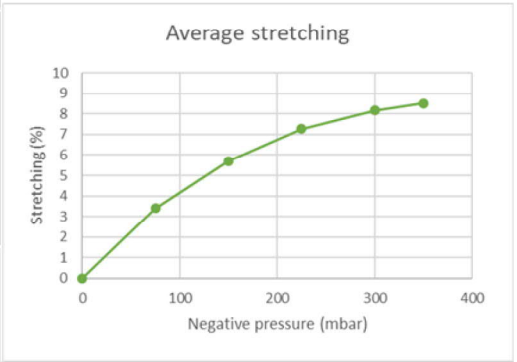

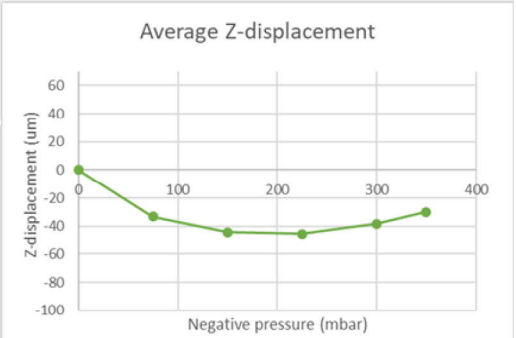

Spot 1 measure 1				Spot 1 measure 2				Spot 1 measure 3				Spot 1 measure 4				Spot 1 measure 5			
Pressure	Stretch	St. Dev.	Z	Pressure	Stretch	St. Dev.	Z	Pressure	Stretch	St. Dev.	Z	Pressure	Stretch	St. Dev.	Z	Pressure	Stretch	St. Dev.	Z
0-75	3.18	0.03	-45.41	0-75	3.28	0.04	-36.40	0-75	3.29	0.04	-33.16	0-75	3.31	0.03	-43.37	0-75	3.28	0.03	-37.21
0-150	5.42	0.06	-60.79	0-150	5.53	0.06	-58.07	0-150	5.53	0.06	-50.01	0-150	5.54	0.04	-59.93	0-150	5.52	0.04	-53.10
0-225	7.03	0.08	-69.58	0-225	7.07	0.09	-58.29	0-225	7.13	0.09	-66.40	0-225	7.11	0.07	-73.65	0-225	7.08	0.07	-64.27
0-300	8.01	0.09	-68.20	0-300	8.05	0.10	-72.18	0-300	8.06	0.09	-59.52	0-300	8.04	0.08	-75.98	0-300	8.02	0.09	-64.25
0-350	8.34	0.10	-73.87	0-350	8.44	0.12	-56.07	0-350	8.49	0.09	-59.37	0-350	8.44	0.08	-69.33	0-350	8.45	0.10	-68.03
Spot 2 measure 1				Spot 2 measure 2				Spot 2 measure 3				Spot 2 measure 4				Spot 2 measure 5			
Pressure	Stretch	St. Dev.	Z	Pressure	Stretch	St. Dev.	Z	Pressure	Stretch	St. Dev.	Z	Pressure	Stretch	St. Dev.	Z	Pressure	Stretch	St. Dev.	Z
0-75	3.55	0.01	-29.32	0-75	3.60	0.02	-30.00	0-75	3.59	0.01	-28.67	0-75	3.58	0.01	-26.47	0-75	3.58	0.01	-26.46
0-150	5.93	0.02	-43.90	0-150	5.98	0.01	-34.92	0-150	5.97	0.01	-35.31	0-150	5.97	0.01	-28.51	0-150	5.97	0.01	-35.40
0-225	7.50	0.02	-32.88	0-225	7.58	0.01	-25.92	0-225	7.59	0.01	-31.85	0-225	7.56	0.01	-27.94	0-225	7.57	0.01	-27.68
0-300	8.38	0.02	-20.33	0-300	8.44	0.02	-13.31	0-300	8.48	0.02	-17.37	0-300	8.47	0.01	-14.30	0-300	8.47	0.02	-12.48
0-350	8.72	0.02	-7.40	0-350	8.81	0.02	-5.41	0-350	8.78	0.02	2.50	0-350	8.80	0.02	-3.20	0-350	8.80	0.02	-2.41
Spot 3 measure 1				Spot 3 measure 2				Spot 3 measure 3				Spot 3 measure 4				Spot 3 measure 5			
Pressure	Stretch	St. Dev.	Z	Pressure	Stretch	St. Dev.	Z	Pressure	Stretch	St. Dev.	Z	Pressure	Stretch	St. Dev.	Z	Pressure	Stretch	St. Dev.	Z
0-75	3.42	0.02	-33.94	0-75	3.39	0.01	-32.73	0-75	3.40	0.03	-32.26	0-75	3.38	0.02	-31.29	0-75	3.39	0.02	-33.21
0-150	5.70	0.03	-37.97	0-150	5.69	0.02	-46.64	0-150	5.65	0.02	-32.06	0-150	5.68	0.03	-36.04	0-150	5.68	0.02	-38.52
0-225	7.24	0.03	-38.57	0-225	7.23	0.02	-43.19	0-225	7.22	0.03	-35.84	0-225	7.22	0.03	-36.73	0-225	7.24	0.03	-41.56
0-300	8.03	0.03	-28.71	0-300	8.03	0.03	-27.39	0-300	8.04	0.03	-23.57	0-300	8.06	0.03	-26.08	0-300	8.05	0.03	-20.18
0-350	8.28	0.03	-9.97	0-350	8.30	0.03	-17.75	0-350	8.29	0.03	-12.61	0-350	8.32	0.03	-12.05	0-350	8.32	0.03	-12.49
Spot 4 measure 1				Spot 4 measure 2				Spot 4 measure 3				Spot 4 measure 4				Spot 4 measure 5			
Pressure	Stretch	St. Dev.	Z	Pressure	Stretch	St. Dev.	Z	Pressure	Stretch	St. Dev.	Z	Pressure	Stretch	St. Dev.	Z	Pressure	Stretch	St. Dev.	Z
0-75	3.36	0.01	-39.19	0-75	3.33	0.02	-30.42	0-75	3.30	0.01	-25.50	0-75	3.38	0.01	-35.67	0-75	3.34	0.01	-31.72
0-150	5.68	0.03	-53.09	0-150	5.66	0.03	-44.18	0-150	5.65	0.03	-44.13	0-150	5.66	0.02	-44.07	0-150	5.67	0.03	-49.15
0-225	7.23	0.05	-52.13	0-225	7.21	0.05	-45.69	0-225	7.21	0.05	-48.46	0-225	7.20	0.04	-41.54	0-225	7.24	0.05	-47.67
0-300	8.16	0.06	-50.30	0-300	8.13	0.07	-46.91	0-300	8.12	0.06	-40.98	0-300	8.15	0.06	-42.10	0-300	8.17	0.07	-43.63
0-350	8.55	0.07	-42.70	0-350	8.52	0.07	-35.83	0-350	8.52	0.07	-36.25	0-350	8.55	0.07	-39.74	0-350	8.55	0.08	-34.99

Device 5

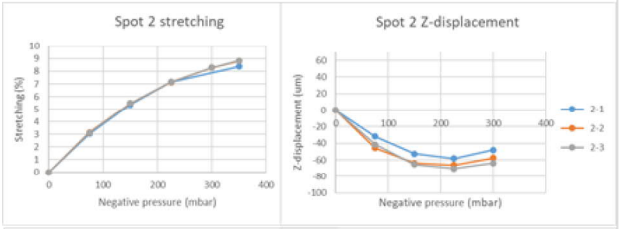

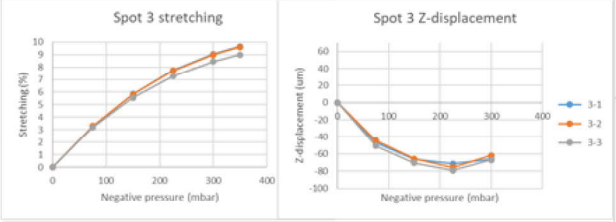

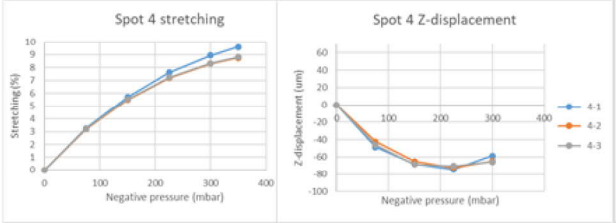

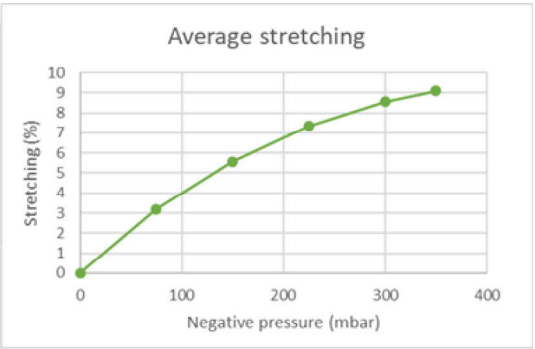

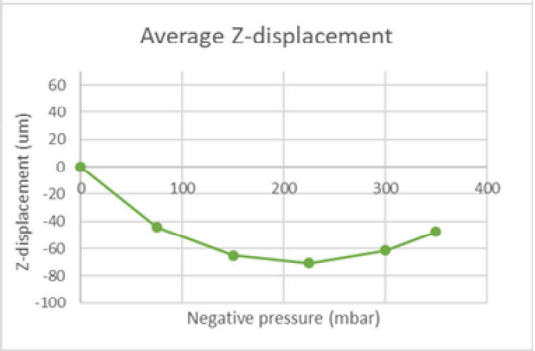

Spot 2 measure 1			
Pressure	Stretch	St. Dev.	Z
0-75	3.05	0.03	-31.72
0-150	5.36	0.03	-52.41
0-225	7.15	0.04	-58.25
0-300	8.37	0.04	-47.90
0-350	8.84	0.04	-36.87

Spot 2 measure 2			
Pressure	Stretch	St. Dev.	Z
0-75	3.14	0.02	-45.77
0-150	5.47	0.03	-63.71
0-225	7.15	0.04	-66.04
0-300	8.28	0.04	-57.51
0-350	8.81	0.04	-43.05

Spot 2 measure 3			
Pressure	Stretch	St. Dev.	Z
0-75	3.12	0.02	-41.25
0-150	5.46	0.03	-65.46
0-225	7.16	0.04	-70.38
0-300	8.30	0.04	-63.68
0-350	8.83	0.04	-49.01

Spot 3 measure 1			
Pressure	Stretch	St. Dev.	Z
0-75	3.28	0.01	-47.28
0-150	5.84	0.01	-66.35
0-225	7.72	0.02	-71.40
0-300	9.03	0.04	-66.10
0-350	9.64	0.04	-45.50

Spot 3 measure 2			
Pressure	Stretch	St. Dev.	Z
0-75	3.31	0.01	-44.40
0-150	5.82	0.01	-65.72
0-225	7.71	0.03	-75.44
0-300	9.00	0.04	-61.75
0-350	9.60	0.05	-48.27

Spot 3 measure 3			
Pressure	Stretch	St. Dev.	Z
0-75	3.20	0.01	-50.63
0-150	5.54	0.02	-70.47
0-225	7.28	0.03	-79.08
0-300	8.44	0.02	-66.88
0-350	8.99	0.02	-53.30

Spot 4 measure 1			
Pressure	Stretch	St. Dev.	Z
0-75	3.25	0.03	-48.48
0-150	5.71	0.05	-67.80
0-225	7.60	0.05	-74.33
0-300	8.93	0.04	-58.63
0-350	9.59	0.04	-51.23

Spot 4 measure 2			
Pressure	Stretch	St. Dev.	Z
0-75	3.18	0.02	-42.33
0-150	5.49	0.03	-64.99
0-225	7.18	0.04	-72.10
0-300	8.29	0.04	-64.74
0-350	8.75	0.07	-46.72

Spot 4 measure 3			
Pressure	Stretch	St. Dev.	Z
0-75	3.21	0.02	-46.05
0-150	5.52	0.04	-68.46
0-225	7.23	0.05	-70.21
0-300	8.32	0.06	-65.67
0-350	8.81	0.06	-54.51

Device 6

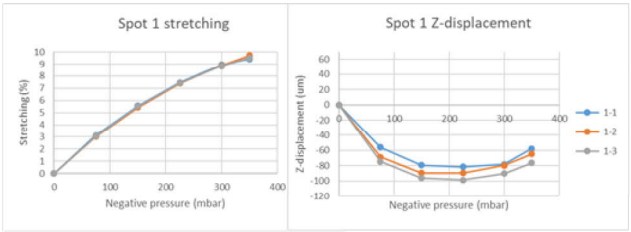

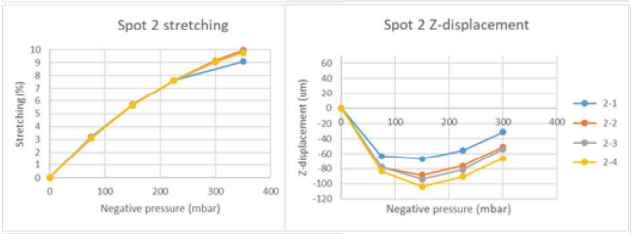

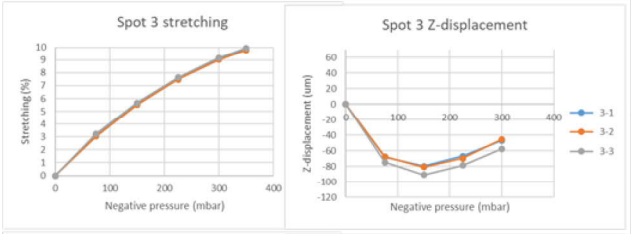

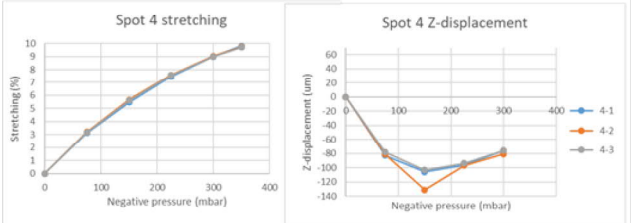

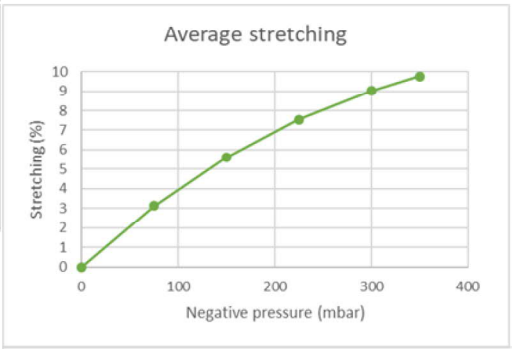

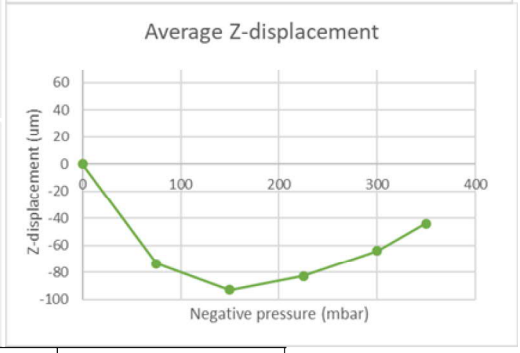

Spot 1 measure 1				Spot 1 measure 2				Spot 1 measure 3				Spot 1 measure 4			
Pressure	Stretch	St. Dev.	Z	Pressure	Stretch	St. Dev.	Z	Pressure	Stretch	St. Dev.	Z	Pressure	Stretch	St. Dev.	Z
0-75	3.11	0.02	-55.94	0-75	3.00	0.02	-68.65	0-75	3.05	0.00	-74.43	0-75			
0-150	5.55	0.03	-79.38	0-150	5.43	0.02	-89.35	0-150	5.52	0.01	-95.99	0-150			
0-225	7.44	0.02	-81.45	0-225	7.38	0.01	-89.39	0-225	7.43	0.02	-98.67	0-225			
0-300	8.94	0.03	-78.13	0-300	8.88	0.01	-79.80	0-300	8.83	0.03	-90.03	0-300			
0-350	9.54	0.15	-57.57	0-350	9.71	0.02	-64.75	0-350	9.52	0.04	-76.43	0-350			
Spot 2 measure 1				Spot 2 measure 2				Spot 2 measure 3				Spot 2 measure 4			
Pressure	Stretch	St. Dev.	Z	Pressure	Stretch	St. Dev.	Z	Pressure	Stretch	St. Dev.	Z	Pressure	Stretch	St. Dev.	Z
0-75	3.21	0.02	-63.38	0-75	3.11	0.02	-78.50	0-75	3.21	0.02	-78.14	0-75	3.13	0.02	-83.63
0-150	5.67	0.02	-66.90	0-150	5.70	0.04	-88.73	0-150	5.65	0.03	-94.35	0-150	5.67	0.03	-103.62
0-225	7.63	0.04	-55.47	0-225	7.64	0.06	-76.58	0-225	7.61	0.03	-81.50	0-225	7.64	0.04	-90.79
0-300	9.09	0.05	-31.13	0-300	9.16	0.07	-50.57	0-300	9.04	0.04	-53.84	0-300	9.08	0.05	-66.19
0-350	9.85	0.06	-8.40	0-350	9.95	0.07	-28.81	0-350	9.81	0.04	-35.88	0-350	9.76	0.06	-43.26
Spot 3 measure 1				Spot 3 measure 2				Spot 3 measure 3				Spot 3 measure 4			
Pressure	Stretch	St. Dev.	Z	Pressure	Stretch	St. Dev.	Z	Pressure	Stretch	St. Dev.	Z	Pressure	Stretch	St. Dev.	Z
0-75	3.08	0.02	-67.94	0-75	3.05	0.03	-67.62	0-75	3.25	0.02	-74.70	0-75			
0-150	5.58	0.04	-79.45	0-150	5.52	0.05	-80.74	0-150	5.66	0.03	-90.67	0-150			
0-225	7.53	0.04	-66.90	0-225	7.49	0.07	-69.49	0-225	7.63	0.04	-78.66	0-225			
0-300	9.07	0.05	-46.77	0-300	9.02	0.07	-45.22	0-300	9.17	0.05	-57.61	0-300			
0-350	9.86	0.04	-23.66	0-350	9.78	0.07	-24.96	0-350	9.94	0.04	-32.85	0-350			
Spot 4 measure 1				Spot 4 measure 2				Spot 4 measure 3				Spot 4 measure 4			
Pressure	Stretch	St. Dev.	Z	Pressure	Stretch	St. Dev.	Z	Pressure	Stretch	St. Dev.	Z	Pressure	Stretch	St. Dev.	Z
0-75	3.13	0.01	-82.68	0-75	3.21	0.01	-81.20	0-75	3.17	0.01	-77.93	0-75			
0-150	5.48	0.27	-105.88	0-150	5.66	0.01	-130.97	0-150	5.60	0.02	-103.13	0-150			
0-225	7.46	0.28	-95.79	0-225	7.59	0.01	-96.66	0-225	7.56	0.03	-93.68	0-225			
0-300	8.98	0.28	-76.04	0-300	9.03	0.03	-80.58	0-300	8.99	0.05	-75.44	0-300			
0-350	9.79	0.28	-58.27	0-350	9.73	0.04	-60.63	0-350	9.69	0.06	-57.54	0-350			

No stabilator ring, 4 mm vacuum chamber

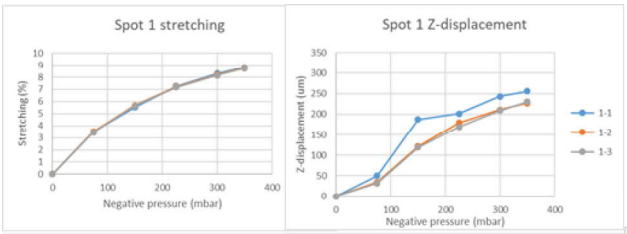

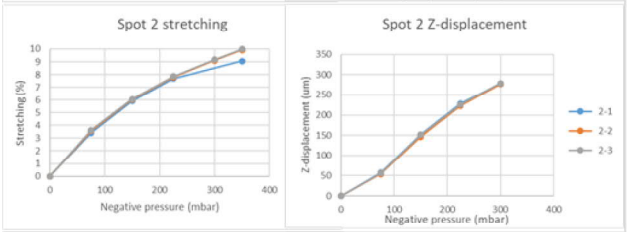

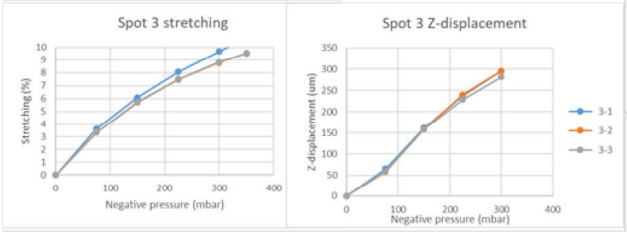

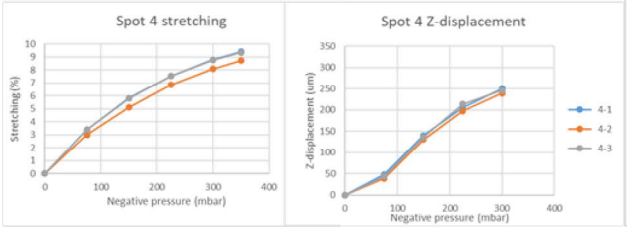

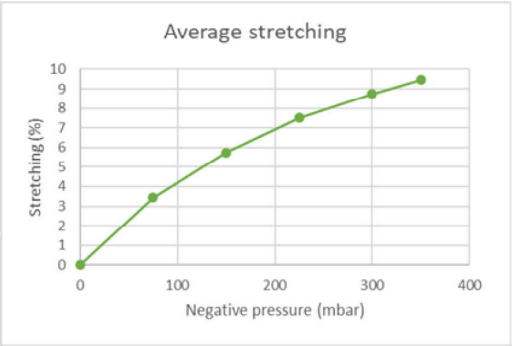

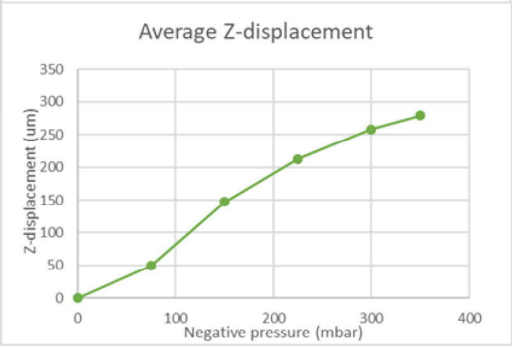

Spot 1 measure 1				Spot 1 measure 2				Spot 1 measure 3			
Pressure	Stretch	St. Dev.	Z	Pressure	Stretch	St. Dev.	Z	Pressure	Stretch	St. Dev.	Z
0-75	3.49	0.06	50.33	0-75	3.51	0.03	34.88	0-75	3.46	0.07	32.08
0-150	5.52	0.02	187.24	0-150	5.70	0.04	121.50	0-150	5.65	0.08	118.78
0-225	7.25	0.05	201.26	0-225	7.22	0.05	179.12	0-225	7.18	0.08	169.09
0-300	8.31	0.04	243.43	0-300	8.22	0.05	210.66	0-300	8.16	0.06	208.71
0-350	8.83	0.05	256.16	0-350	8.80	0.04	226.77	0-350	8.73	0.04	230.25
Spot 2 measure 1				Spot 2 measure 2				Spot 2 measure 3			
Pressure	Stretch	St. Dev.	Z	Pressure	Stretch	St. Dev.	Z	Pressure	Stretch	St. Dev.	Z
0-75	3.41	0.88	57.35	0-75	3.56	0.08	53.58	0-75	3.63	0.05	55.96
0-150	5.91	0.85	151.70	0-150	6.01	0.10	146.82	0-150	6.06	0.07	151.35
0-225	7.70	0.86	228.53	0-225	7.80	0.13	223.26	0-225	7.85	0.09	225.88
0-300	9.06	0.88	277.32	0-300	9.09	0.16	276.69	0-300	9.17	0.13	278.81
0-350	9.88	0.90	303.59	0-350	9.92	0.18	298.32	0-350	9.99	0.15	299.19
Spot 3 measure 1				Spot 3 measure 2				Spot 3 measure 3			
Pressure	Stretch	St. Dev.	Z	Pressure	Stretch	St. Dev.	Z	Pressure	Stretch	St. Dev.	Z
0-75	3.64	0.10	64.64	0-75	3.37	0.08	58.58	0-75	3.36	0.07	59.22
0-150	6.08	0.14	162.25	0-150	5.73	0.11	159.51	0-150	5.71	0.12	158.60
0-225	8.07	0.17	237.46	0-225	7.47	0.15	239.76	0-225	7.50	0.15	228.55
0-300	9.68	0.19	295.42	0-300	8.78	0.18	295.12	0-300	8.82	0.18	281.59
0-350	10.80	0.17	311.04	0-350	9.54	0.18	310.57	0-350	9.53	0.19	312.27
Spot 4 measure 1				Spot 4 measure 2				Spot 4 measure 3			
Pressure	Stretch	St. Dev.	Z	Pressure	Stretch	St. Dev.	Z	Pressure	Stretch	St. Dev.	Z
0-75	3.38	0.05	47.61	0-75	3.01	0.64	38.40	0-75	3.40	0.06	43.14
0-150	5.80	0.05	140.29	0-150	5.10	0.78	130.36	0-150	5.78	0.07	136.22
0-225	7.53	0.06	204.73	0-225	6.85	0.80	196.96	0-225	7.54	0.08	213.14
0-300	8.79	0.06	249.51	0-300	8.09	0.81	238.88	0-300	8.76	0.08	245.41
0-350	9.41	0.05	270.80	0-350	8.72	0.82	256.91	0-350	9.34	0.07	272.87

3 mm vacuum chamber with stabilator ring

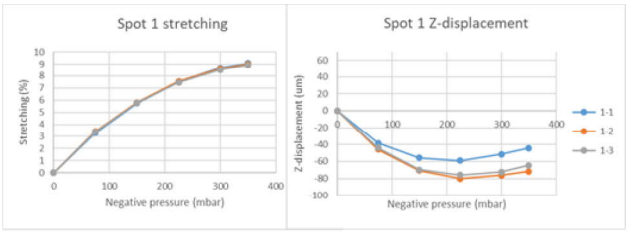

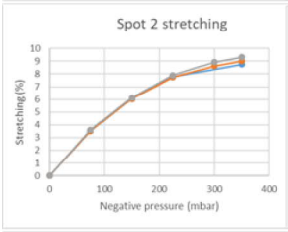

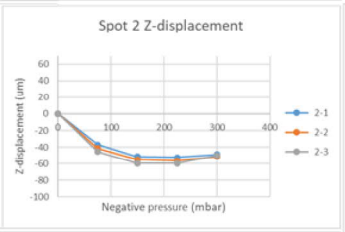

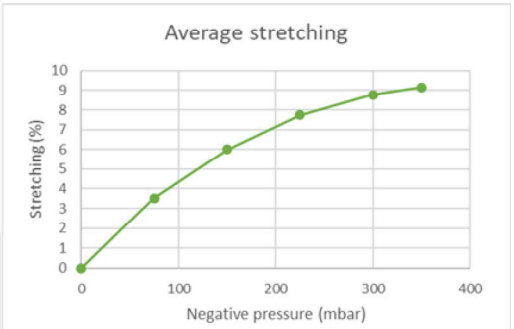

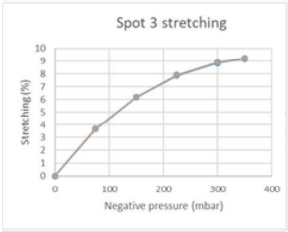

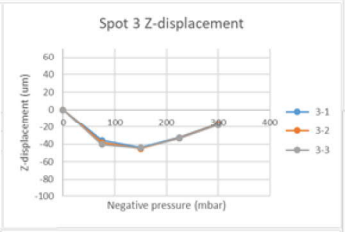

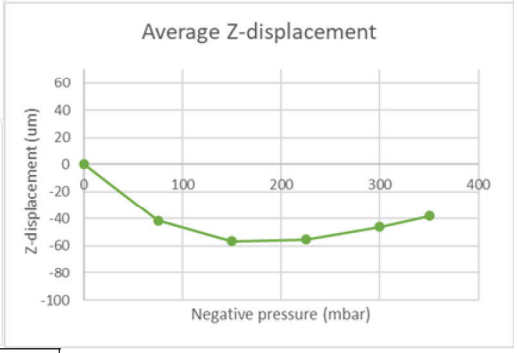

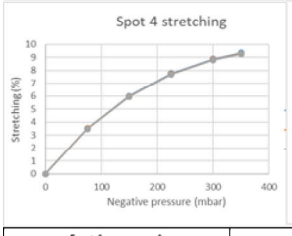

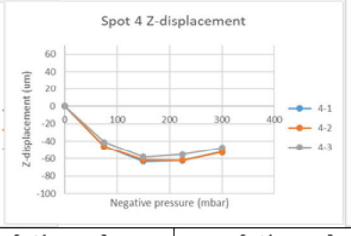

Spot 1 measure 1				Spot 1 measure 2				Spot 1 measure 3			
Pressure	Stretch	St. Dev.	Z	Pressure	Stretch	St. Dev.	Z	Pressure	Stretch	St. Dev.	Z
0-75	3.28	0.06	-38.48	0-75	3.41	0.02	-45.86	0-75	3.37	0.03	-43.80
0-150	5.74	0.08	-55.79	0-150	5.81	0.02	-70.83	0-150	5.79	0.03	-69.88
0-225	7.53	0.10	-59.06	0-225	7.56	0.03	-80.14	0-225	7.47	0.03	-75.86
0-300	8.69	0.08	-51.39	0-300	8.63	0.05	-76.34	0-300	8.51	0.04	-72.27
0-350	9.07	0.07	-44.23	0-350	9.00	0.09	-71.56	0-350	8.93	0.08	-64.63
Spot 2 measure 1				Spot 2 measure 2				Spot 2 measure 3			
Pressure	Stretch	St. Dev.	Z	Pressure	Stretch	St. Dev.	Z	Pressure	Stretch	St. Dev.	Z
0-75	3.53	0.01	-37.18	0-75	3.53	0.01	-41.48	0-75	3.61	0.01	-45.45
0-150	6.04	0.03	-51.42	0-150	6.03	0.02	-54.95	0-150	6.12	0.02	-59.67
0-225	7.77	0.04	-52.35	0-225	7.75	0.03	-56.24	0-225	7.89	0.04	-59.66
0-300	8.74	0.06	-48.71	0-300	8.63	0.20	-51.42	0-300	8.92	0.07	-50.15
0-350	9.12	0.09	-46.95	0-350	9.01	0.20	-45.43	0-350	9.32	0.10	-43.76
Spot 3 measure 1				Spot 3 measure 2				Spot 3 measure 3			
Pressure	Stretch	St. Dev.	Z	Pressure	Stretch	St. Dev.	Z	Pressure	Stretch	St. Dev.	Z
0-75	3.67	0.03	-35.74	0-75	3.65	0.02	-38.13	0-75	3.68	0.02	-40.28
0-150	6.16	0.07	-43.99	0-150	6.17	0.02	-45.02	0-150	6.18	0.02	-44.35
0-225	7.86	0.07	-32.46	0-225	7.91	0.03	-33.11	0-225	7.91	0.03	-33.47
0-300	8.84	0.07	-16.31	0-300	8.89	0.05	-16.92	0-300	8.89	0.06	-17.89
0-350	9.18	0.09	-4.94	0-350	9.20	0.08	-2.75	0-350	9.25	0.10	-5.10
Spot 4 measure 1				Spot 4 measure 2				Spot 4 measure 3			
Pressure	Stretch	St. Dev.	Z	Pressure	Stretch	St. Dev.	Z	Pressure	Stretch	St. Dev.	Z
0-75	3.51	0.01	-45.80	0-75	3.51	0.02	-45.62	0-75	3.49	0.02	-40.71
0-150	6.01	0.02	-63.38	0-150	5.96	0.01	-61.70	0-150	5.96	0.02	-58.40
0-225	7.76	0.04	-62.39	0-225	7.72	0.03	-62.18	0-225	7.71	0.05	-55.52
0-300	8.87	0.09	-51.96	0-300	8.84	0.09	-52.84	0-300	8.81	0.10	-47.46
0-350	9.35	0.14	-46.25	0-350	9.27	0.15	-44.49	0-350	9.25	0.17	-37.13

3 mm vacuum chamber without stabilator ring

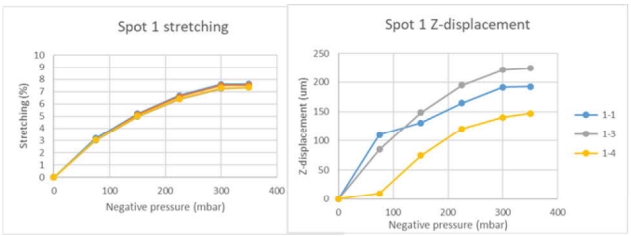

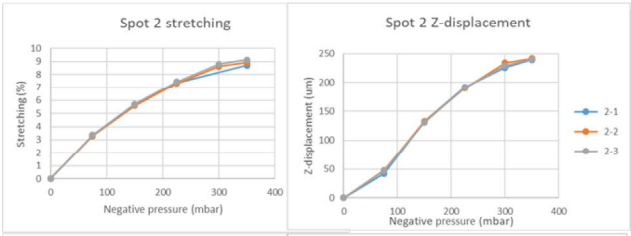

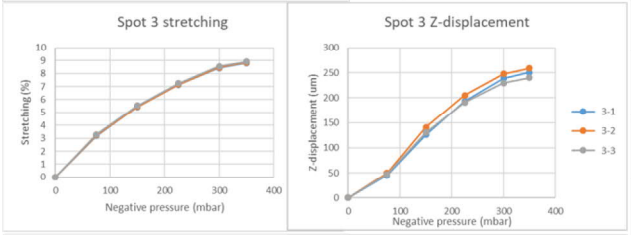

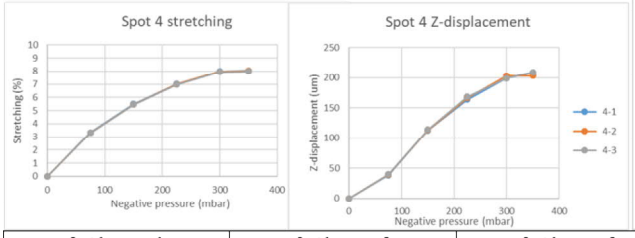

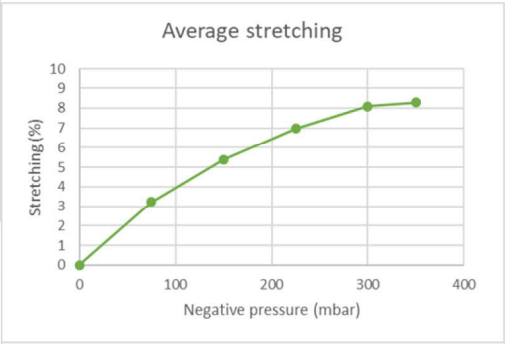

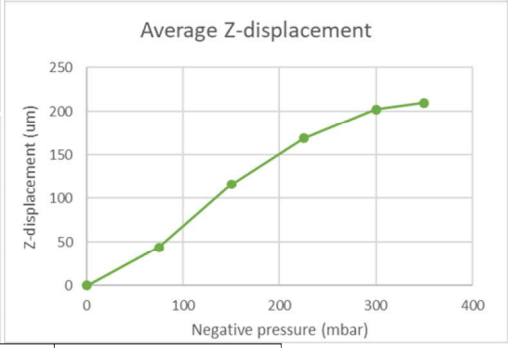

Spot 1 measure 1				Spot 1 measure 2				Spot 1 measure 3				Spot 1 measure 4			
Pressure	Stretch	St. Dev.	Z	Pressure	Stretch	St. Dev.	Z	Pressure	Stretch	St. Dev.	Z	Pressure	Stretch	St. Dev.	Z
0-75	3.16	0.04	110.00	0-75	3.05	0.04	-32.91	0-75	2.98	0.04	85.01	0-75	3.03	0.02	9.74
0-150	5.21	0.06	130.85	0-150	5.15	0.06	19.72	0-150	4.99	0.07	148.50	0-150	5.02	0.02	74.43
0-225	6.69	0.08	164.68	0-225	6.60	0.08	55.33	0-225	6.39	0.11	194.74	0-225	6.41	0.05	120.48
0-300	7.58	0.10	191.68	0-300	7.50	0.11	71.92	0-300	7.25	0.14	221.41	0-300	7.28	0.08	140.38
0-350	7.62	0.10	192.76	0-350	7.53	0.11	72.18	0-350	7.33	0.15	224.11	0-350	7.34	0.07	146.84
Spot 2 measure 1				Spot 2 measure 2				Spot 2 measure 3				Spot 2 measure 4			
Pressure	Stretch	St. Dev.	Z	Pressure	Stretch	St. Dev.	Z	Pressure	Stretch	St. Dev.	Z	Pressure	Stretch	St. Dev.	Z
0-75	3.30	0.12	41.95	0-75	3.30	0.15	48.13	0-75	3.37	0.14	47.04	0-75	0.00	0.00	0.00
0-150	5.60	0.17	132.19	0-150	5.59	0.20	132.34	0-150	5.70	0.19	130.60	0-150	0.00	0.00	0.00
0-225	7.34	0.20	191.55	0-225	7.32	0.24	189.55	0-225	7.44	0.22	190.47	0-225	0.00	0.00	0.00
0-300	8.71	0.21	225.60	0-300	8.61	0.31	233.93	0-300	8.78	0.23	229.22	0-300	0.00	0.00	0.00
0-350	9.04	0.20	239.07	0-350	8.92	0.31	241.78	0-350	9.13	0.22	240.03	0-350	0.00	0.00	0.00
Spot 3 measure 1				Spot 3 measure 2				Spot 3 measure 3				Spot 3 measure 4			
Pressure	Stretch	St. Dev.	Z	Pressure	Stretch	St. Dev.	Z	Pressure	Stretch	St. Dev.	Z	Pressure	Stretch	St. Dev.	Z
0-75	3.18	0.13	44.76	0-75	3.23	0.13	49.62	0-75	3.29	0.12	47.04	0-75	0.00	0.00	0.00
0-150	5.43	0.16	125.85	0-150	5.46	0.15	141.07	0-150	5.54	0.15	130.60	0-150	0.00	0.00	0.00
0-225	7.13	0.16	193.65	0-225	7.16	0.15	204.99	0-225	7.24	0.15	190.47	0-225	0.00	0.00	0.00
0-300	8.42	0.16	238.54	0-300	8.47	0.15	247.28	0-300	8.54	0.15	229.22	0-300	0.00	0.00	0.00
0-350	8.80	0.13	250.41	0-350	8.85	0.12	258.54	0-350	8.91	0.11	240.02	0-350	0.00	0.00	0.00
Spot 4 measure 1				Spot 4 measure 2				Spot 4 measure 3				Spot 4 measure 4			
Pressure	Stretch	St. Dev.	Z	Pressure	Stretch	St. Dev.	Z	Pressure	Stretch	St. Dev.	Z	Pressure	Stretch	St. Dev.	Z
0-75	3.33	0.08	38.36	0-75	3.32	0.08	39.37	0-75	3.31	0.08	39.70	0-75	0.00	0.00	0.00
0-150	5.50	0.08	112.86	0-150	5.46	0.09	113.04	0-150	5.46	0.07	114.19	0-150	0.00	0.00	0.00
0-225	7.02	0.08	163.46	0-225	6.99	0.09	166.52	0-225	6.97	0.08	168.10	0-225	0.00	0.00	0.00
0-300	7.99	0.08	199.61	0-300	7.95	0.09	202.98	0-300	7.95	0.08	199.04	0-300	0.00	0.00	0.00
0-350	8.05	0.10	208.48	0-350	8.02	0.11	202.98	0-350	7.99	0.10	209.23	0-350	0.00	0.00	0.00

APPENDIX C: CROSS-SECTIONAL CELL AREAS

Controls: Each sample was imaged from three different spots. The average cross-sectional cell area and standard deviation was calculated for each spot, and an average of the three values per control sample were calculated.

Compression test: The sample was imaged from three to five spots at each time point. The average cross-sectional cell area and standard deviation was calculated for each spot. The averages were calculated for each time point.

		Spot 1		Spot 2		Spot 3		Spot 4		Spot 5			
		Area (μm^2)	σ (μm^2)	Area (μm^2)	σ (μm^2)	Area (μm^2)	σ (μm^2)	Area (μm^2)	σ (μm^2)	Area (μm^2)	σ (μm^2)	Average area (μm^2)	Average σ (μm^2)
Controls	Marienfeld High Precision cover glass	152.65	60.47	206.22	76.63	255.02	114.91					204.63	84.00
	SILPURAN®	156.13	58.27	232.36	80.75	159.22	62.42					182.57	67.15
Compression test	Before compression	135.75	56.30	124.11	59.03	128.58	44.84					129.48	53.39
	0 h	111.67	48.72	106.84	33.55	84.10	33.17					100.87	38.48
	0.5 h	78.96	27.75	80.40	27.48	59.71	27.07					73.02	27.43
	1 h	83.25	22.20	76.30	20.21	76.61	23.34					78.72	21.91
	1.5 h	70.22	25.46	57.23	18.82	50.54	18.33	67.52	23.10	67.52	24.70	62.60	22.08
	2 h	54.09	21.01	54.40	18.82	48.93	14.51	73.82	25.80	75.74	36.83	61.40	23.39
	2.5 h	77.19	26.71	57.08	21.98	61.36	21.26	89.57	26.77	92.71	32.46	75.58	25.84
	3 h	77.99	26.76	66.50	28.91	63.98	27.98	88.17	31.06	83.31	31.18	75.99	29.18
	3.5 h	57.43	24.24	58.76	28.69	72.74	30.09	89.16	29.80	92.05	25.30	74.03	27.62
	4 h	75.25	28.73	65.43	29.93	76.88	75.57	89.62	30.32	83.79	29.63	78.19	38.83